UNIVERSIDADE FEDERAL DO PARANÁ

JÚLIO WERNER YOSHIOKA BERNARDO

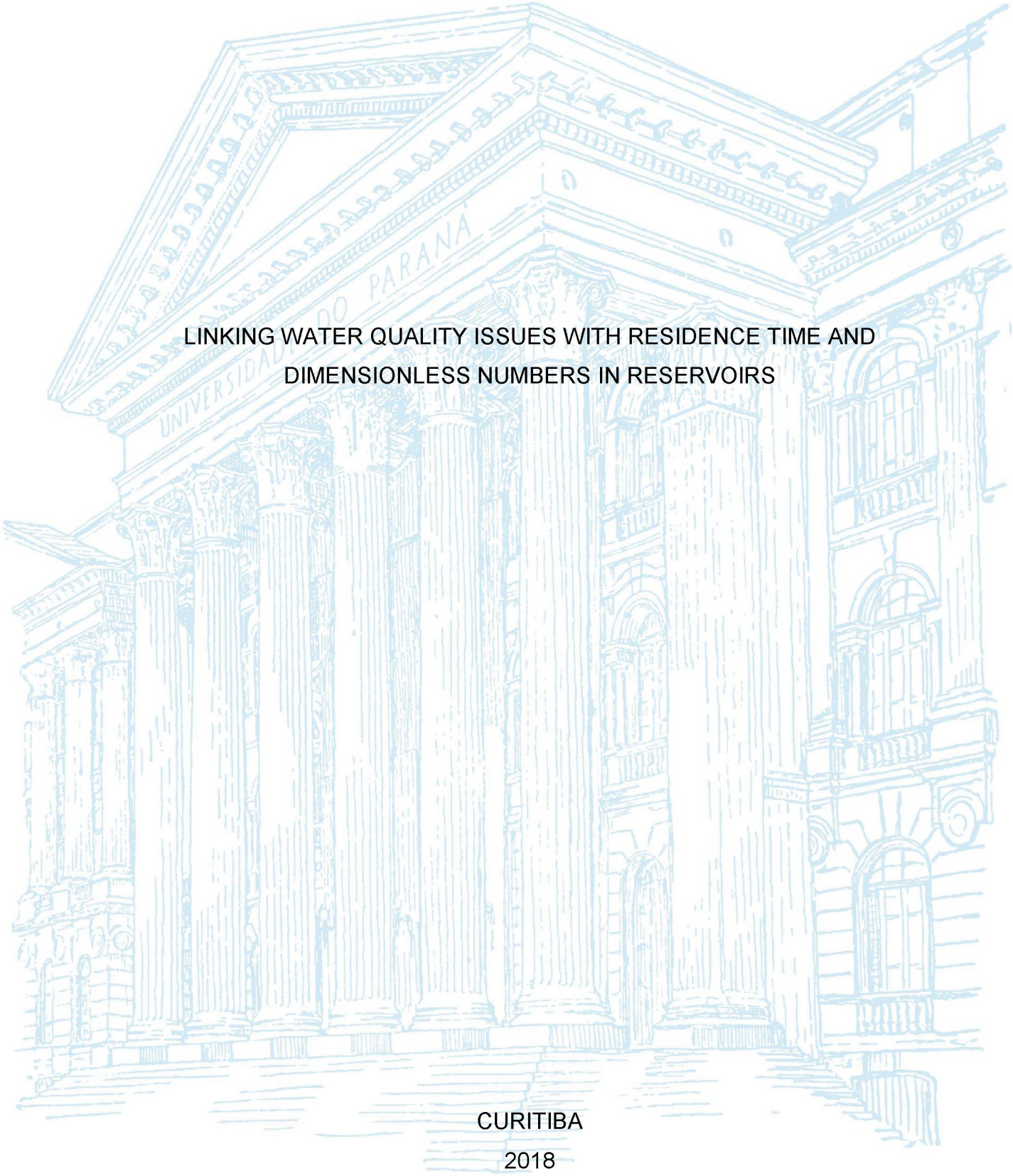

LINKING WATER QUALITY ISSUES WITH RESIDENCE TIME AND DIMENSIONLESS NUMBERS IN RESERVOIRS

CURITIBA

2018

JÚLIO WERNER YOSHIOKA BERNARDO

LINKING WATER QUALITY ISSUES WITH RESIDENCE TIME AND DIMENSIONLESS NUMBERS IN RESERVOIRS

Trabalho apresentado como requisito parcial para a obtenção do grau de Doutor em Engenharia de Recursos Hídricos e Ambiental no curso de Pós-graduação em Engenharia de Recursos Hídricos e Ambiental, Setor de Tecnologia da Universidade Federal do Paraná.

Orientador: Prof. Dr.-Ing. Tobias Bleninger

CURITIBA

2018

Catalogação na Fonte: Sistema de Bibliotecas, UFPR
Biblioteca de Ciência e Tecnologia

B523l Bernardo, Julio Werner Yoshioka
Linking water quality issues with residence time and dimensionless numbers in reservoirs / Julio Werner Yoshioka Bernardo. – Curitiba, 2018.

Tese - Universidade Federal do Paraná, Setor de Tecnologia, Programa de Pós-Graduação em Engenharia de Recursos Hídricos e Ambiental, 2018.

Orientador: Tobias Bleninger.

1. Água – qualidade. 2. Reservatórios. 3. Modelagem. I. Universidade Federal do Paraná. II. Bleninger, Tobias. III.Título.

CDD: 631.7

Bibliotecária: Vanusa Maciel CRB- 9/1928

MINISTÉRIO DA EDUCAÇÃO
SETOR SETOR DE TECNOLOGIA
UNIVERSIDADE FEDERAL DO PARANÁ
PRÓ-REITORIA DE PESQUISA E PÓS-GRADUAÇÃO
PROGRAMA DE PÓS-GRADUAÇÃO ENGENHARIA DE RECURSOS HÍDRICOS E AMBIENTAL

TERMO DE APROVAÇÃO

Os membros da Banca Examinadora designada pelo Colegiado do Programa de Pós-Graduação em ENGENHARIA DE RECURSOS HÍDRICOS E AMBIENTAL da Universidade Federal do Paraná foram convocados para realizar a arguição da Tese de Doutorado de **JULIO WERNER YOSHIOKA BERNARDO**, intitulada: **LINKING WATER QUALITY ISSUES WITH RESIDENCE TIME AND DIMENSIONLESS NUMBERS IN RESERVOIRS**, após terem inquirido o aluno e realizado a avaliação do trabalho, são de parecer pela sua aprovação no rito de defesa.

A outorga do título de Doutor está sujeita à homologação pelo colegiado, ao atendimento de todas as indicações e correções solicitadas pela banca e ao pleno atendimento das demandas regimentais do Programa de Pós-Graduação.

Curitiba, 27 de Novembro de 2018.

TOBIAS BERNWARD BLENINGER
Presidente da Banca Examinadora

STEPHAN HILGERT
Avaliador Externo (KIT)

CRISTOVÃO VICENTE SCAPULATEMPO FERNANDES
Avaliador Interno (UFPR)

JOSÉ RODOLFO SCARATI MARTINS
Avaliador Externo (USP)

WILLIAM BONINO RAUEN
Avaliador Interno (UFPR)

FERNANDO OLIVEIRA ANDRADE
Avaliador Interno

ACKNOWLEDGEMENTS

I would like to express my very great appreciation to Dr. Tobias Bleninger for his valuable and constructive suggestions during the planning and development of this thesis. His willingness to assist in my formation as a scientist and his enthusiastic manner to face all kind of situations has been very much appreciated. I would also like to thank my committee members, Dr. Cristovão V. S. Fernandes, Dr. Fernando O. Andrade, Dr. William B. Rauen, Dr. Stephan Hilgert, and Dr. José R. Scarati Martins. I would especially like to thank the staff and students of PPGERHA to provide an enjoyable and productive environment to work. I would like to thank the organizations that supported this research: the Brazilian National Council for Scientific and Technological Development (CNPq), Brazilian National Council for the Improvement of Higher Education (CAPES), the exchanges with the Karlsruhe Institute of Technology (KIT) which were supported by BWS plus Scholarships provided by the Baden-Württemberg Stiftung, Germany. Finally, I wish to thank my family for their support and encouragement throughout my study.

"Between stimulus and response there is a space.
In that space is our power to choose our response."
Anonymous

RESUMO

A qualidade da água de um reservatório é de grande importância para as necessidades humanas, mas difícil de se medir, devido à sua alta variabilidade espacial e temporal. Portanto, em muitos casos, indicadores são usados para prever danos hídricos, sendo alguns desses indicadores baseados apenas em parâmetros físicos, especialmente os hidrodinâmicos, como o tempo de residência. Há evidências que comprovam a relação entre a qualidade da água e o tempo de residência para sistemas uniformes e totalmente misturados, por exemplo, o modelo proposto por Vollenweider que classifica o estado trófico de reservatórios e lagos. No entanto, ainda faltam métricas para reservatórios estratificados e não permanentes. Uma abordagem dedutiva utilizando-se da análise dimensional e de manipulação algébrica das soluções da equação de advecção, difusão e reação foi realizada para produzir um conjunto de métricas relacionadas à concentração máxima. As métricas resultantes foram números não dimensionais, escalas características de espaço e de tempo, incluindo o tempo de residência. O número do estuário foi identificado como sendo o mais relacionado à concentração máxima local e, portanto, foi escolhido parar ser avaliado por meio de análise de escala e sensibilidade. A aplicabilidade desta métrica para sistemas não uniformes e não permanente foi testada e discutida em um estudo de caso para avaliação da eutrofização de um reservatório subtropical. Os resultados indicaram que a transferência de massa é dominada pela difusão e reação quando o número do estuário é maior que um, e pela advecção e reação quando o número do estuário é menor que um. Além disso, na simulação do estudo de caso, a probabilidade de concentração de fosfato exceder o limite foi 60 % menor nas regiões onde o número de estuários ficou a maior parte do tempo, isso quando comparado com as regiões onde o número do estuário era inferior a um.

Palavras-chave: Escalas de tempo. tempo de residência. Números adimensionais. Transporte. Modelagem.

ABSTRACT

Reservoir water quality is of high importance for human needs, but difficult to measure, due to its high spatial and temporal variability. Therefore, often indicators are used to predict water impairment and some of them are based on physical parameters, especially hydrodynamic parameters only, such as the residence time. There are pieces of evidence proving the relationship between water quality and residence time for uniform, fully mixed systems, for example using the trophic state classification by the Vollenweider plot. However, metrics are missing for stratified and unsteady reservoirs. A deductive approach using dimensional analysis and algebraic manipulation of solutions of the advection-diffusion-reaction-equation were carried out to deduce a set of metrics related to maximum concentration. The resulting metrics are non-dimensional numbers, length and time scales, including residence time. The estuary number was identified to be the most related to local maximum concentration thereby this metric was chosen to be assessed through scale and sensitivity analysis. The applicability of estuary number for non-uniform and unsteady systems was tested and discussed in a case study for eutrophication assessment of a subtropical reservoir. Estuary number application allowed to classify the relative dominance of mixing, transport and transformation processes. Results indicated that the mass transfer is dominated by diffusion and reaction for large estuary numbers, and by advection for smaller estuary numbers. Case study results showed that the probability of orthophosphate concentration exceeding the concentration limit was 60% lower in regions where the estuary number was greater than one most of the time.

Key-words: Time scales. Residence time. Dimensionless numbers. Transport. Modeling.

LIST OF FIGURES

LIST OF TABLES

LIST OF SYMBOLS

C	Concentration [$kg.m^{-3}$].
C_f	Courant number [–].
D	Eddy diffusivity [m^2s^{-1}].
D_H	Horizontal eddy difussity [m^2s^{-1}].
D_V	Vertical eddy difussity [m^2s^{-1}].
Da	Damkholer number [–].
DaI	Damkhöler number I [–].
$DaII$	Damkhöler number II [–].
H	Water depth [m].
L	Characteristic Length [m].
L_n	Lake number [–].
M	Mass [kg].
M_e	Mass of elements leaving the system [kg].
N_e	Number of elements [–].
N_t	Total number of elements [–].
P	Pressure [Pa].
Pe	Peclet number [–].
Q	Discharge [m^3].
Re	Reynolds number [–].
S	Source or sink term [$kg.m^{-2}.s^{-1}$].
S_c	Schmidt number [–].
Δs	Maximum displacement [m].
Δt	Time interval [s].
Δx	Grid size in x direction [m].
Δy	Grid size in y direction [m].
η	Estuary number [–].
ν_H	horizontal eddy viscosity [m^2s^{-1}].
ν_V	Vertical eddy viscosity [m^2s^{-1}].
f	Coriolis parameter [s^{-1}].

$f(t_r)$	Probability density function of residence time.
g	Acceleration due to gravity $[ms^{-2}]$.
n	Random number uniformly distributed [–].
t_a	Age, average time since a substance entered in the system [s].
t_r	Bulk residence time [s].
t_{max}	Time when maximum concentration occurs [s].
u	Velocity in x direction $[ms^{-1}]$.
v	Velocity in y direction $[ms^{-1}]$.
w	Velocity in z direction $[ms^{-1}]$.
x	First coordinate of three-dimensional Cartesian system $[m]$.
y	Second coordinate of three-dimensional Cartesian system $[m]$.
z	Third coordinate of three-dimensional Cartesian system $[m]$.

CONTENTS

1 INTRODUCTION

The storage of water in reservoirs is a common solution to overcome the seasonality and uneven territorial distribution of water. According to Lehner et al. (2011), ICOLD (2007), the most common purposes of large reservoirs are irrigation and hydropower. Hydropower provides about 20% of the world's electricity, in Brazil the proportion is more expressive being 69% of the total capacity. Furthermore, the growing Brazilian population and economy increases the demand for electricity, and consequently for new hydropower plants. The construction of 18 large hydropower plants is planned in Brazil until 2023 (EPE, 2014). This is also a global trend, i.e. for emerging countries, where at least 3,700 dams are planned or under construction according to Zarfl et al. (2015). Consequently, sustainability issues of reservoirs which include the change of water quality are a world-wide issue.

Approximately, two in ten Brazilian's water quality monitoring sites were classified having fair, poor or very poor water quality through the national water quality index within the years of 2001 to 2010 (ANA, 2013). Furthermore, about 6 in 10 water quality monitoring points within lakes, reservoirs, and ponds were classified as eutrophic and hypereutrophic. Thus, an expressive number of Brazilian reservoirs, lakes, and ponds may suffer effects of eutrophication processes. Those numbers highlight that Brazil has a remarkable quantity of water quality issues which may increase with the planned reservoirs and population growth. Although water quality monitoring systems are more available and increasingly installed, they bring additional challenges to water management systems. The data produced from different sources like satellites, unmanned vehicles, terrestrial and aquatic stations, mobile network sensor allows the analysis of spatial and temporal variability in much higher resolutions, allowing to setup and calibrate three-dimensional and unsteady models for reservoir management purposes. As consequence, the spatial and temporal variability of hydrodynamics and related water quality issues can be measured, estimated and predicted. However, a huge amount of information is generated compromising their processing and analysis.

Even with ongoing technology, hydrodynamic models require a lot of computational power and improvements to achieve faster and precise simulations (AFZAL et al.,

2017). Due to this computational constraint, current applications on environmental systems work with coarse grids, short scenario periods and long running times. Furthermore, water quality issues require additional models being coupled with a hydrodynamic model increasing, even more, the simulation time. Additionally, the post-processing stage of two and three-dimensional models requires innovative techniques for visualization and interpretation of model output. Thus, time is a constraint to perform modeling activities.

This thesis proposes to develop metrics relating water quality with hydrodynamics, which could create insights beforehand and using advanced modeling only in cases where metrics indicate when necessary, thus saving time and working hours. As a consequence, the saved time can be used to refine the hydrodynamic model, to carry out other scenarios, or just to get faster insights. Metrics summarize a set of aspects of the system to simplify the analysis and to provide insights and drive decisions for a specific issue (Figure 1).

Residence time is a well-known metric which relates water quality and hydrodynamics (EVANS et al., 2017; CATALÁN et al., 2016; CHAPRA, 2008; RENNELLA; QUIRÓS, 2006; VOLLENWEIDER, 1975). Common applications are classifications of the trophic state (ANA, 2010; VOLLENWEIDER, 1975) and the distinction between lotic and lentic systems (JONES et al., 2017; CONAMA, 2005). In that regard, this metric states that a system with a long residence time is more susceptible to eutrophication. Thus, a rapid and simple solution arose from this metric: shortening the residence time. Furthermore, lotic systems (short residence time) are usually considered more resilient than lentic systems. As a consequence, water quality regulations usually distinguish concentration limits of estuaries, rivers, lakes, and reservoirs (U.S.EPA, 2017; CONAMA, 2005).

Existing relationships between residence time and eutrophication were established assuming steady, and completely mixed systems. However, environmental systems usually present spatial and temporal variability of water quality and hydrodynamic parameters. In that regard, additional methods have been explored to use residence time concepts considering that variability. These recent concepts are called here generically a local residence time (JIANG et al., 2017; MAHANTY et al., 2016; DELHEZ et al., 2014; DEFNE; GANJU, 2015). However, these studies miss the link between local

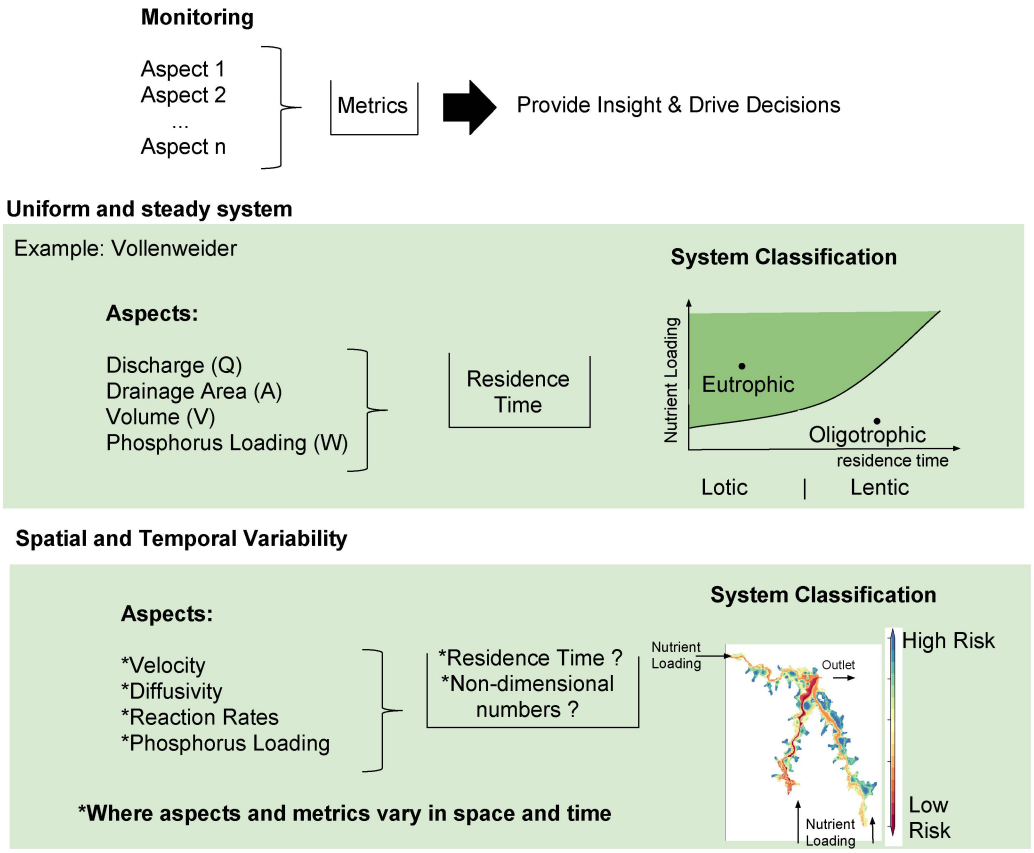

Figure 1 – Graphical summary of the research problem addressed in this thesis. Metrics are useful to simplify the system to provide insights and drive decisions more easily. A well-known metric for reservoirs is the residence time which was derived for uniform and steady systems. However, the correct metric for systems with spatial and temporal variability is still unclear.

residence time and water quality. Usually, the basic assumption of these studies relies on evidence from earlier concepts which assume a uniform system.

Often, correlations between residence times and concentrations are used to establish their relationship (ROGERS et al., 2017; QI et al., 2016; LI; ZHANG; YAO, 2015; BERNARDO; BLENINGER, 2015; DELESALLE; SOURNIA, 1992). However, the correlation approach does not imply in causation and the results may be site-specific results only. This problem and its related challenge is illustrated in Figure 1.

Instead of searching only for correlations, the herein proposed method is to extract the link from the theory of solute transport in a fluid system, i.e. the advection-diffusion-reaction equation (ADRE). The hypothesis is that there are suitable metrics to establish and assess the link between hydrodynamics and water quality aspects in system with spatial and temporal variability. The expected benefits of this approach are: (i) the metric is derived from the theory without simplifications, (ii) the theory already contains the link between a metric and water quality, thus the links rely on a fundamental concept of transport phenomena.

1.1 OBJECTIVE

The objective is to find a link between water quality and hydrodynamic and physicochemical metrics, such as time or length scales and non-dimensional numbers, for non-uniform and unsteady reservoirs. The following goals were proposed to assess the hypothesis:

- To find a set of potential hydrodynamic parameters related with water quality;
- To identify a metric which defines the dominant hydrodynamic processes;
- To assess the relationship between the parameter and a water quality aspect (maximum concentration and lentic/lotic classification);
- To define a key metric and verify its potential application to assess eutrophication in a subtropical reservoir.

1.2 THESIS OUTLINE

The introduction will be followed by chapter 2, which explores the theoretical background and describes the governing equations. The derivation of the potential metrics relating water quality, hydrodynamics, and physicochemical parameters is presented in Chapter 3 including their assessment. This part focused on the link of the metrics and the water quality aspects. The results of the assessment are presented in Chapter 4 followed by the conclusions and recommendations in Chapter 5.

2 THEORETICAL BACKGROUND

This chapter presents the background on four fundamental topics covered by this thesis: reservoirs, eutrophication, transport phenomena, and residence time. The first topic describes the studied environment. The second describes main causes and effects of eutrophication, followed by a detailed review of residence time concepts and their relationship to eutrophication, as well as extensions to systems with spatial and temporal variability. The fourth topic shows a review on the governing equations of transport phenomena and presents existing analytical solutions for one-dimensional ideal systems.

2.1 RESERVOIRS

The disruption of a river caused by a dam changes the hydrodynamics of the system as depicted in Figure 2. Consequently, damming a river produces positive and negative impacts. Among the benefits of building a dam are the flood protection, water supply, electricity generation, navigability enhancement, and recreation. The impacts are enhanced deposition of nutrients and sediments, ecological disturbance, blockage of sediment transport, changes on microclimate, and increased decomposition of organic matter producing methane and/or carbon dioxide.

Most of North American and European rivers already present a high degree of regulation as shown in Figure 3 reproduced from Lehner et al. (2011). Furthermore, the growing number of planned and built dams is fast-paced in emerging economies countries and specially in Brazil (ZARFL et al., 2015). Therefore, studies about the environmental impact of river damming must go along with the same pace to avoid or diminish its effects on nature, and to reduce the future impacts of this current trend, especially for emerging economies to achieve long-term preservation of reservoir water quality.

Most man made reservoir characteristics are similar to natural lakes like slow, mainly wind induced motions, large surface area and volume. Low velocities promote an environment with higher sedimentation rates than in the rivers, which have larger

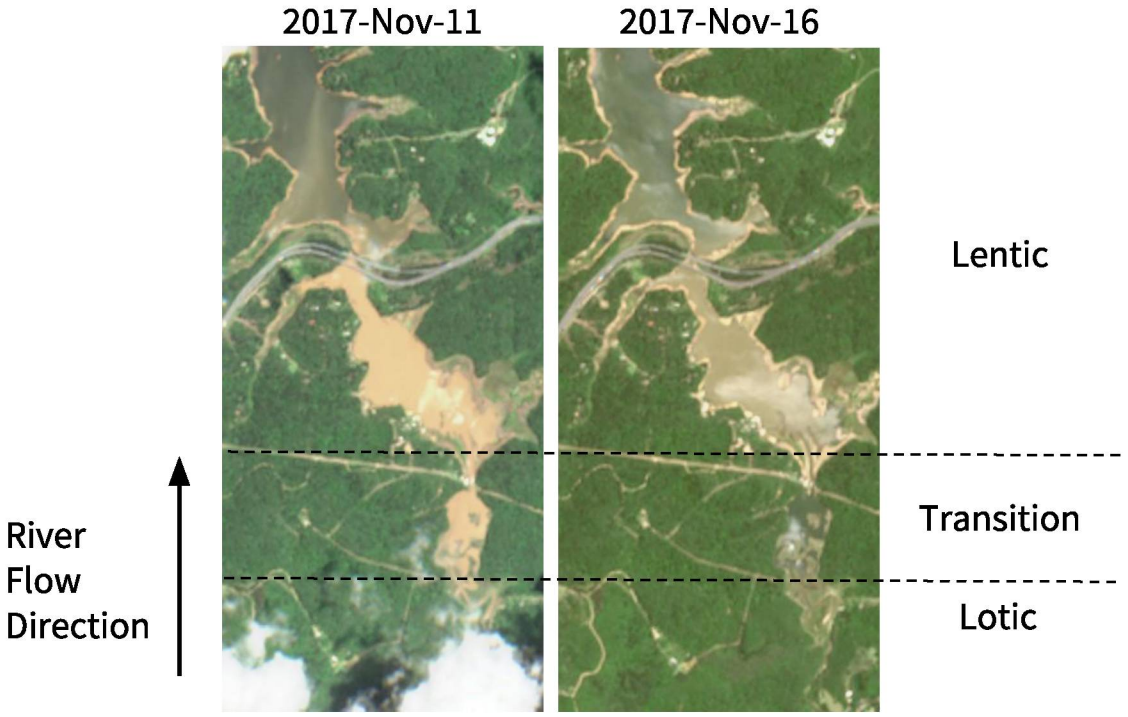

Figure 2 – River disruption caused by damming and related zones. Satellite image acquired after an intense rainfall. Modified Copernicus Sentinel data 2018/Sentinel Hub.

carrying capacities. Solar radiation is more effective than in riverine system due to those slow motions, less shadow, and the large surface area, creating temperature stratifications. Light abundance in addition, favors primary productivity. Usually, oxygen gradients occur over the vertical because of photosynthesis and air exchanges happening at the surface layer and decomposition processes consuming oxygen at the bottom, and less re-aeration rates due to temperature induced density stratification. Table 1 shows typical characteristics comparing riverine and reservoir systems.

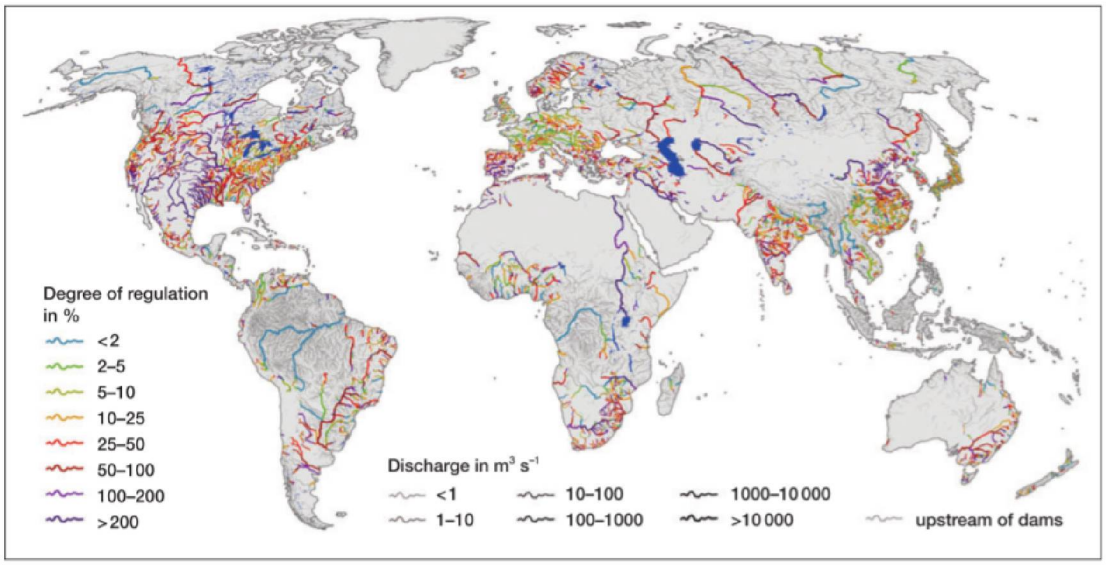

Figure 3 – Degree of regulation of world's main rivers. Source: (LEHNER et al., 2011)

Table 1 – Typical characteristics differentiating riverine system from reservoirs.

Rivers	**Reservoirs**
lotic	lentic
transport	sedimentation
allochthonous	autochthonous
vertically mixed	vertically stratified
oxic conditions	anoxic conditions

2.2 EUTROPHICATION

Eutrophication is the limnologic term for algae blooms and associated issues induced by the excessive loading of nutrients into a water body (SCHINDLER, 2012; WETZEL, 2001). Figure 4 is a schematic diagram of eutrophication showing the main processes involved (e.g. internal loading, settling, feeding, excretion, and decomposition) and the effects on the environment (e.g. oxygen depletion, fish killing, ecosystem instability, toxins release, and gas production). Such impairment of water quality is a worldwide concern because of the increasing nutrient loadings on waterbodies, caused mainly by rapid population growth and associated agricultural and urbanization effects

(SEITZINGER et al., 2010).

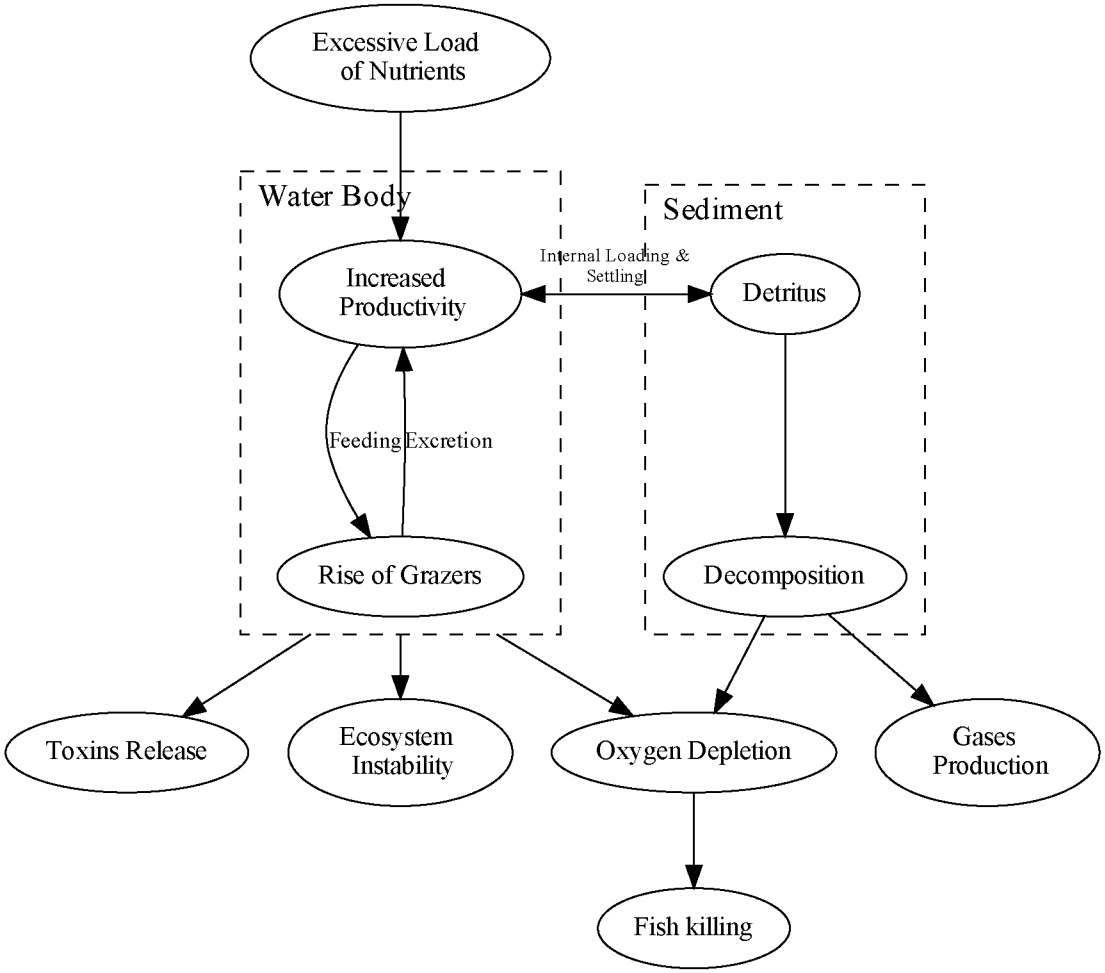

Figure 4 – Major processes and effects of eutrophication in rivers, lakes, and reservoirs.

Concentrations of Chlorophyll-a, total phosphorus, total nitrogen, water transparency (Secchi depth),and low dissolved oxygen are common indicators for eutrophication. Chlorophyll-a, water transparency, and dissolved oxygen estimate the increased productivity, whilst total phosphorus and total nitrogen estimate the nutrient enrichment.

The relevance of nitrogen and phosphorus is based on the photosynthesis/respiration processes and plant stoichiometry as shown by the following chemical equation (STUMM; MORGAN, 2012):

$$106\,CO_2 + 16\,NO_3^- + HPO_4^{2-} + 122\,H_2O + 18\,H^+ \overset{\text{energy}}{\rightleftharpoons} \underbrace{C_{106}H_{263}O_{110}N_{16}P}_{algae} + 138\,O_2$$

$$106\,CO_2 + 16\,NH_4^+ + HPO_4^{2-} + 108\,H_2O + 18\,H^+ \overset{\text{energy}}{\rightleftharpoons} \underbrace{C_{106}H_{263}O_{110}N_{16}P}_{algae} + 107\,O_2 + 14\,H^+$$

As shown above, nitrate, ammonium, and orthophosphate are essential nutrients for algae growth. Furthermore, from stoichiometry, the mass ratio of C:N:P is 40:7.2:1 considering that 1% of dry-weight of the plant protoplasm is composed of phosphorus. The chemical equation represents a system in equilibrium where any change of concentration on a substance will force a new equilibrium state. The algae growth is associated to increasing oxygen, however respiration and decomposition consumes oxygen producing carbon dioxide under oxic conditions and methane under anoxic conditions. Consequently, those equations state the limiting stoichiometric conditions and the energy dependency for eutrophication enhancement, and also emphasizes the importance of loading which impacts the chemical equilibrium.

The effect of hydrodynamics and ecology does not appear directly in the chemical equations, however, they can change the availability of substances and enhance energy retention in the fluid. Biological interaction between organisms, such as predation alters the populations unbalancing the chemical equation. Transport and mixing can also unbalance the chemical equation because they can act on the availability of substances and energy. For example, transport can alter the availability of substances by routing their sources to a given location. Moreover, according to the collision theory, the reactants must collide with enough energy to react. As a consequence, turbulent mixing through the energy cascade can transfer energy from large scales of motion to smaller scales promoting more collisions.

In essence, eutrophication depends on several aspects related to system loadings, reaction rates, biological interactions, and hydrodynamics. Furthermore, environmental systems are subject to spatial and temporal changes on those three aspects. Land-use change, new industrial plants, among others can alter the loading of nutrients into a reservoir. Reaction kinetics may change according to meteorological conditions (e.g temperature and pressure) and the presence of a catalyst. Introduction of alien species can provoke ecological instabilities. Damming of a river, stratification, meteorological

seasonality can change the hydrodynamics. Thus, the challenges to manage reservoirs to avoid eutrophication are huge because of the large number of variables to be considered and their inherent variability in time and space.

Therefore, there are numerous approaches to use indicators or characteristic numbers to embed those variations and dependencies in simplified descriptions. Interestingly, and aside from nutrient loadings and water quality conditions, residence time has been used as a key physical parameter because it summarizes the physical characteristics of a reservoir and its dynamics. First attempts were made to relate physical parameters with eutrophication focused on light, temperature, latitude, and depth (CHAPRA, 2008; SCHINDLER, 2006). However, Vollenweider (1975) observed that deep and faster flushing reservoirs are less susceptible to eutrophication than shallow reservoirs with longer residence times. Figure 5 shows Vollenweider's plot which relates the areal phosphorus loading (L_p $[kg.m^{-2}s^{-1}]$) with depth (z) and residence time. The areal phosphorus loading is the phosphorus loading (W $[kg.s^{-1}]$) divided by the surface area of the reservoir (A_{sup} $[m^2]$) and residence time (t_r $[s]$) is the mean volume (V $[m^3]$) divided by the mean annual outflow (Q $[m^3.s^{-1}]$).

The phosphorus loading is not directly linked to residence time but to the ratio between depth and residence time which is dimensionally a velocity, i.e. a hydrodynamic parameter. In 1976, Vollenweider refined his previous model by adding a new factor, $\frac{H}{t_r}(1+\sqrt{t_r})$, to improve model agreement with measured data. Further attempts were undertaken to extend this new model to predict chlorophyll, oxygen demand, and Secchi-disk depth (CHAPRA, 2008, p.539).

Chapra (2008) also showed that Vollenweider's plot is an approximation of phosphorus mass balance in a completely mixed tank

$$V\frac{dp}{dt} = W - Qp - k_S V p, \tag{2.1}$$

where p is the phosphorus concentration, t is time, and k_S is the phosphorus settling loss rate ($[s^{-1}]$). For the steady solution ($dp/dt = 0$), i.e., when the system reached equilibrium, the phosphorus concentration is

$$p = \frac{W}{Q + k_S V} = \frac{L_p}{\frac{H}{t_r}(1 + k_S t_r)}. \tag{2.2}$$

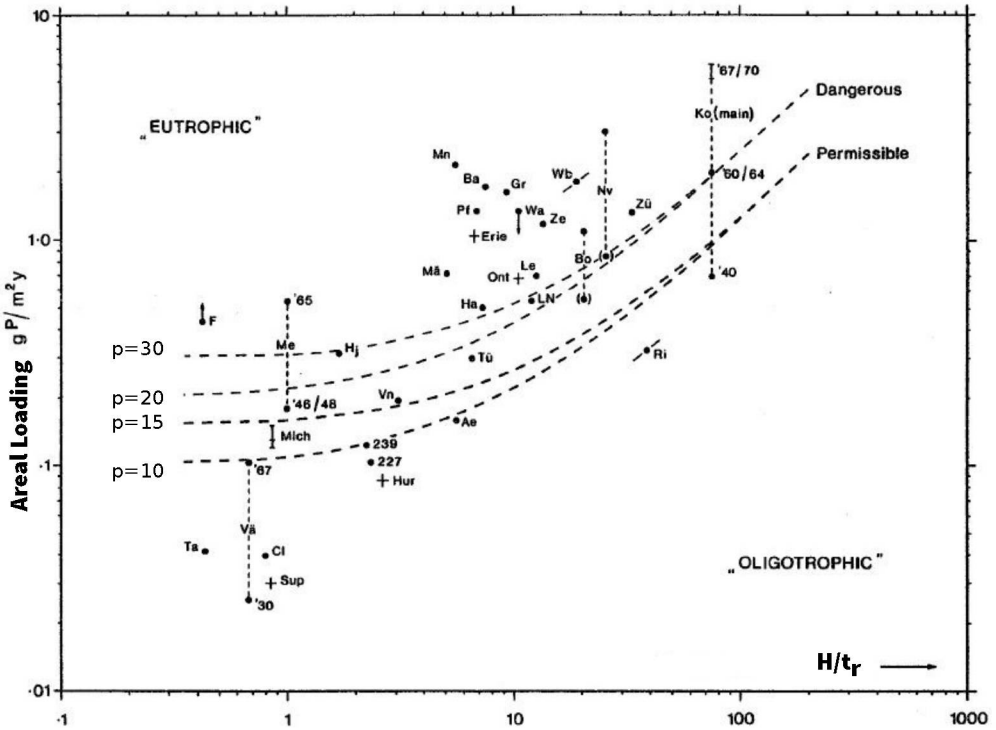

Figure 5 – Results from Vollenweider (1975) showing the relationship between areal phosphorus loading (y-axis) and the ratio of depth to residence time (x-axis). Points represent a lake or reservoir. When a lake or reservoir has multiple loadings they are tied together by a dashed vertical line. Exponentially varying dashed lines represent phosphorus concentration limits to distinguish between eutrophic and Oligotrophic states.

Thus, the relationship of phosphorus concentration in the reservoir (p) depends on the area loading (L_p) and the ratio of depth (H) to residence time (t_r) as shown in the Vollenweider plot, however, missing k_S.

Further investigations, using larger datasets were conducted by other researchers and different settling loss rates (k_S) were obtained. Rast & Lee (1978) approximated the loss rate by $k_S = 1/\sqrt{t_r}$ for North American reservoirs and Salas, Martino et al. (1990) by $k_S = 2/\sqrt{t_r}$ for tropical lakes and reservoirs. This model is still widely used, as well as the concept of residence times, despite the significant simplifications of a steady-state and completely mixed systems, and the variability of the loss rate between tropical and temperate lakes, seen in the dispersion of measured data present in the log-log plot. For example, applications for water use licenses for a hydropower dam in

Brazil require the analysis of eutrophication assessment using the Vollenweider plot (regulation from the Brazilian National Water Agency, (ANA, 2010)). Only for complex systems, authorities may demand for a more sophisticated water quality modeling approach.

In summary, residence times can be applied to summarize hydrodynamic conditions, and also as a simple approach to predict trophic states of lakes and reservoirs. However, spatial variability of those systems cannot be addressed by this metric due to its inherent simplifications. The influence and consequences of those limitations are described as follows by discussing residence times and transport processes in more detail.

2.3 RESIDENCE TIME

A residence time is a time scale applied for a wide range of subjects like environmental sciences, chemical engineering, water resources, geosciences, chemistry, public health, and more, as shown in Figure 6. The main application of residence time is to understand flowing systems. According to Nauman (2008), the theory of residence time started in 1908 due to Irving Langmuir's chemical reactor model and the theory has been evolving since. Furthermore, the popularity of residence time is increasing over the past years according to the results obtained from through a literature survey using two popular search engines for research publications: Web of Science (CLARIVATE, 2018) and Google Scholar (GOOGLE, 2018). This upward trend is shown in Figure 7. Altogether, residence time is a popular scale applied over a wide range of fields. Other metrics also used to classify reservoir systems is presented in Appendix B.

calculated by the following equation:

$$a_{rad} = \frac{1}{k} ln \left(\frac{C_r}{C_p} \right) \tag{2.12}$$

where C_r is the concentration of the radioactive tracer and C_p is the concentration of the passive tracer and k is the decay rate. The ratio of C_r to C_p is the fraction of mass decayed along the path, thus the time required to decay this fraction is the age of the tracer.

This method is simple to implement in any hydrodynamic model which supports the simulation of a passive and a radioactive tracer, and the radio-age method can be applied also experimentally. For example, time scales for world ocean ventilation (air-water exchanges) are measured through radio-age methods using natural carbon isotopes present in the ocean surface layer (FUENTE et al., 2015; BROECKER et al., 1990).

2.3.4 Spatial and Temporal Distribution of Residence Time

After the description of the residence time (probability) distribution, and the calculation of spatial distributions of residence times, the concept of temporal variability of those times is described as follows.

General Theory of Age

The general theory of age was introduced by Delhez et al. (1999) to provide a general scheme to calculate time scales pointwise and also over varying times in an Eulerian framework. Furthermore, this approach distinguishes the age of pure water from the age of its constituents (e.g. pollutants, algae, salt, suspended solids, etc.). This theory has been improved throughout the years widening the range of applications (MOUCHET et al., 2016; DELHEZ et al., 2014; DELHEZ, 2013). As a consequence, the theory became generic enough to be applied for a variety of situations in waterbodies from lakes to the ocean to get insights about the fate of transport (QI et al., 2016; MOUCHET et al., 2016; DU; SHEN, 2015; REN et al., 2014; BRYE et al., 2013).

The main idea of this theory is the concept that a fluid element is composed of water and dissolved or particulate constituents with different ages. Thus, concentration is a function of space, time, and age so that the total concentration at a given position

and time is

$$C(\vec{x},t) = \int_0^\infty c(\vec{x},t,\tau)d\tau \tag{2.13}$$

This new concept was called concentration distribution function ($c(\vec{x},t,\tau)$) by Delhez et al. (1999) which also proved to obey the mass balance equation for a constituent:

$$\frac{\partial c}{\partial t} = p - d - \nabla \cdot (\vec{u}c - D \cdot \nabla c) - \frac{\partial c}{\partial \tau} \tag{2.14}$$

where p and d are production and decay rates respectively, and $\frac{\partial c}{\partial \tau}$ is the aging function, i.e., the rate in which age increases, $\vec{u}$ is the velocity vector, and D is the diffusivity.

The solution of this five-dimensional equation can be avoided by considering the mean value of age of a fluid element. In this case, mean age (a) is estimated by the solution of the following system of equations (DELHEZ et al., 1999):

$$\frac{\partial C}{\partial t} = -\nabla \cdot (\vec{u}C - D \cdot \nabla C) \tag{2.15}$$

$$\frac{\partial C_{age}}{\partial t} = C - \nabla \cdot (\vec{u}C_{age} - D \cdot \nabla C_{age}) \tag{2.16}$$

$$a(\vec{x},t) = \frac{C_{age}(\vec{x},t)}{C(\vec{x},t)} \tag{2.17}$$

Those equations are similar to the transport equation, so they can be implemented using the same numerical schemes, which are commonly applied for hydrodynamic models. Deleersnijder, Delhez & Beckers (2001) showed that some of the previous methods to calculate water age is a particular case of the general theory of age. For example, the radio-age method is obtained by neglecting the diffusive processes.

The general theory of age is a generic framework to estimate time scales. Depending on the boundary and initial conditions a time scale can be determined. For example, in a river, if C is set constant at the inlet and C_{age} is set initially zero, the age is the arrival time. In studies of ocean ventilation, the understanding of the renewal of deep water and surface layer water is described by setting the tracer constant at the surface (DELEERSNIJDER et al., 2002).

Although this theory provides benefits, the complexity to obtain the time scales is similar to obtain concentration distributions from a water quality model because

both solve the advection-diffusion-reaction equations. However, when water quality measurements are scarce the approach can be useful as it relies just on the hydrodynamic results and avoids the calibration of chemical and biological process rates.

In summary this section showed that residence time methods evolved and nowadays temporally and spatially varying residence times can be calculated by for example radio-age methods or the general theory of age. Thus, a lot of effort was put in the improvement of residence time calculations in past years. The following topic covers case studies and applications on how these methods have been used in practice.

2.3.5 Residence Time Applications

Residence times have been applied to achieve a variety of objectives in environmental sciences and water resources. Hydrologists have been investigating times scales, usually called transit times, to understand the connectivity between water storages in watersheds (BIRKEL; SOULSBY, 2016; HUIJGEVOORT et al., 2016). In coastal zones, Andutta, Kingsford & Wolanski (2012), Largier et al. (2004) showed that locations with long local residence times may have ecological benefits providing convenient habitats for early live stage of fishes. For sanitation issues, Alosairi, Imberger & Falconer (2011) investigated flushing behavior of the Persian Gulf to provide a guide for the assessment of future effluent dispersion in the region. In lakes and reservoirs, residence times have been associated to eutrophication. The pioneer work of Vollenweider pointed out that systems with slow flushing characteristics require a small amount of nutrient loadings to become hypereutrophic (VOLLENWEIDER, 1975). Soballe & Kimmel (1987) noted that the algae abundance was similar in rivers, lakes and reservoirs with similar residence times. In conclusion, residence times have a wide range of applications and they have been applied in all kind of waterbodies. Furthermore, residence times are claimed to establish the link between hydrodynamics and biology and chemistry aspects of waters.

Management and regulatory applications

The concept of residence time is simple thus attractive for decision makers. In Brazil, the application for a water use license includes a study of residence times among other requirements (ANA, 2010). Also, Brazilian regulations differ between lentic and lotic systems by means of residence time: the system is considered lotic when residence

time is less than 2 days and lentic when longer than 40 days, and in between 2 and 40 day considered as intermediate (CONAMA, 2005). The lentic/lotic classification is a ecosystem type classification of the flow. Recently, a new classification also using residence times was proposed by Jones et al. (2017) to classify coastal regions in lentic, lotic, or oscillatory (i.e. when systems oscillate between lotic and lentic behavior). Furthermore, The Brazilian water agency uses a water quality index for reservoirs (IqAR) developed by the Paraná state environmental protection agency (IAP, 2004). which is composed of oxygen deficit, chlorophyll-a, total phosphorous, secchi depth, chemical oxygen demand, residence time, inorganic nitrogen, Cyanobacteria, and depth. The weight applied to residence time in this index is 10% of all parameters.

Engineering applications

Typical engineering solutions to prevent nutrient transport to critical regions are pre-dams, flow diversions or other engineering structures, thus prevent harmful algae blooms when the reduction of nutrients loading cannot be achieve fast enough (LEE et al., 2010). In that regard, the assessment of residence time has been useful. The study of local residence time in a reservoir in the La Plata River basin showed that the drinking water intake was located in an area with long residence time and low turbidity providing conditions to promote the growth of algae nearby the intake (SILVA; MARTI; IMBERGER, 2014a). The simulations of groynes being added close to the water intake reduced the residence time by 33-50% and decreased by 30-40% (SILVA; MARTI; IMBERGER, 2014b). Trying to avoid microbial contamination from inlets, Morillo, Imberger & Antenucci (2006) aimed to change residence times and dilution ratio by means of submerged curtains. In this case, the solution aimed for the increase of residence time to avoid underflow, and therefore maximize microbial death by contact of these organisms with UV light. In conclusion, long or short residence time may bring benefits or disadvantages depending on the issue the waterbody is facing.

In summary, local residence times have been applied in many fields to understand the hydrodynamics pathways within a system, and to identify causes and to assess engineering solutions. The concept of residence allows to decompose the flow according to a feature of interest. This decomposition is especially useful in systems with spatial and temporal variability because of the variety of phenomena occurring simultaneously distracting or even hiding important features of the flow. The decomposition feature

owes the direct link of residence time with tracer experiments and its inherent Lagrangian aspect. Most of the applications herein mentioned took advantage of this feature, for example, by trying to understand the impact of inflowing river water on the reservoir (RUEDA; MORENO-OSTOS; ARMENGOL, 2006) or the role of suspended sediments in the Coastal Zone (MERCIER; DELHEZ, 2007). However, in contrary to Vollenweider's plot, the previous examples are not applicable universally and require intensive efforts to compute residence times for unsteady and non-uniform systems.

2.3.6 Relation with Water Quality

The majority of residence time applications for water quality problems used bulk metrics. For example, applications of the Vollenweider model for eutrophication (SALAS; MARTINO, 1991; RAST; LEE, 1978; VOLLENWEIDER, 1975), or Mari et al. (2007) who found a relationship between bulk residence time and the ratio of transparent exopolymeric particles to dissolved organic matter in an estuary. Even nowadays, with plenty of methods to estimate local residence times, bulk residence times are still being used. In very recent papers, bulk residence time was related to organic carbon reactivity and decomposition rates (EVANS et al., 2017; CATALÁN et al., 2016). Most probably, the popularity of bulk metrics owe to its simple and rapid assessment, and using few data only.

However, bulk metrics cannot handle spatial variability and despite many efforts have been spent on finding relation with bulk residence time, few research has been conducted to verify the relation of water quality and local residence times. Most of the applications using local residence times rely on the assumption that the relationship between water quality and bulk residence time is still valid for local residence times. Furthermore, there are plenty of methods to estimate local residence time and each of them presents different results. Thus, it is unlikely that the relationship found with bulk scales is still valid for all local residence time concepts. Because of that, many authors, e.g. Monsen et al. (2002), have been advocating the verification of method assumptions before their implementation.

As concluded in the applications section, the local residence time can provide interesting information on bulk system dynamics using a simple calculation. However, it also can be a poor and misleading estimate for unsteady and non-uniform systems.

Some of the relations between local residence time and water quality are based on this tracking feature of local residence times. For example, retention zones seem to be important to early live stage of fishes (ANDUTTA; KINGSFORD; WOLANSKI, 2012; LARGIER et al., 2004), thus hotspots can be found through local residence time analysis. However, this is just a requirement from biology and it does not establish a general link with water quality.

Another approach to seek for a link between residence time and water quality is through correlations. Bernardo & Bleninger (2015) found a correlation between residence time and dissolved carbon dioxide in subtropical reservoir. However, there is no guarantee that this correlation can be extended for other reservoirs because, in general, correlation does not necessarily mean causation. Correlation can produce reliable results just when enough samples confirm a trend. In a review about the relationship between residence time and phytoplankton biomass, Lucas, Thompson & Brown (2009) found negative, positive, and no significant correlations, i.e., they could not identify a consistent trend in the relationship between phytoplankton and local residence time.

In essence, few studies addressed the relationship of water quality and local residence time. Furthermore, most of the applications of local residence times are used to understand the mass transport in a system, with focus on the identification of retention zones and fast flushing areas only. These zones can be hotspots for the occurrence of certain live beings that require slow or fast flow. But still the link from biology/ecology to hydrodynamics is required. Here, the aim is the opposite, i.e. to find how hydrodynamics can change water quality/biology. Because of that, the following investigation focused on the mass transport theory to understand how the physicochemical parameters change mass fluxes providing good or bad conditions for an environmental development of water quality issues. In that regard, the theory of mass transport is presented in the following section.

2.4 TRANSPORT PHENOMENA

This section presents the theoretical background of the transport of dissolved mass by a fluid. The focus is given on the Advection-Diffusion-Reaction-Equation (ADRE) which is the link between hydrodynamics and water quality. Completely mixed

systems and one-dimensional analytical solutions of the ADRE are presented.

Advection, diffusion, and reaction are the basic processes of mass transport in a fluid. Advection is the transport by the dominant (mean) motion of the fluid, diffusion transport is the result of concentration gradients and random motions of the fluid, and reaction is the transformation of mass by contact with the substances, live beings, and energy sources as radiation. The following equation includes those three processes (in Einstein notation):

$$\frac{\partial C}{\partial t} + \underbrace{u_i \frac{\partial C}{\partial x_i}}_{\text{Advection}} = \underbrace{D_i \frac{\partial^2 C}{\partial x_i^2}}_{\text{Diffusion}} - \underbrace{kC}_{\text{Reaction}} + \gamma, \tag{2.18}$$

where C is the mass concentration $[kg.m^{-3}]$, $u_i(t, x_i)$ are the velocity components in i direction $[m.s^{-1}]$, $D_i(t, x_i)$ is the molecular and turbulent diffusivity in i direction $[m^2.s^{-1}]$, $k(t, x_i)$ is the first-order rate of reaction $[s^{-1}]$, and $\gamma(t, x_i)$ is a source/sink term, all implicitly including effects of temperature stratification or density currents, for example provided by measurements or the momentum and energy equations. The source/sink, for example representing internal loadings or intakes were not considered in the following analyses. External loadings are considered in the boundary conditions.

2.4.1 Non-dimensional Form

The relative magnitude of dynamic processes (advection, diffusion, and reaction) becomes apparent when the ADRE is converted into its non-dimensional form. Their importance is measured by non-dimensional parameters which may be used to describe the dynamics of the system. Four non-dimensional forms of ADRE are presented here. The difference among those are the scales used to deduce them as shown in Table 2. The table does not show the non-dimensional concentration because all forms use $C' = C/C_0$, where C_0 is the source concentration. Note that notations of scales are used indistinctly, in the sake of simplicity, to avoid four different notations but remember that each form has its own scale definition.

Combinations of non-dimensional scales generate parameters which relate the dynamic processes of advection, diffusion, and reaction. The relation of advection time and diffusion time is known as the Peclet Number:

$$Pe = \frac{uL}{D}, \tag{2.19}$$

Table 2 – Scales used to deduce each of non-dimensional forms of the ADRE.

Scale	Form I	Form II	Form III	Form IV	Form V
x'	$\frac{x}{L}$	$\frac{x}{L}$	$\frac{kx}{u}$	$\sqrt{\frac{k}{D}}x$	$\frac{u}{D}x$
t'	$\frac{Dt}{L^2}$	$\frac{ut}{L}$	kt	kt	kt

the relation of reaction time and advection time is called Damköhler I:

$$Da_I = \frac{kL}{u}, \tag{2.20}$$

and Damköhler II is the relation of reaction time and diffusion time:

$$Da_{II} = \frac{kL^2}{D} \tag{2.21}$$

The non-dimensional form I and II are similar, and both include a characteristic length. The non-dimensional equation for these forms are respectively:

$$\frac{\partial C'}{\partial t'} + Pe\frac{\partial C'}{\partial x_i'} = \frac{\partial^2 C'}{\partial x'^2} - Da_{II}C' \tag{2.22}$$

$$\frac{\partial C'}{\partial t'} + \frac{\partial C'}{\partial x_i'} = \frac{1}{Pe}\frac{\partial^2 C'}{\partial x'^2} - Da_I C' \tag{2.23}$$

On the other side, the non-dimensional forms III and IV do not have any characteristic length defined, and are respectively:

$$\frac{\partial C'}{\partial t'} + \frac{\partial C'}{\partial x_i'} = \frac{Da_I}{Pe}\frac{\partial^2 C'}{\partial x'^2} - C' \tag{2.24}$$

$$\frac{\partial C'}{\partial t'} + \sqrt{\frac{Pe}{Da_I}}\frac{\partial C'}{\partial x_i'} = \frac{\partial^2 C'}{\partial x'^2} - C' \tag{2.25}$$

$$\frac{\partial C'}{\partial t'} + \frac{Pe}{Da_I}\frac{\partial C'}{\partial x_i'} = \frac{Pe}{Da_I}\frac{\partial^2 C'}{\partial x'^2} - C' \tag{2.26}$$

Thus, the advantage of form III and IV is the presence of just one non-dimensional parameter which shapes the solution of the equation. (CHAPRA, 2008) called this number the Estuary number.

Due to the fact that the non-dimensional forms III and IV do not include a characteristic length, they are more suitable for describing non-uniform system where

the definition of a characteristic length is prone to uncertainty. Furthermore, such non-dimensional numbers can be estimated for each location in the system, what we call hereafter local non-dimensional number. The ability of local Peclet, Damköhler I, and Damköhler II to predict the dominant processes will be investigated.

2.4.2 Analytical Solutions

Instantaneous loading, step loading, and oscillatory loading are typically studied boundary conditions. The instantaneous or pulse loading may represent for example a spill or strong and short rainfall with subsequent strong and short substance transport into the reservoir. The step change can represent the long-term effects of land use changes in reservoir's drainage area, that is, the introduction of new sources in the system. The oscillatory release represents a system with loadings varying with a period or season of high and low emissions. Besides the idealization, such more boundary conditions may build up insights regarding the behavior of the transport of mass in a system. In this section, solutions for completely mixed and one-dimensional systems are presented with these types of boundary conditions.

2.4.2.1 Completely Mixed System

Complete mixing assumes an instantaneous mixture of mass in the system, that is, the coefficient of diffusivity tending to infinity (Figure 10). Consequently, the input at the boundary is represented by a source and the governing equation becomes:

$$\frac{dC}{dt} + \left(\frac{Q}{V} + k\right) C = \frac{W}{V} \tag{2.27}$$

where Q is the outflow $[m^3.s^{-1}]$, V is the system volume $[m^3]$, and W is the loading function $[kg.s^{-1}]$.

The Loading function represents a boundary condition. Thus, the representations of instantaneous loading, step loading, and the oscillatory are:

$$W = \frac{m\delta(t)}{V}, \tag{2.28}$$

$$W(t) = 0 \quad \text{for} \quad t < 0 \quad \text{and} \quad W(t) = W \quad \text{for} \quad t \geq 0, \tag{2.29}$$

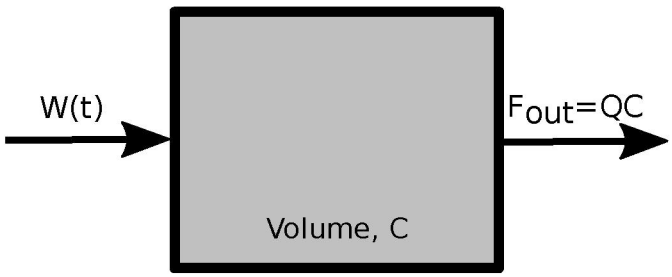

Figure 10 – Scheme of a completely mixed system. The absence of spatial variations defines it as an ideal system. The system is represented by a volume where a loading changing in time ($W(t)$) is released in the system which is instantaneously mixed and then it leaves the system with the rate (F_{out}).

$$W(t) = \overline{W} + W_a \sin(\omega t - \theta) \tag{2.30}$$

, where m is the discharged mass, $\overline{W}$ is the mean loading $[kg.s^{-1}]$, W_a is the loading amplitude $[kg.s^{-1}]$, ω is the angular frequency $[s^{-1}]$, and θ is the phase shift [radians].

The solutions using the previous boundary conditions of instantaneous loading, step loading, and oscillatory loading were compiled by (CHAPRA, 2008), and are respectively:

$$C = \frac{m}{V} \exp(-\lambda t) \tag{2.31}$$

$$C = \frac{W}{\lambda V}(1 - \exp(-\lambda t)) \tag{2.32}$$

$$C = \frac{W}{\lambda V} + \frac{W_a}{V\sqrt{\lambda^2 + \omega^2}} \sin(\omega t - \omega - \phi) \tag{2.33}$$

, where $\lambda = \frac{Q}{V} + k$ and $\phi = \tan^{-1}\left(\frac{\omega}{\lambda}\right)$.

Figure 11 shows the results of each boundary condition, as well as some shape parameters as temporal extent to achieve 95% of the initial concentration (t_{95}), phase shift, angular frequency, oscillation period (T_p), steady concentration $\overline{c}$, and the amplitude of the concentration (C_a), respectively. Although the solutions represent an ideal system, the inspection of shape parameters reveals how the system response changes according to the dynamic processes. Until now, such approach is limited to completely mixed systems and the extension of this method to a non-uniform system is explored in this thesis.

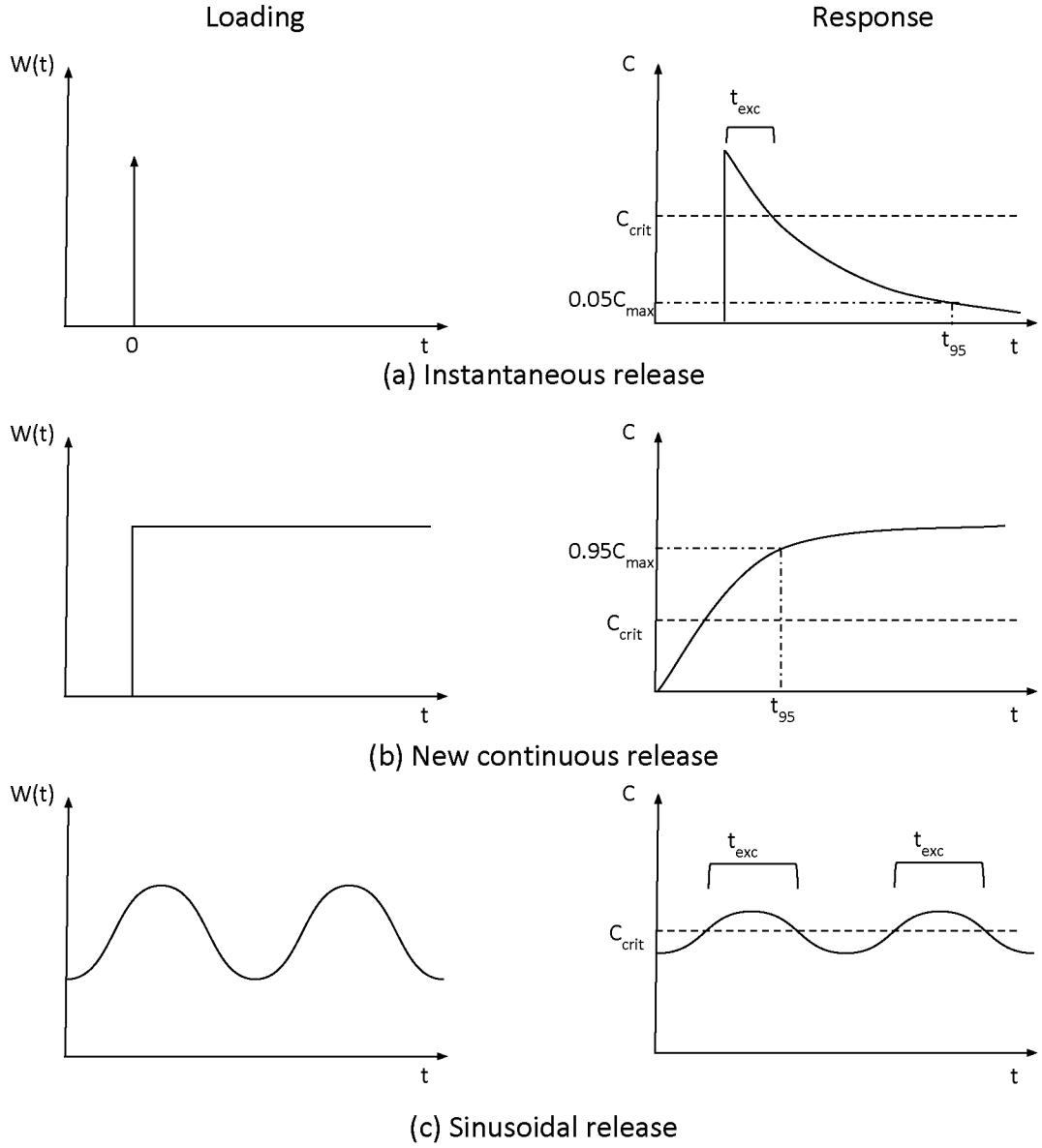

Figure 11 – Solutions for completely mixed systems adapted from Chapra (2008). Boundary conditions (inlet conditions) are represented on the left and the response (outlet concentration distributions) to them on the right.

2.4.2.2 One-dimensional Incompletely Mixed System

The effect of non-uniformity is explored first for a one-dimensional system, that is, completely mixed in two dimensions only (laterally and vertically). This choice was made to increase confidence in the results by growing complexity step-by-step. This section just describes and summarizes the main assumptions to solve the one-dimensional ADRE to obtain the solution for the instantaneous loading, step loading, and oscillatory loading (Figure 12) conditions. These solutions were used to reveal the links between water quality and shape parameters in a non-uniform system in analogy to completely mixed systems.

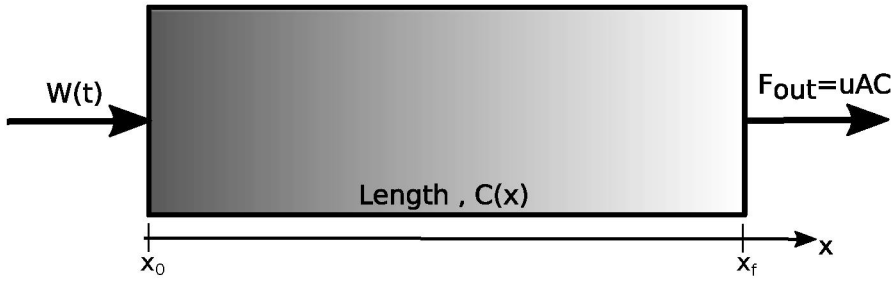

Figure 12 – Scheme of a one-dimensional incompletely mixed system (only mixed laterally and vertically, but not horizontally). The spatial variation occurs in one direction (here horizontal, x). The system is defined by a characteristic length where a loading changing in time ($W(x_0, t)$) is released at the initial position ($x = x_0$) and then transported until the end of the system ($x = x_f$). The mass released in the system is partially mixed and then removed from the system with the rate F_{out}.

For all cases, the initial condition is a system without substance,

$$C(x, t = 0) = C(t = 0) = 0. \tag{2.34}$$

The boundary condition at $x = 0$ for an instantaneous loading is

$$C(x = 0, t) = m\delta(t), \tag{2.35}$$

where $\delta(t)$ is the Dirac delta function. The boundary condition for the step loading is

$$-D\frac{\partial C}{\partial x} + uC\Big|_{x=0} = uC_0, t > 0, \tag{2.36}$$

and for the oscillatory loading is

$$-D\frac{\partial C}{\partial x} + uC\bigg|_{x=0} = uC_0\cos(\omega t). \tag{2.37}$$

The second boundary condition at the system end was set to

$$C(x=\infty, t) = 0. \tag{2.38}$$

Solutions for instantaneous and step loading were deduced for example by (GENUCHTEN; ALVES, 1982), and are respectively:

$$C(x,t) = \frac{M}{\sqrt{4\pi Dt}}\exp\left(\frac{-(x-ut)^2}{4Dt} - kt\right) \tag{2.39}$$

$$\begin{aligned} C(x,t) = C_0\Bigg\{ & \frac{u}{u+\zeta}\exp\left[\frac{(u-\zeta)x}{2D}\right]\operatorname{erfc}\left[\frac{x-\zeta t}{2\sqrt{Dt}}\right] \\ & + \frac{u}{u-\zeta}\exp\left[\frac{(u+\zeta)x}{2D}\right]\operatorname{erfc}\left[\frac{x+\zeta t}{2\sqrt{Dt}}\right] \\ & + \frac{u^2}{2kD}\exp\left(\frac{ux}{D} - kt\right)\operatorname{erfc}\left[\frac{x+ut}{2\sqrt{Dt}}\right]\Bigg\}, \end{aligned} \tag{2.40}$$

where

$$\zeta = \sqrt{u^2 + 4kD} = u\sqrt{1 + 4\frac{kD}{u^2}} = u\sqrt{1+4\eta}, \tag{2.41}$$

and, as shown by (LOGAN; ZLOTNIK, 1995), the oscillatory solution is:

$$C(x,t) = \frac{uC_0}{\sqrt{(u+\alpha D)^2 + \rho^2 D^2}}\exp(-\alpha x)\cos(\omega t - \rho x - \gamma), \tag{2.42}$$

where

$$\alpha = \mu - \frac{u}{2D}, \tag{2.43}$$

$$\mu = \sqrt{\frac{\sqrt{\phi^2+\psi^2}+\psi}{2}}, \tag{2.44}$$

$$\rho = \sqrt{\frac{\sqrt{\phi^2+\psi^2}-\psi}{2}}, \tag{2.45}$$

$$\phi = \frac{\omega}{D}, \tag{2.46}$$

$$\psi = \frac{u^2}{4D^2} + \frac{k}{D} = \frac{\zeta^2}{4D^2}, \tag{2.47}$$

$$\gamma = \tan^{-1}\left(\frac{\rho}{\frac{u}{2D} + \mu}\right). \tag{2.48}$$

2.5 CHAPTER OVERVIEW

Regarding reservoirs and lakes, eutrophication is a worldwide concern mainly caused by excessive loading of nutrients into a waterbody. Previous studies have pointed out residence times as relevant parameter relating directly or indirectly physical, chemical, and biological aspects. However, it is a metric for completely mixed systems, thus showing a scientific gap when considering non-uniform and unsteady systems. Recently, researchers focused on the development of methods for calculating residence time also considering spatial and temporal variability (local metrics). However, few validations and fundamental deduction were conducted to verify if previous associations between bulk residence times and water quality still hold for local residence time concepts. Furthermore, it looks like within eutrophication studies too much attention is given to residence time, probably due to historic reasons, than on other metrics.

In that context, non-dimensional forms of the ADRE and some ideal solutions were presented as they represent a fundamental part of the investigation conducted in this thesis. In theory, the ADRE already ties together the main aspects of hydrodynamics and water quality. This statement has the intrinsic assumption that concentration is the major indicator of water quality. To accomplish this task, a non-empirical, but the deterministic approach has been chosen to derive these metrics from dimensional analysis and the theory of mass transport.

3 METRICS DERIVATION AND ASSESSMENT

This chapter shows the metric derivation and delineates the methods applied in this thesis to verify the link between metrics and water quality aspects. The hypothesis is that parameters other than residence time may also be relevant for water quality issues, especially in systems with spatial and temporal variability.

The term water quality is a wide concept related with the main characteristics of water and its physical, chemical, and biological features. Usually, these characteristics are associated with requirements to maintain a healthy ecosystem and/or to allow the safe use of water by human activities. Often, those requirements are measured trough concentrations of a substance or a set of characteristics building an index (e.g. Water Quality Index).

The thesis objectives were addressed in the following methodological framework and Figure 13 shows a graphical summary of the methods.:

- Finding Potential hydrodynamic parameters related with water quality:
  - Metrics derivation through dimensional analysis;
- Assessment of relationship:
  - Analytical analysis of the relationship of metrics with maximum concentration by inspection of solutions of the 1D ADRE;
  - Conduct a sensitivity analysis to understand the relationship of physicochemical parameters;
  - Qualitatively compare concentration with related non-dimensional numbers;
- Identification of metric defining the dominant hydrodynamic processes:
  - Qualitative compare metrics and classify dominant processes;
- Definition of the key metric and verification
  - Verification of metric through a case study.

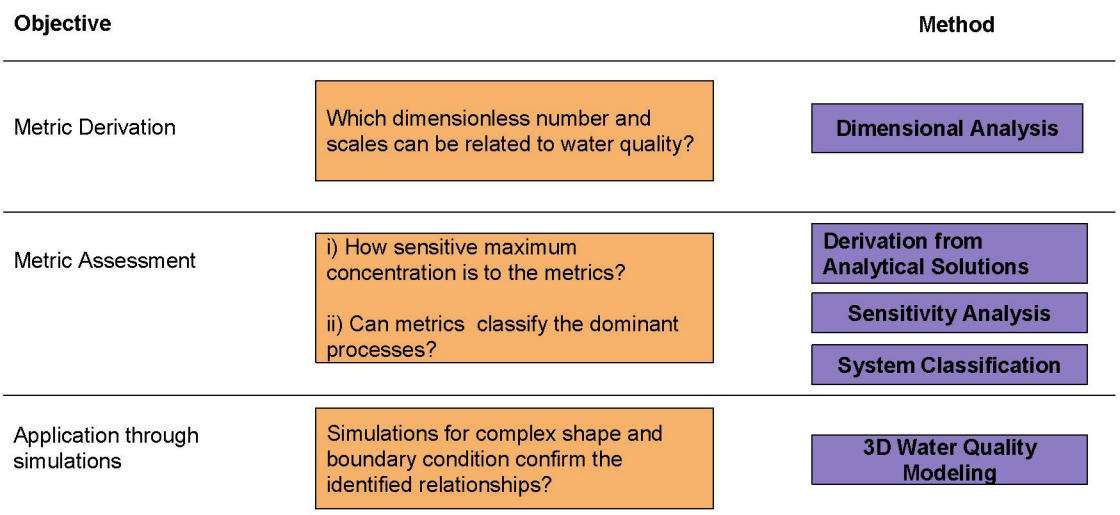

Figure 13 – Graphical summary of the methods which were divided in three parts: Metrics derivation, metric assessment, and an application of a metric in a case study.

3.1 METRICS DERIVATION

The aim of this chapter is to show the derivation of metrics related to hydrodynamics and potential links to water quality. The content covered herein represents the first result of the thesis.

The method used to derive the metrics was dimensional analysis. This approach is commonly used in Fluid Dynamics and usually applied through the well-known Buckingham Π theorem. The aim of this theorem is to find Π sets of non-dimensional numbers related to a phenomenon. A typical application of using non-dimensional numbers are similarity concepts, where the model and real-world systems are considered similar when one or a set of non-dimensional numbers are equal.

Dimensional analysis requires the definition of a dependent variable and a set of independent parameters. The dependent variable represents the phenomenon and the independent parameters are the quantities that may affect the dependent variable. For example, the duration of a plane flight (dependent variable) may be related with the plane velocity and the distance to travel (independent parameters).

Herein, the dependent variable is the maximum concentration divided by the concentration of the loading concentration (C_0) which is already in a non-dimensional form. Velocity, diffusivity, reaction rate, path length traveled since the release (L), and age (t_a) were set as the independent parameters, written in the functional form,

$$\frac{C_{\max}}{C_0} = f(u, D, K, L, t_a) \tag{3.1}$$

The water quality aspect is represented by the maximum concentration and the hydrodynamics by velocity, diffusivity, and reaction rate. Age and path were chosen arbitrarily, however they can represent other time or length scales indistinctly.

The Buckingham Π theorem was modified to derive all forms of non-dimensional scales, but also characteristic time and length scales. This was achieved by modifying the system of equations.

A total of 18 metrics were identified, where nine of them are non-dimensional numbers, five are characteristic length scales, and four are characteristic time scales. Table 3 shows the characteristic scales, five of them do not have a formal name (Π_5, Π_6, Π_7, Π_8, and Π_9).

Through dimensional analysis, a comprehensive list of non-dimensional, length and time scales were derived. Estuary, L1, L2, L3, T1, and T3 can all be calculated locally because they only depend on physical-chemical parameters. Remaining scales depend either on the path or on age or both, thus they are site or time specific. The name estuary number was kept following the definition from Chapra (2008) even tough the work focuses on reservoirs. Surprisingly, this number was not found in other works in this context.

This derivation of metrics was included here with the aim to illustrate the wide range of simple metrics that take into account fundamental hydrodynamic parameters. Those metrics are potentially linked to water quality. Furthermore, dimensional analysis is a traditional method often used in fluid mechanics to proof model and prototype similarity. Thus, the presented metrics may be used to assess similarities of reservoirs, models, and related water quality aspects.

Table 3 – List of characteristic scales and non-dimensional numbers related to the resilience of the system. The id column is the symbol given to the scale.

id	non-dimensional	Name	id	Length Scale	id	Time Scale
Π_1, η	$\frac{KD}{u^2}$	Estuary	L1	u/D	T1	L/u
Π_2, Pe	$\frac{u}{DL}$	Peclet	L2	u/K	T2	L^2/D
Π_3, DaI	$\frac{KL}{u}$	Damköhler I	L3	$\sqrt{D/K}$	T3	D/u^2
$\Pi_4, DaII$	$\frac{L^2K}{D}$	Damköhler II	L4	ut_a	T4	t_a
Π_5	$\frac{ut_a}{L}$	–	L5	Dt_a/L		
Π_6	$\frac{Dt_a}{L^2}$	–				
Π_7	$\frac{D}{U^2t_a}$	–				
Π_8	Kt_a	–				
Π_9	$\frac{C_{\max}}{C_0}$	–				

3.2 METRICS ASSESSMENT

The one-dimensional channel is one the most simple example of a non-uniform system, which provides an excellent environment to test the metrics because the spatial variability occurs only in one direction. Thus, the 1D channel isolates any complexity caused by further dimensions and the effect of spatial variability can be evaluated in a controlled situation.

The assessment is conducted through the inspection of solutions of the ADRE for a 1D channel. Three boundary conditions were evaluated: (i) instantaneous loading, (ii) new continuous loading, and (iii) oscillatory loading. The goal of the assessment is to find a mathematical relationship between a water quality aspect and physicochemical metrics.

From the solutions of the 1D ADRE, the equation to determine a maximum concentration was derived for each boundary condition. Then, the identification of

parameters that define the shape was conducted. These parameters are called shape parameters, for example, the shape parameters of a line are the slope and the intercept. Thus, each parameter has a known influence on the shape of the solution what may be fundamental to understand the relation between a metric and the water quality aspect.

The identification of shape parameters was followed by a sensitivity analysis. The sensitivity analysis was designed to evaluate how the physicochemical variables (velocity, diffusivity, and reaction rate) and the related metrics affect the shape parameters. The changing one-factor-at-time approach was applied. In the first approach, diffusivity, velocity and reaction were changed one-at-a-time keeping the other constant and equal to the median value of the typical range. Table 4 shows the range of values used which were based on typical values for small lakes presented in literature (WÜEST; LORKE, 2003; PEETER A. WUEST, 1996).

Table 4 – Range of values used for sensitivity analysis.

Parameter	Min	Max
Velocity ($m.s^{-1}$)	1e-4	1e-2
Diffusivity ($m^2.s^{-1}$)	1e-5	1
Decay rate (day^{-1})	0.01	0.1
Length (m)	200	3000

Dimensional analysis was chosen to reduce the complexity of the system into few important parameters.

The second method explores the non-dimensional form of the 1D-ADRE. Two aspects were assessed: the relationship with concentration and the relative dominance of hydrodynamic and chemical processes.

Classification of dominant processes

The prevalence of a transport process over the other(s) may vary in time and space in unsteady and non-uniform systems. Furthermore, this prevalence of a process may be useful to better understand the mass transport at certain locations. For example, a fast concentration decay is expected in a region of a system where reactive processes dominate in comparison with regions dominated by advective processes. Thus, the objective of this method is to verify if the parameters can classify regions within a system dominated by advection, diffusion or reaction processes at a given moment.

The significance of advection, diffusion/dispersion, and reaction were classified by comparison of the mass flux rate induced by each process. Then, advection is classified as dominant when $u\frac{\partial c}{\partial x}$ is bigger than $D\frac{\partial^2 C}{\partial x^2}$ and kC, respectively.

3.3 CASE STUDY APPLICATION

Simulations were conducted to assess the scales in a complex system with spatial and temporal variability of water quality and physicochemical parameters. Therefore, a three dimensional hydrodynamic and water quality model of Vossoroca reservoir, a dendritic reservoir, was setup and configured considering a specified loading of nutrients.

Vossoroca reservoir was modeled using measured data as boundary conditions for hydrodynamics thereby producing an unsteady and non-uniform simulation. The substance loadings were determined by water quality field campaigns carried out in 2012 (MANNICH, 2013, p. 108). The concentration at the inlet changes accordingly to the varying discharge. The parameters of the water quality model were: a decayable tracer, orthophosphate, nitrate, ammonium, and algae. The aim of the water quality simulation was not necessarily to specifically reproduce the water quality in the reservoir, but to produce a realistic distribution in time and space of water quality parameters.

Nowadays, there is a plenty of computational fluid dynamics softwares available. Most of the current models may differ in computational time however most of them produce similar results under the same initial and boundary conditions (SYMONDS et al., 2017). The Delft-3D package was chosen for this work, because it is a 3D hydrodynamic model and an open source model. Furthermore, there are more than 1800 publications using this model for a wide range of applications. The source code, examples and the manual with a full description of the model (DELTARES, 2015) are freely available on the internet[1].

3.3.1 Hydrodynamic and Water Quality Model

Delft3D-Flow is the hydrodynamic module of the package which solves the Navier Stokes equations using the shallow water assumptions (hydrostatic assumption). The equations are solved numerically by finite differences in an orthogonal curvilinear grid

[1] <http://oss.deltares.nl/web/delft3d>

(horizontal grid). The model offers two vertical grid-systems: the Cartesian coordinate system (Z-model) and the so-called σ coordinate system (σ-model).

The vertical boundary conditions are (i) vertical velocity is zero at surface and bottom, (ii) quadratic shear stress formulations are used at the surface and the bottom for wind and friction respectively.

The turbulence closure models implemented in Delft3d are the constant coefficient, algebraic eddy viscosity closure model, $k - L$ model, and $k - \epsilon$ model. The eddy viscosities used in the horizontal terms are the sum of the horizontal background eddy viscosity (user defined) and the computed vertical eddy viscosity computed by the turbulence closure model.

The relationship among eddy diffusivity coefficients in the transport equation and eddy viscosity is given by the Schmidt number (S_c), a non-dimensional number, which is the ratio of the eddy viscosity (ν) and eddy diffusivity (D_e). Delft3d-Flow sets $S_c = 0.7$ for the transport of tracer concentrations, $S_c = 1.3$ for transport of turbulent kinetic energy dissipation (ϵ) and $S_c = 1.0$ for the transport of turbulent kinetic energy (κ).

The transport of heat is modeled by the advection-diffusion equation and there are five options for the equations of heat balance at the surface. The ocean model was chosen herein where the net radiation was specified. The effective back radiation and the heat losses due to evaporation and convection are computed by the model. Additionally, free convection of latent and sensible heat is also computed by the model.

Delft3D-FLOW solves the three-dimensional shallow water equations using a time stepping scheme called Alternating Direction Implicit (ADI) to solve equations in time and offering accuracy and stability for the model. In theory the ADI method is unconditionally stable however, in cases with irregular boundaries, this is not always guaranteed.

Under these conditions Deltares (2015) recommends that the Courant number (C_f) must satisfy the criteria:

$$C_f = 2\Delta t \sqrt{gH \left(\frac{1}{\Delta x^2} + \frac{1}{\Delta y^2} \right)} < 4\sqrt{2} \tag{3.2}$$

where Δx and Δy are the horizontal grid sizes and Δt the time step. This is the most critical situation, but for general practical situations a Courant number up to 10 still gives stable and accurate results.

When the horizontal large eddy simulation (HLES) model is used, Reynolds stresses are integrated explicitly leading to an additional stability condition:

$$2\Delta t \nu_H \left(\frac{1}{\Delta x} + \frac{1}{\Delta y} \right) \leq 1 \tag{3.3}$$

Such time step limitations are for σ-grids.

Delft3D-WAQ is the water quality model of the package. The model solves the three-dimensional form of advection-diffusion-reaction equation (2.18) by the finite volume method. Delft3d-WAQ includes a comprehensive set of substances and processes for water quality. There are two models available for eutrophication: DYNAMO and BLOOM. The BLOOM module was used.

The BLOOM module is a multi-species competition model for phytoplankton. The model has been applied and validated worldwide creating a knowledge database with default species characteristics for distinct uses. The model selects the optimum composition based on the net growth rate and the requirements for each resource. Every species has its own growth response to light condition, temperature, available nutrients and stoichiometry composition. Stochiometry variability is modeled through the subdivision of a specie in three types, energy limited, phosphorous limited and nitrogen limited. BLOOM computes the optimal combination of types by linear optimization. Thus, types can convert into each other instantaneously, however species take more time.

The aim of the water quality model was not to produce realistic results but to assess metrics in a complex geometry system subject to environmental conditions varying in time. Thus, a simple eutrophication model was setup with minimal parameters and processes as depicted in Figure 14. This simple eutrophication model considers the growth rate of algae varying in function of nutrients and processes related with nitrogen cycle, nitrification and denitrification. Additionally, the rates are temperature dependent. More detailed about equations and parameters can be found in Smits & Beek (2013), Deltares (2015).

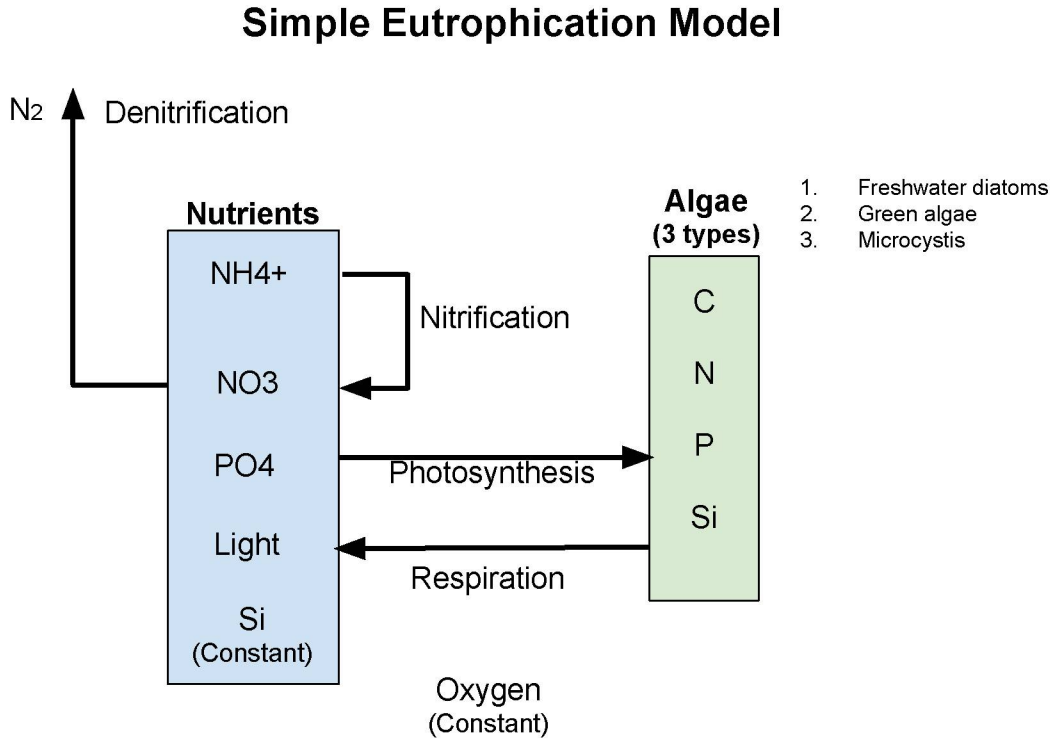

Figure 14 – Diagram of process modeled in Delft3D-WAQ.

3.3.2 Study Area: Vossoroca Reservoir

The Vossoroca Reservoir is located approximately 60 km south-east from Curitiba, within the municipality Tijucas do Sul (Figure 15) and was impounded at 1949. The reservoir has two main inlets, named São João and São Joãozinho rivers respectively. The reservoir is used as storage for energy production by the Chaminé Hydroelectric Power Plant which has 18 MW of installed power.

Vossoroca reservoir is located in a temperate climate, its monthly mean air temperature is between 18°C and 22°C, there is no well defined dry season, with annual accumulated rainfall in between 1400 mm and 1800 mm and annual mean relative humidity in between 80% and 85% (AVIGLIONE et al.,).

The reservoir's surface area is approximately 4.1 km^2 and the reservoir's volume is approximately 35.7 hm^3 both for maximum water elevation condition (814.7 m). The

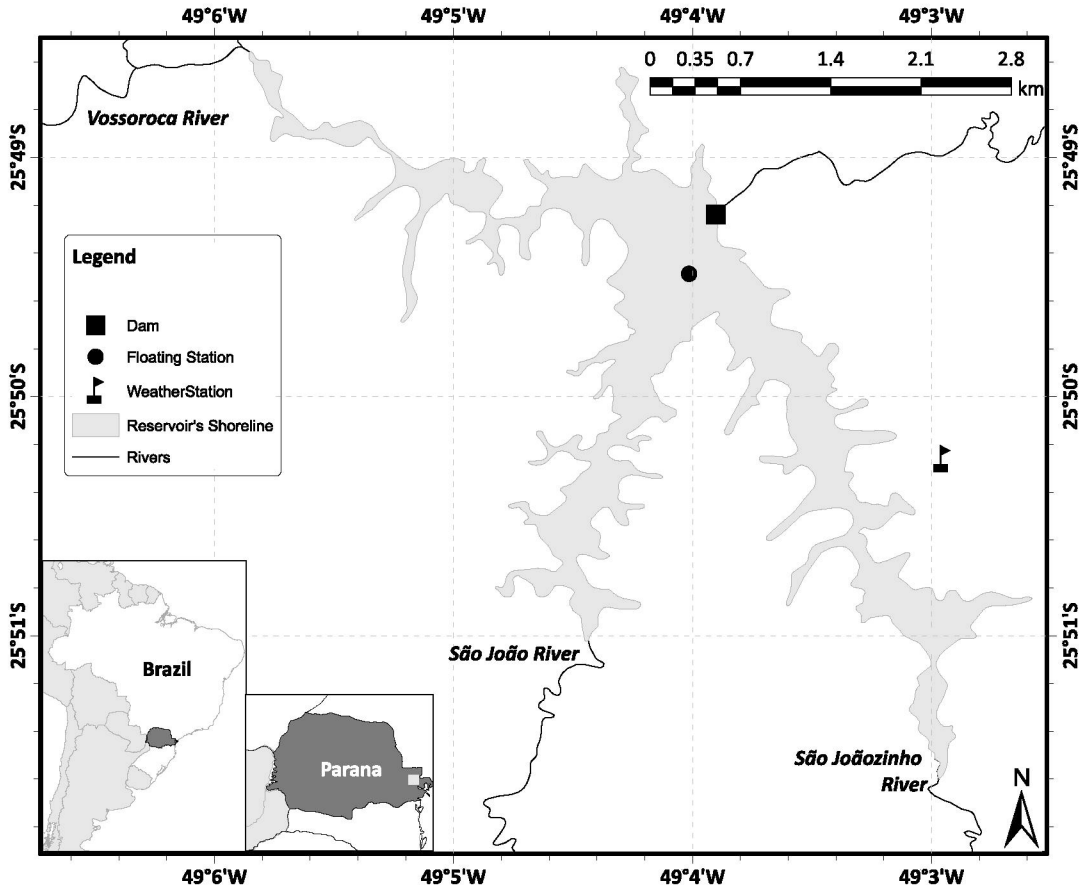

Figure 15 – Map depicting localization of the study area, the weather station, the floating platform, dam, and main tributaries.

mean depth is 8 meters and the maximum depth is 17 m. The annual mean flow is 3.5 m^3/s and the drainage area is 151 km^2. Thus, it is a small reservoir regarding its extension. Further information are presented in Table 5 and hydrometeorological data, bathymetry, and water quality data are presented in Appendix A.

Table 5 – Morphological description of the Vossoroca reservoir and mean discharge and reasidence time.

Parameter	Value
Longitude	-49.07°
Latitude	-25.82°
Maximum water elevation (MWE)	814.7 m
Maximum depth	17 m
Mean depth	8 m
Volume at MWE	35.7 hm^3
Surface area at MWE	4.1 km^2
Drainage area	151 km^2
Mean annual discharge	3.5 m^3/s
Mean residence time	116 days

3.3.3 Model Setup

Hydrodynamic simulations were performed from July 1st, 2012 to October 2nd, 2012. This particular period includes the transition from a vertically mixed to a temperature stratified system. Furthermore, the water level dropped two meters within this period. In that matter, the simulation of Vossoroca reservoir represents a complex case with the spatial and temporal variability. The hydrodynamic model was set up to represent those changes accordingly. Therefore a grid size of 15 m was chosen in the horizontal dimension, and 20 layers (z-grid) equally distributed over the vertical (90 cm) were used over the vertical to capture the stratification processes. Figure 16 shows a zoom of the grid overlay over a reservoir image. The model was forced with temporally varying inflows and outflows, and inflow temperatures, as well as varying atmospheric conditions, such as wind, air temperature, and humidity. The time step chosen was 3 s, to meet numerical stability (Courant number < 10). The first month of the simulation (June) was chosen as the warm-up period for the hydrodynamic simulation. The latitude was -25.82^o, Manning coefficient was 0.02 $m^{-1/3}s$ (uniformely), background eddy viscosity and background eddy diffusivity was set to 0 $m^2.s^{-1}$. The chosen turbulent model was the $\kappa - \epsilon$ model. Free slip condition was considered as lateral wall roughness. The time series of solar radiation were prescribed and Secchi depth of $1.84\ m$ were set using measured data. The initial condition for the water

level was set to -0.42 m for the maximum water level and a uniform temperature of $14.5\ ^oC$.

The hydrodynamic model was coupled with a water quality model, calculating the concentrations of phosphorus and chlorophyll a. Concentrations of the water quality model were kept initially equal to the average mean value obtained from water quality measurements (Appendix A). A warm-up period was not set for water quality model, the aim was to analyze the effect of a loading over a system in equilibrium.

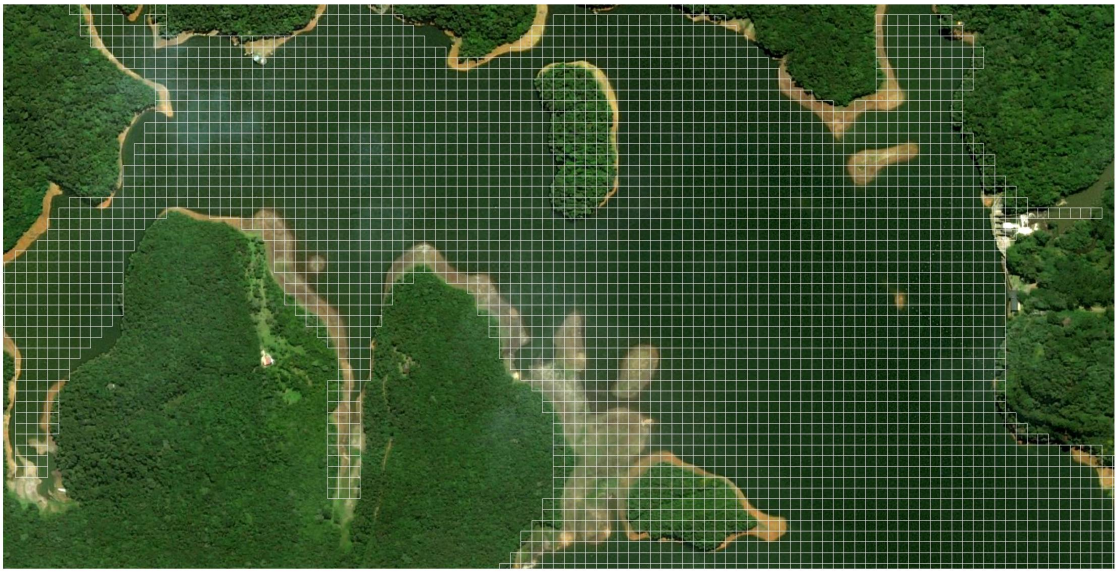

Figure 16 – Illustration of the numerical grid over a satellite image (World Imagery from ArcGIS).

The boundary conditions for temperature and discharge are shown in A. Boundary conditions for water quality were based on a loading proportional to the discharge. The average loading was estimated using water quality measurement done in the inflowing rivers in 2012 as reported by Mannich (2013). The loadings for total dissolved nitrogen and total phosphorus were calculated for each campaign by the multiplication of the daily discharge and the measured concentration. The average of those campaigns resulted in a mean nitrogen loading of 0.591 gN/s and a mean phosphorus loading of 0.0404 gP/s.

Actually, reactive phosphorus (PO_4), nitrate (NO_3), and ammonium (NH_4)

are the nutrients modeled by Deflt3d in the eutrophication module. Reactive phosphorus is a fraction of total phosphorus as well as nitrate and ammonium are a fraction of total dissolved nitrogen. Therefore, the mean fraction of these substance was estimated through measurements. Altogether, the concentration was calculated using

$$C = f\frac{C_{avg}}{Q_{avg}}Q(t) \tag{3.4}$$

where f is the fraction of the substance, C_{avg} is the average concentration, and Q_{avg} is the average discharge. This was an artifact to consider the concentration proportional to the discharge. The estimated fraction for reactive phosphorus was 0.6, for nitrate 0.48 and for ammonium 0.23. The magnitude of the term $\frac{C_{avg}}{Q_{avg}}$ was considered equal to the magnitude of loading to create a critical scenario.

The algorithms used to post-process Delft3d data is available on github (http://github.com/juliowerner/thesis). The algorithms were written in python. The diagram explaining step procedures as some of the input and output parameters are shown in Figure /reffig:Algorithms. Delft3d output data were converted to hdf5, only extracting necessary variables. Then, for each variable a transpose version were append in the same file. This procedure was required because the output matrix is big and there was not available RAM to load the entire matrix to start any algorithm. Thus, the solution were to create two datasets: one for spatial analysis and a second to time series analysis.

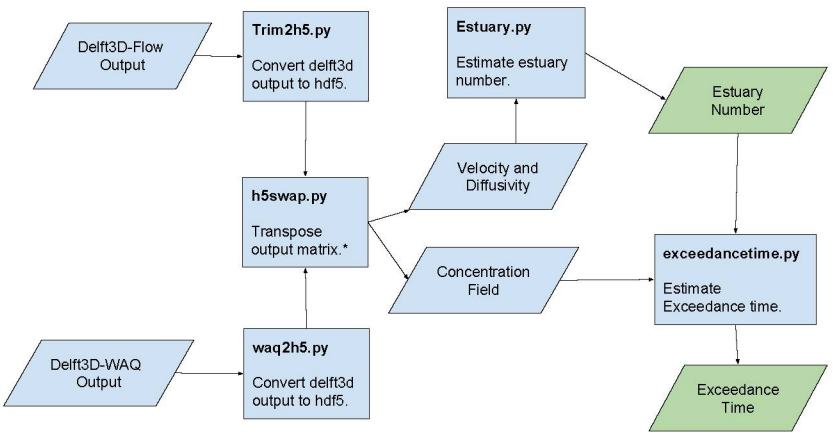

Figure 17 – Diagram showing the main routines to process Delft3d output data. Bold titles indicate the names of python scripts that can be download at github.

4 RESULTS AND DISCUSSION

A modified dimensional analysis was performed to derive metrics potentially linked to water quality. The results were divided in the analytical part and the application part. In the analytical part, a set of metrics was assessed to identify the relationship to water quality. These metrics are tested in a case study in the application part.

The role of the scales, which consistently appeared in both previous methods, was analyzed through a sensitivity analysis. The aim of the sensitivity analysis was to measure the sensitivity of a water quality aspect with respect to the scales. The maximum concentration was the water quality aspect assessed in this study. The result of this part are quantitative relationships on how much scale changes affect maximum concentration, i.e., if a scale indicates 5% of change how much per cent of the maximum concentration is expected to change for this system.

Furthermore, the assessment of the potential metrics indicate the dominant transport processes which were verified comparing the metric with the system classification and providing information on regions being dominated by different processes.

4.1 ANALYTICAL METRIC ASSESSMENT

The first method to assess the potential metrics was the inspection of the ADRE ideal solutions for a 1D channel. The aim was to find a mathematical relationship between maximum concentration and physicochemical metrics from the solution of the 1D ADRE. This approach takes advantage of the well-known shapes of mathematical functions and the fact that the ADRE already combines water quality (concentration) and physicochemical parameters in one equation.

The simplest example of shape parameters is a line which has two shape parameters, the slope, and intercept, where the slope represents the rate of change and the intercept a displacement. Thus, if the solution of the ADRE is a line, the slope indicates the rate of concentration changes.

That is a first step to establish a meaning to the identified metrics. The link

between concentration (water quality) and a metric is given by the ADRE (Section 2.4). Thus, the task is to identify the shape parameters. For the sake of simplicity, just the one-dimensional ADRE was analyzed.

Only maximum concentration was investigated because it indicates the intensity of the impact caused by a mass release into the system. As the system is not uniform, the maximum concentration is a local estimation, i.e, each location through the system has its own maximum concentration. Some of the following equations were derived and represent the maximum local concentrations for instantaneous loading. The detailed derivation can be found in Appendix C.

$$C_{\max}(x) = \frac{M}{\sqrt{4\pi D t_{\max}}} \exp\left(\frac{-(x - u t_{\max})^2}{4 D t_{\max}} - k t_{\max}\right) \tag{4.1}$$

$$t_{\max} = \frac{\sqrt{D^2 + 4KDx^2 + u^2x^2} - D}{u^2 + 4kD} \tag{4.2}$$

a new continuous loading (GENUCHTEN; ALVES, 1982),

$$C_{\max}(x) = C_0(\frac{2u}{u+\zeta}) \underbrace{\exp\left[-\frac{(\zeta - u)x}{2D}\right]}_{\text{Exponential Decay}} \tag{4.3}$$

$$t_{\max} \to \infty \tag{4.4}$$

and an oscillatory loading based on Logan & Zlotnik (1995) solution:

$$C_{\max}(x) = C_0 \frac{u}{\sqrt{(u + \alpha D)^2 + \rho^2 D^2}} \underbrace{\exp(-\alpha x)}_{\text{Exponential Decay}} \tag{4.5}$$

Previous equations can be divided into two terms, one composed by the part outside the exponential and the part inside the exponential, i.e., $C_{max} = A^{-1}\exp(-Bx)$. Figure 18 shows the exponential function for different shape parameters ($B > 0$). The parameter A is an amplitude measure and B is the decay constant. Larger decay constant make concentration decrease faster . Thus, the parameter B indicates the efficiency of the system in reducing the concentration while it is distributed through the system. Hereafter, the shape parameter A is called initial dilution and the shape

parameter B as recovery rate. The naming was based on the fact that when A increases the higher is the initial dilution and B indicates how far concentration diminishes along the system.

For the instantaneous loading, the previous generic equation does not hold because the parameter inside the exponential cannot be reduced to Bx. Therefore, the instantaneous loading is not under consideration in this analysis.

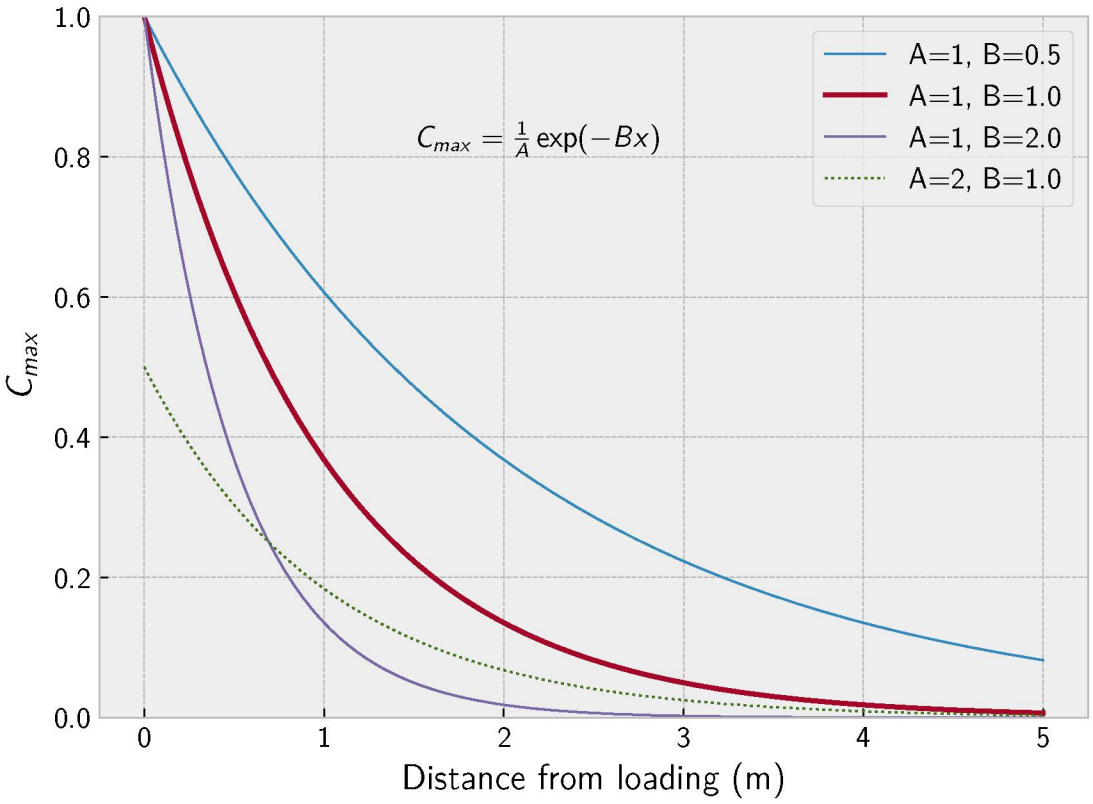

Figure 18 – A set of shape parameters is plotted for the term of a general exponential decay function ($B > 0$). The red solid line is the control line with A and B equal to unity. When B diminishes, the concentration decay is weaker (blue solid line), when B increases the concentration decay is stronger (violet solid line). The shape parameter A indicates the amplitude (grey dashed line).

For oscillatory loading and new continuous loading, the term A does not depend on x, and thus represents the initial dilution, i.e. a dilution factor which holds

exactly at the release point ($x = 0$). The initial dilution factor for the new continuous loading is a non-dimensional number given by

$$A_{ncl} = \frac{u + u\sqrt{1 + 4\eta}}{2u} = \frac{1 + \sqrt{1 + 4\eta}}{2}. \tag{4.6}$$

Initial dilution is proportional to the Estuary Number (η). Therefore, there is no dilution when the estuary number is zero ($A_{ncl} = 1$) and dilution increases according to the rise of the Estuary number.

For the oscillatory loading, the dilution parameter (A_{ol}) is:

$$A_{ol} = \frac{\sqrt{(u - \alpha D)^2 + \rho^2 D^2}}{u} = \left[1 + (\alpha^2 + \rho^2)\frac{D^2}{u^2} - \alpha\frac{2D}{u}\right]^{0.5}. \tag{4.7}$$

In this case, initial dilution includes more terms and the resulting expression is more complex. This is the first time that a frequency is considered, consequently, new terms appeared (α, ρ) which are a function of the angular frequency (ω). The initial dilution factor must converge for new continuous and oscillatory loading ($A_{ncl} = A_{ol}$)for $\omega = 0$ because the oscillating loading is equivalent to a continuous loading when there is no angular velocity.

It can be demonstrated that the dilution factor as function of angular velocity is always decreasing because $\frac{dA_{ol}}{d\omega} \leq 0$. Therefore, a higher frequency of oscillations enhances initial dilution.

The recovery rate for the continuous loading (B_{ncl}) is given by the following equation:

$$B_{ncl} = -\frac{\zeta - u}{2D} = \frac{u}{2D}(1 - \sqrt{1 + 4\eta}), \tag{4.8}$$

showing a dependency between the recovery rate and the estuary number and the length scale L1. Furthermore, the Peclet number is also related to the recovery rate as Bx represents this non-dimensional number weighted by the estuary number. Recovery rate is directly proportional to both the estuary number and L1. Thus, higher estuary numbers consistently induce higher initial dilutions and recovery rates.

For the oscillatory loading, the recovery rate (B_{ol}) is:

$$B_{ol} = -\alpha = \frac{u}{2D} - \mu = \frac{u}{2D}\left\{1 - \sqrt{\frac{1}{2}\left[\sqrt{\frac{16D^2\omega^2}{u^4} + (1 + 4\eta)^2} + (1 + 4\eta)\right]}\right\}, \tag{4.9}$$

which is also a function of estuary number (η) and L1, however the time scale T3 appears with the angular frequency creating a new non-dimensional number ($D\omega/U^2$). It is the first time that this non-dimensional number appears because the frequency of oscillations were not considered in the dimensional analysis.

Figure 19 shows the ratio of A_{ol}/A_{ncl} versus the angular frequency (ω) for some sets of velocities, diffusivities and reaction rates for a typical small lake (Table 4). The logarithm of Estuary number was also estimated for each curve. The shape of the blue curve differs from the other when velocity is small, note that estuary number differs accordingly. It can be observed that oscillatory loadings decrease concentration more efficiently than a constant loading. Furthermore, higher diffusivity coefficients reduce the dilution factors (increasing dilution) indicating that diffusion plays a major role due to mixing induced by larger spatial gradients.

Sensitivity analysis was also conducted to evaluate the recovery rate (Figure 20). Higher recovery rates mean faster reduction of concentration over space. Kumar, Jaiswal & Kumar (2010) had already reported this concentration reduction under oscillating boundary condition when they developed analytical solutions of the 1-D ADRE with variable coefficients. However, the mass loading should be equal in both cases to ensure a fair comparison between constant loading and oscillating loadings.

The estuary number (η) is a common parameter which appeared in all shape parameters of the solutions of 1D-ADRE for continuous and oscillatory loading. Furthermore, this non-dimensional number is direct proportional to shape parameters. Furthermore, the shape parameter suffer expressive changes when velocity, diffusivity or reaction changes the estuary number (η), as can be seen in Figures 19 and 20. Thus, estuary number seems to be a relevant metric which is directly related to the spatial distribution of maximum concentration in a one-dimensional system.

The general behavior of changing diffusivity, velocity and reaction rates cannot be fully understood by the previous sensitivity method, unfortunately, because the one-factor-a-time method contains only a few sets of values. Thus, the insights provided until here are not necessarily valid for all kind of systems. Therefore, subsequent analysis through non-dimensional scales was conducted to reduce the number of plots to be analyzed.

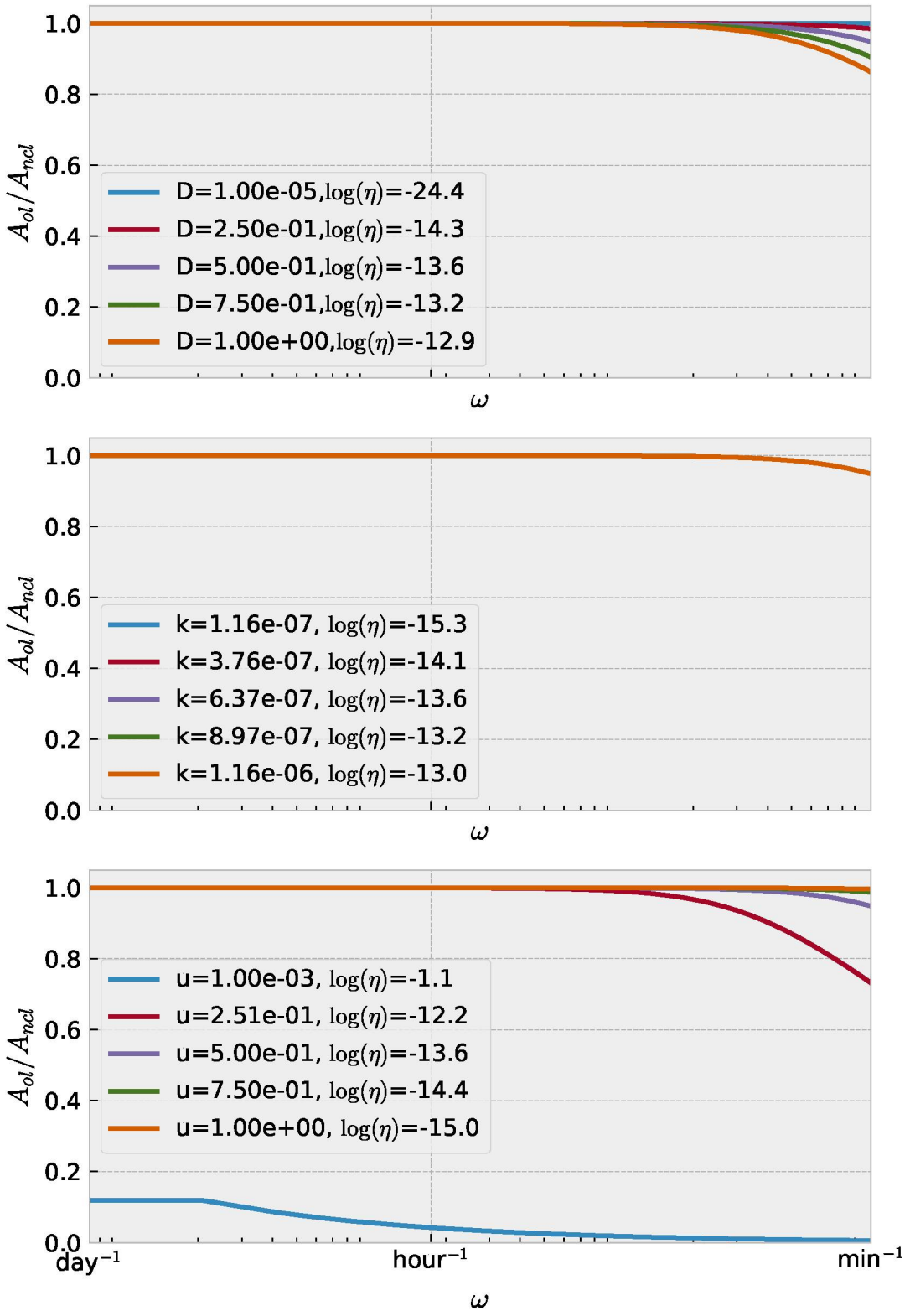

Figure 19 – Results of the sensitivity analysis changing one-factor-at-time to understand the effect or parameter sensitivity on the initial dilution factor. When one factor changes, others are kept unity. Increasing diffusivity increases the initial dilution factor, the opposite relation occurs when changing velocity and reaction rate.

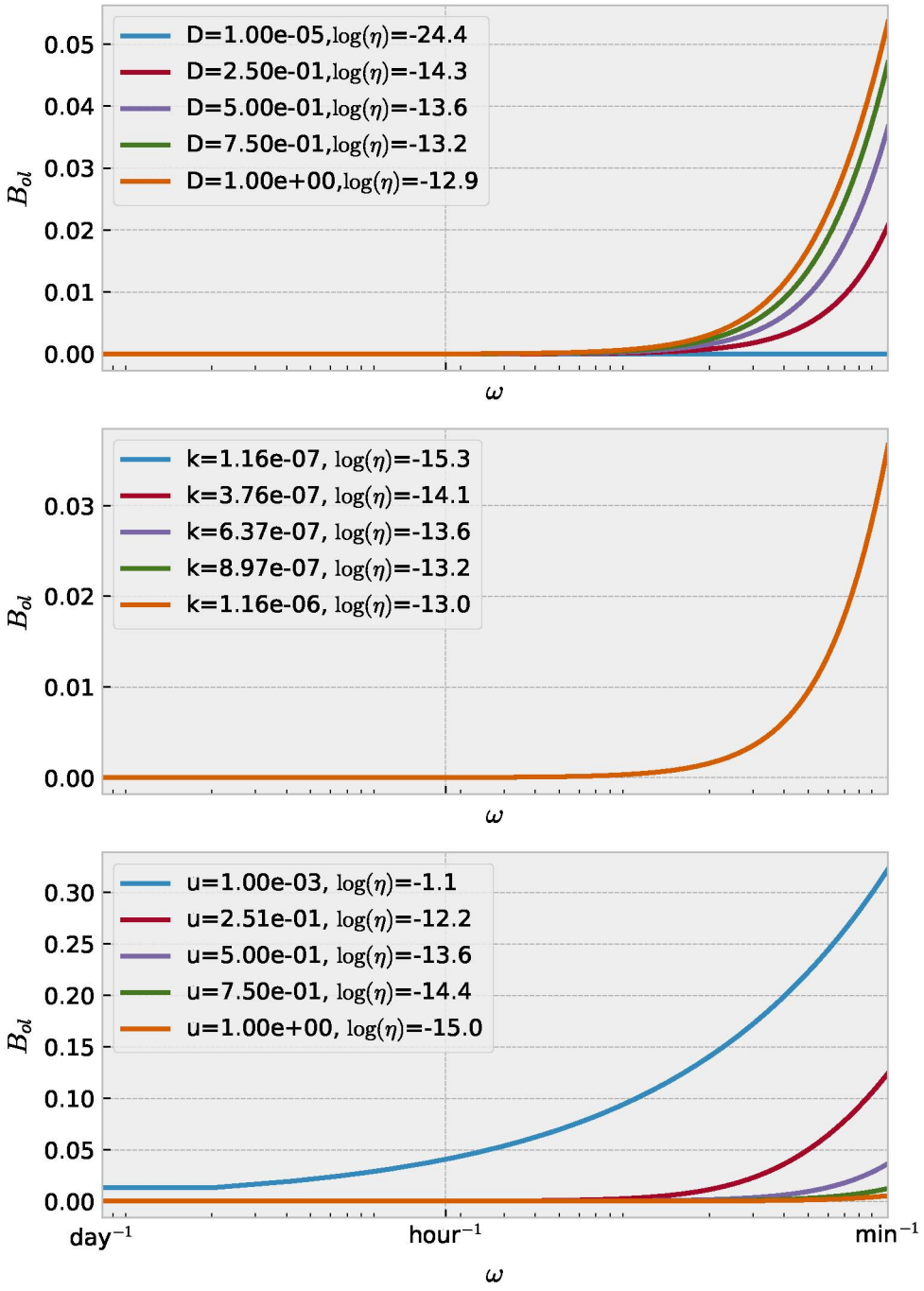

Figure 20 – Results of the sensitivity analysis changing one-factor-at-time to see the effect on recovery rate, when one factor changes other parameters are kept as unity. Increasing diffusivity and velocity increases the recovery factor, the opposite relation occurs when changing reaction rate.

4.1.1 Non-dimensional Numbers & Concentration

The solution of the 1D ADRE for an instantaneous loading and for new constant loadings was used to assess the relation between concentration and the metrics. The objective of this analysis is to associate the concentration distribution with non-dimensional numbers. The advantage of using the non-dimensional form is the reduction of variables to be changed for a sensitivity analysis.

Seven normalized concentration fields (concentration normalized with maximum concentration) were plotted for the estuary numbers (η) varying from 0.01 to 100. The normalized concentrations fields were plotted in a normalized graph with the spatial 1D channel coordinate x being normalized using either Peclet, Damköhler I, and Damköhler II on the horizontal axis versus a normalized time using the reaction rate.

An example of these plots is shown in Figure 21 when the system properties results in an estuary number of 0.1 and Figure 22 when this number results in 10. The surface plot on the upper-left corner of the graph is the concentration distribution throughout the system in the space (x-axis) and time (y-axis). This plot can summarize the spatial and temporal variability in one figure, giving an overall impression of how the system behaves in both dimensions. The plot on the upper-right represents the concentration (y-axis) distribution over the space (x-axis) and the color indicates which transport phenomenon is dominating. The bottom-left plot represents the concentration (y-axis) distribution over the time (x-axis).

The comparison between Figure 21 and Figure 22 shows the concentration distribution stay closes to the source when estuary is greater than one and, when estuary is less than 1, the concentration travels farther distances from the source point. The magnitude of the maximum concentration is also smaller when estuary number is greater than 1.

Figures 23 and 24 show a set of concentration fields for seven estuary numbers in a one-dimensional channel which received an instantaneous loading. The axis of the plot and equations use the non-dimensional form III of the solution (Equation 2.24)). It can be observed that when $t*$ is larger than ≈ 2.3 the non-dimensional concentration is less than 0.1 (horizontal dashed green lines), and this result did not depend on the estuary number.

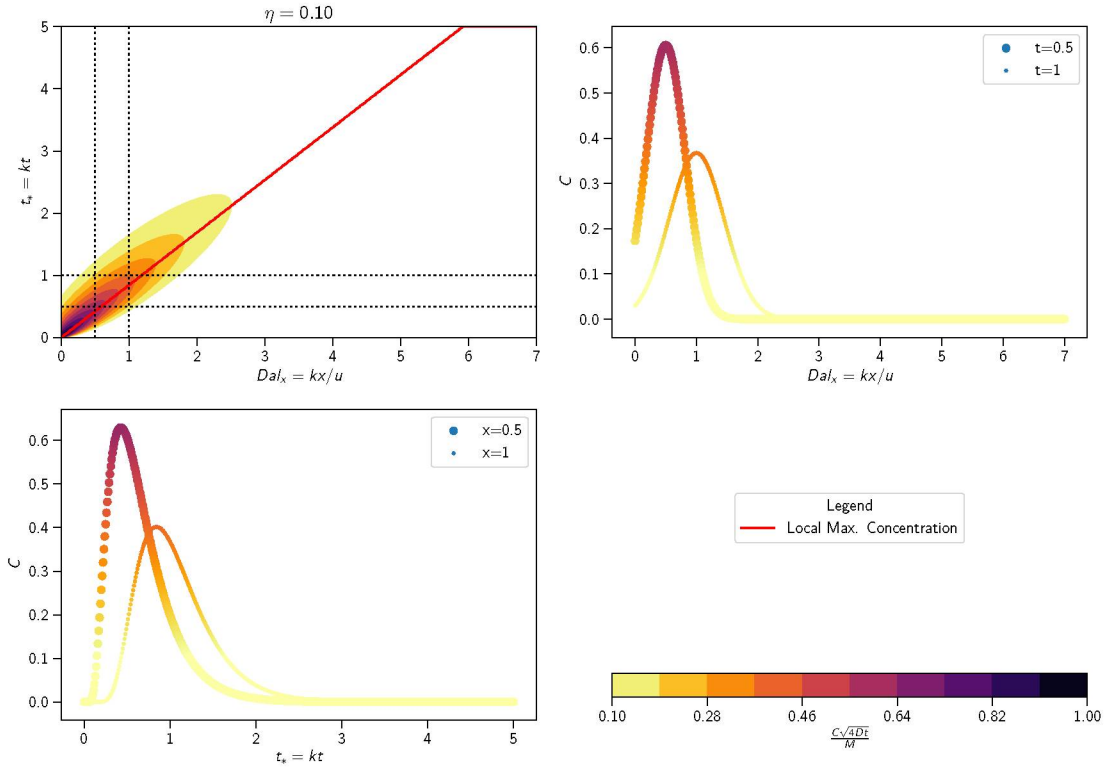

Figure 21 – Concentration distribution in a one dimensional channel where estuary number is equal to 0.1. Upper-left plot is the classification plotted in the space (x-axis) and time (y-axis) plane, the upper-right plot is the concentration evolution distribution over the space for two non-dimensional time, the bottom-left plot is the concentration distribution over the time for two non-dimensional space.

Figure 25 combines Figures 23 and 24 showing that for Estuary numbers larger than 1, Damköhler II indicates how far an instantaneous loading can reach, when Estuary number is lower than 1, Damkhöhler I indicates how far an instantaneous loading can reach. Thus, Damköhler indicates the length where the loading can impact.

The same plot was produced for a continuous loading (Figure 26) and Damkhöler II still delimiting the extension of the plume.

Pattern of the concentration field depends on the estuary number. Furthermore, the estuary number defines the relevance of each scale in the spatial plane. When $\eta > 1$, Da_II is relevant to define a spatial scale and Da_I when $\eta < 1$. Thus, the extent of

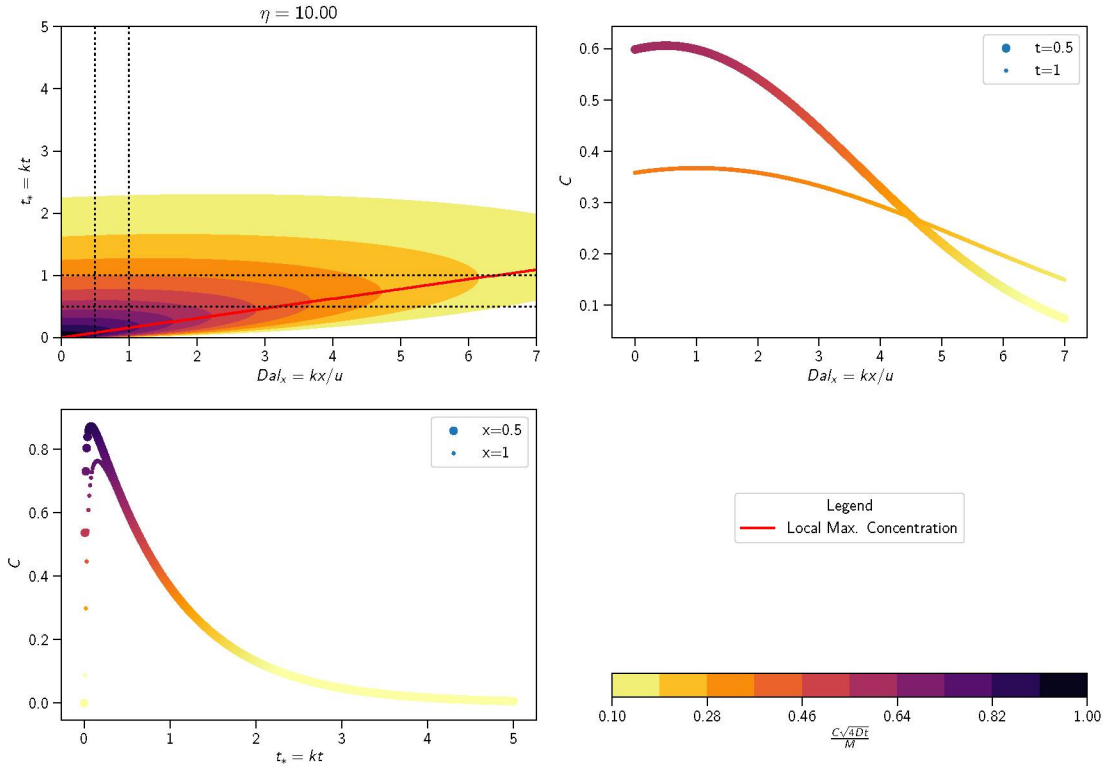

Figure 22 – Concentration distribution in a one dimensional channel where estuary number of 10. Upper-left plot is the classification plotted in the space (x-axis) and time (y-axis) plane, the upper-right plot is the concentration evolution distribution over the space for two non-dimensional time, the bottom-left plot is the concentration distribution over the time for two non-dimensional space.

continuous loading will depend on the estuary number and Damköhler.

Those results can be applied for example when checking the similarity of lakes or to define regions of influence of different river inflows. Let's use a model/prototype as an example. Table 6 shows a characteristic of a prototype channel and 4 models for this prototype using four different similarities: geometric similarity, Damköhler I similarity, Estuary number similarity, and similarity of Estuary number and Damköhler I. To evaluate this system, the time series of concentration at the outlet was analyzed when the system is subject to a continuous loading. This represents that the channel is initially clean and a continuous loading of waste is released at the inlet.

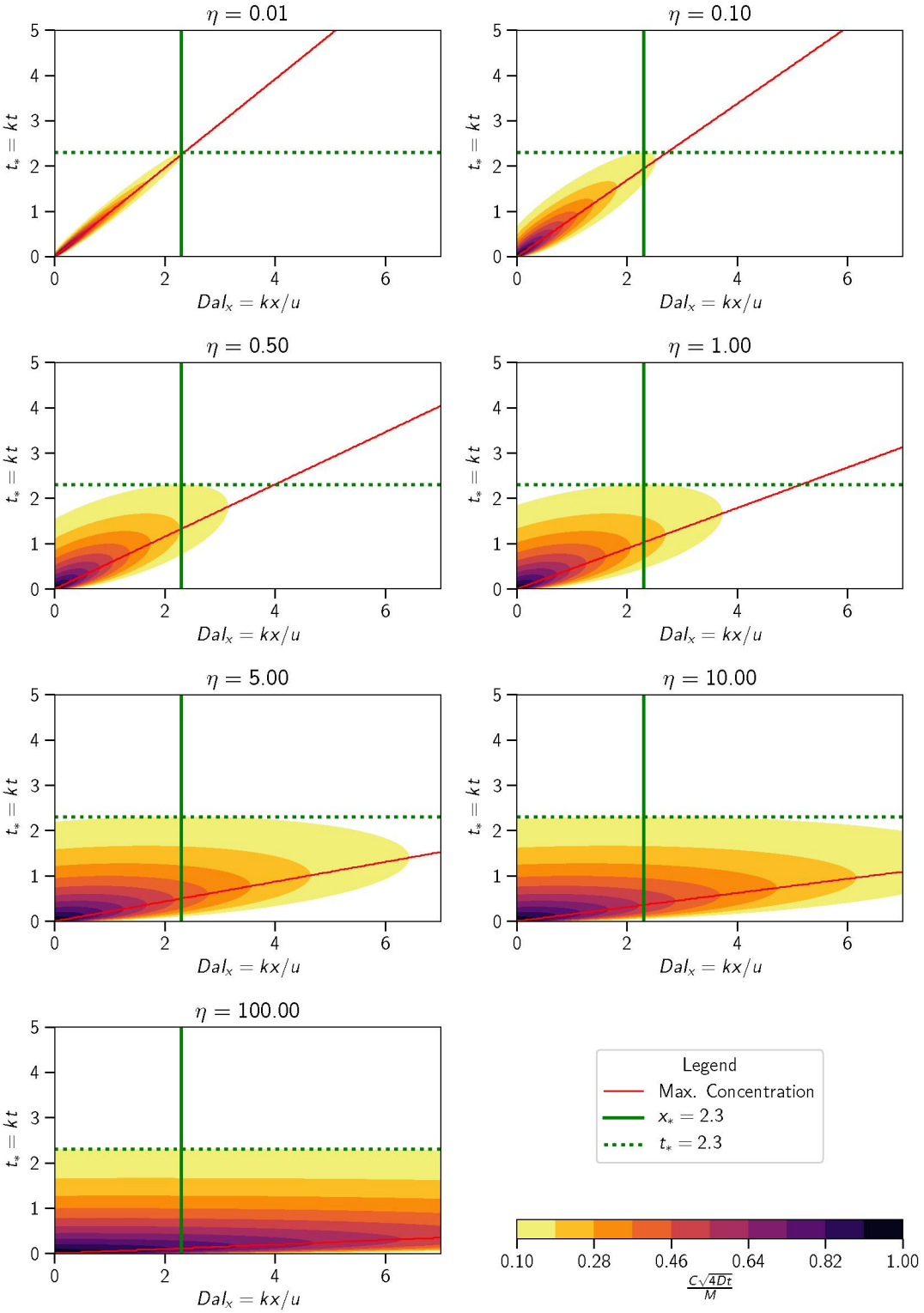

Figure 23 – Typical normalized concentration field for an instantaneous loading using non-dimensional form III. The patterns change according to the estuary number (η).

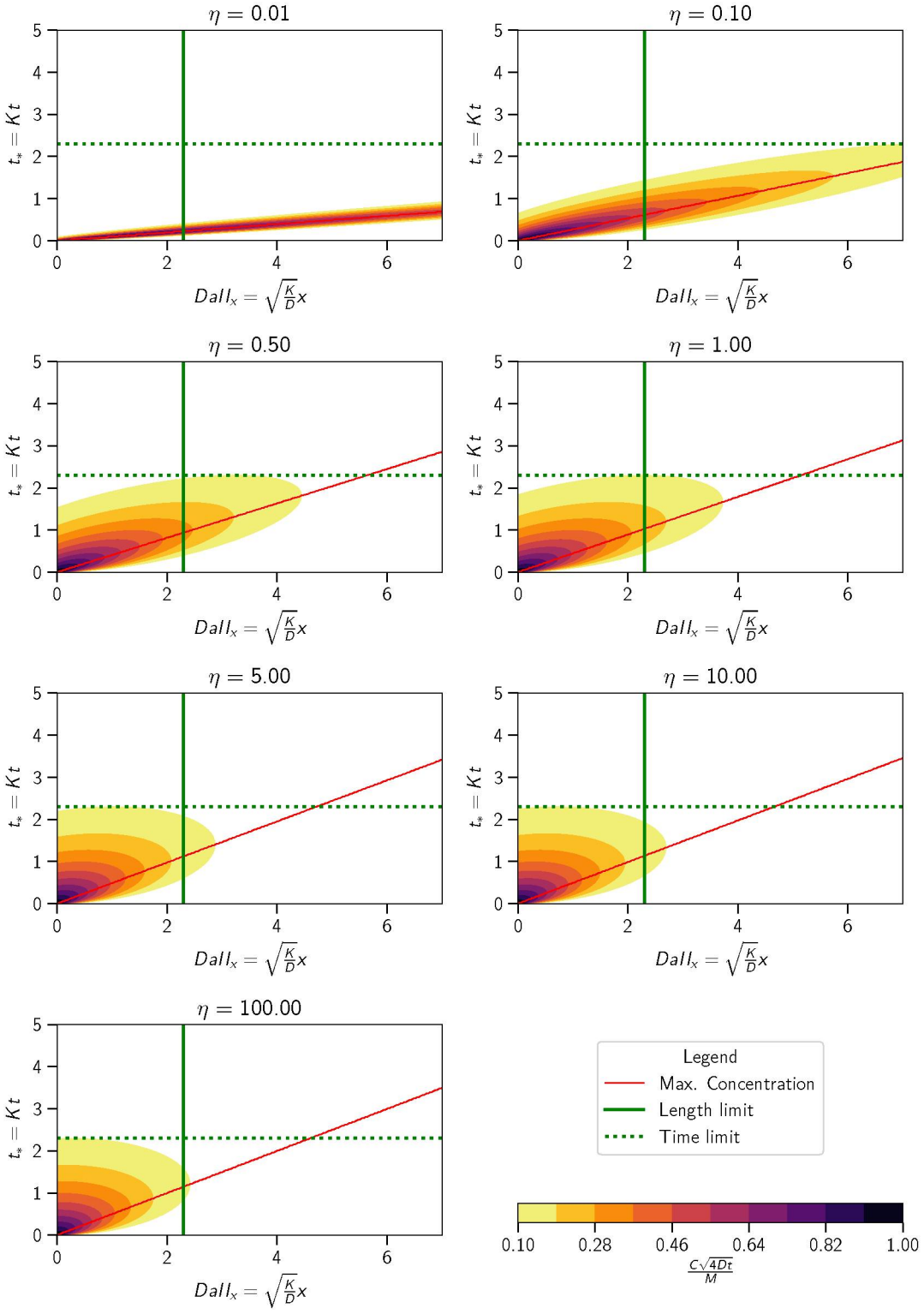

Figure 24 – Typical concentration field for an instantaneous loading using non-dimensional form IV. The pattern change according to the estuary number ((η)).

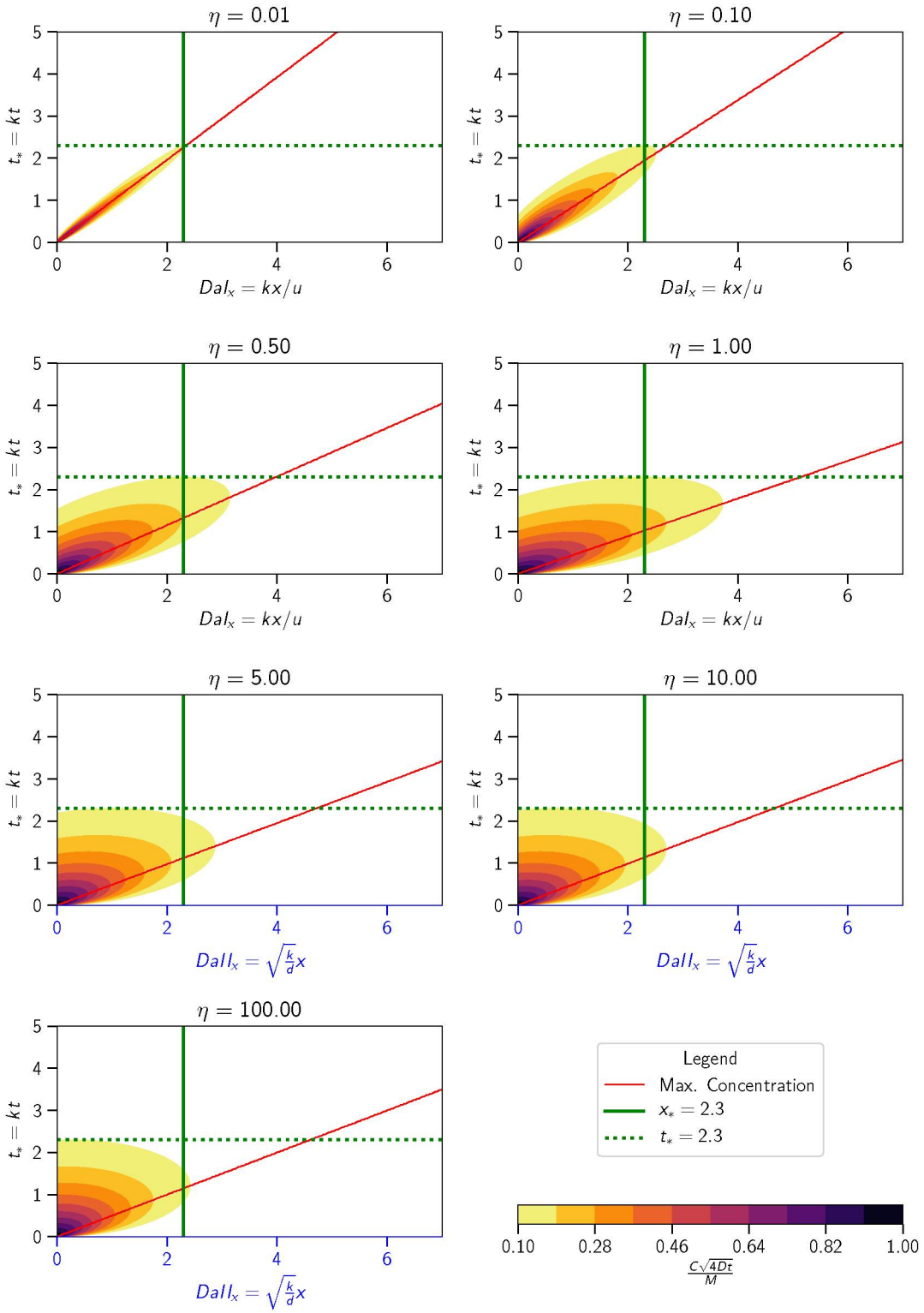

Figure 25 – Typical concentration field for an instantaneous loading using non-dimensional form III and IV. The pattern change according to the estuary number ((η)).

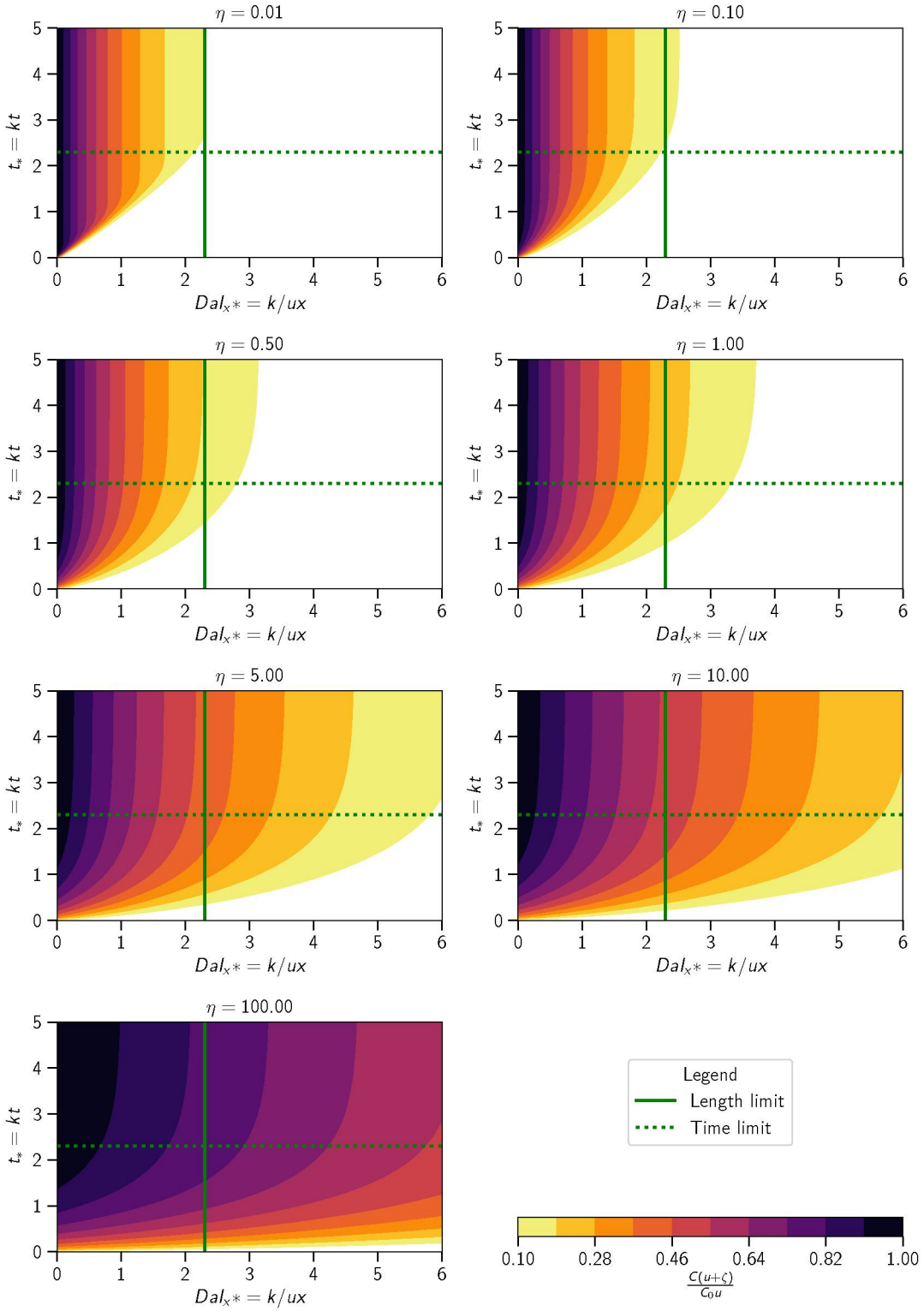

Figure 26 – Typical concentration field for a new continuous loading using non-dimensional form III. The pattern changes according to the estuary number ((η)).

The concentration was estimated through the solutions of 1D-ADRE and the results were plotted in Figure 27. Model was similar to the prototype just when Estuary number and Damköhler I of prototype and model were equals. Thus, Estuary number and Damköhler seems to define the spatio-temporal distribution of a substance in a 1D system.

Table 6 – Morphological and dynamic characteristics for prototype and models tested.

	Prot.	Model1	Scale	Model2	Scale	Model3	Scale	Model4	Scale
Q(m^3/s)	1	0.005	1:200	0.005	1:200	0.005	1:200	0.005	1:200
L(m)	10	1	1:10	5	1:10	1	1:2	5	1:2
W(m)	2	0.2	1:10	2	0.2	1:10	2	0.2	1:10
H(m)	1	0.1	1:10	1	0.1	1:10	1	0.1	1:10
u(m/s)	0.5	0.025	1:20	0.5	0.025	1:20	0.5	0.025	1:20
D(m^2/s)	0.22	0.011	1:20	0.011	1:20	0.055	1:4	0.055	1:4
k(1/hr)	0.05	0.05	1:1	0.05	1:1	0.05	1:1	0.05	1:1

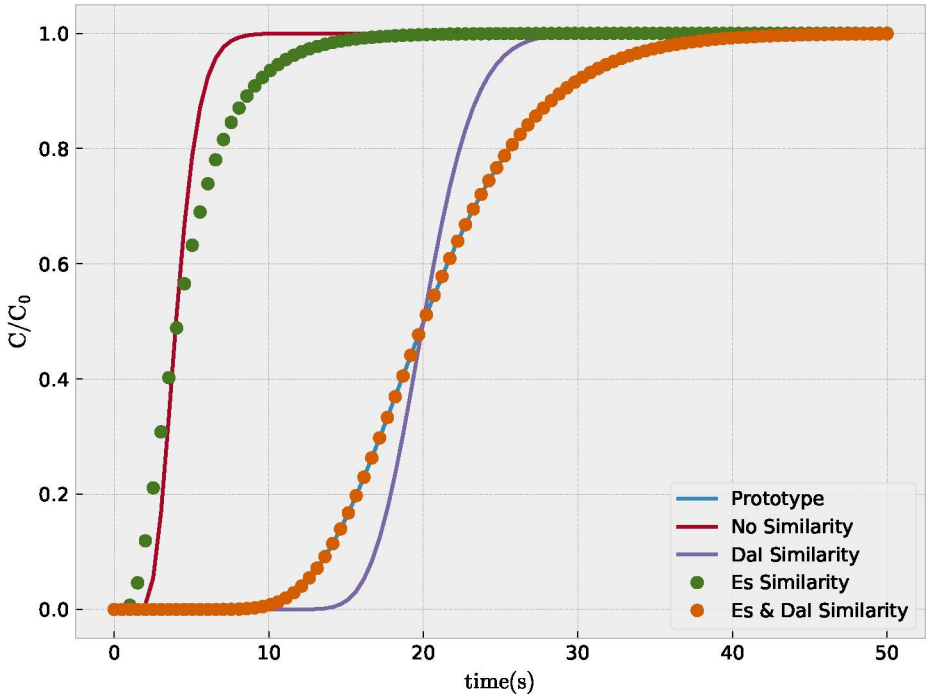

Figure 27 – Concentration time-series at outlet of a prototype and five models with different scales.

4.1.2 Relative Importance of Fluxes - Flux Classification

In this section, the results from the classification of the dominant transport process are presented. The objective of this classification is to compare the relative importance between advective, diffusive or reactive fluxes at a given location and time. A sequence of seven plots varying Estuary number from 0.01 to 100 was produced and combined in one figure. Each plot represents the normalized space-time plane filled with a color representing the regions of the dominant transport processes. A process is relative dominant when its absolute flux is bigger than the others. The difference should be higher than $1e-6$ to be considered relevant. As follows, a qualitative analysis was conducted aiming to find patterns associating metrics and classes.

An example of this classification is shown in Figure 28 for a 1D channel with an estuary number equals to 0.1 and Figure 29 is the classification for a 1D channel with an estuary number of 10. The surface plot on the upper-left corner of the graph is the classification throughout the system in the space (x-axis) and time (y-axis). This plot can summarize the spatial and temporal variability in one figure, giving an overall impression of how system behaves in both dimensions. The plot on the upper-right represents the concentration (y-axis) distribution over the space (x-axis) and the color indicates which transport phenomenon is dominating. The bottom-left plot represents the concentration (y-axis) distribution over the time (x-axis).

Comparison between Figure 28 and Figure 29 shows the concentration distribution stay closes to the source when the estuary is greater than one and, when estuary is less than 1, the concentration can reach places far away the source point. The magnitude of the maximum concentration is also smaller when estuary number is greater than 1. Figure 28 shows the mass fluxes are most of the time and space dominated by advection or reaction when estuary number is less than 1. Figure 29 shows that when estuary number is greater than 1 the mass fluxes are most of the time and space dominated by diffusion or reaction. The rising of the peak is most dominate by advection and the fall by the reaction when estuary is less than 1. When estuary is greater than 1, the rising of the peak is dominated by diffusion.

Figure 30 shows the classification patterns produced for the ADRE solution of the 1D channel subject to an instantaneous loading, and Figure 32 for an oscillatory

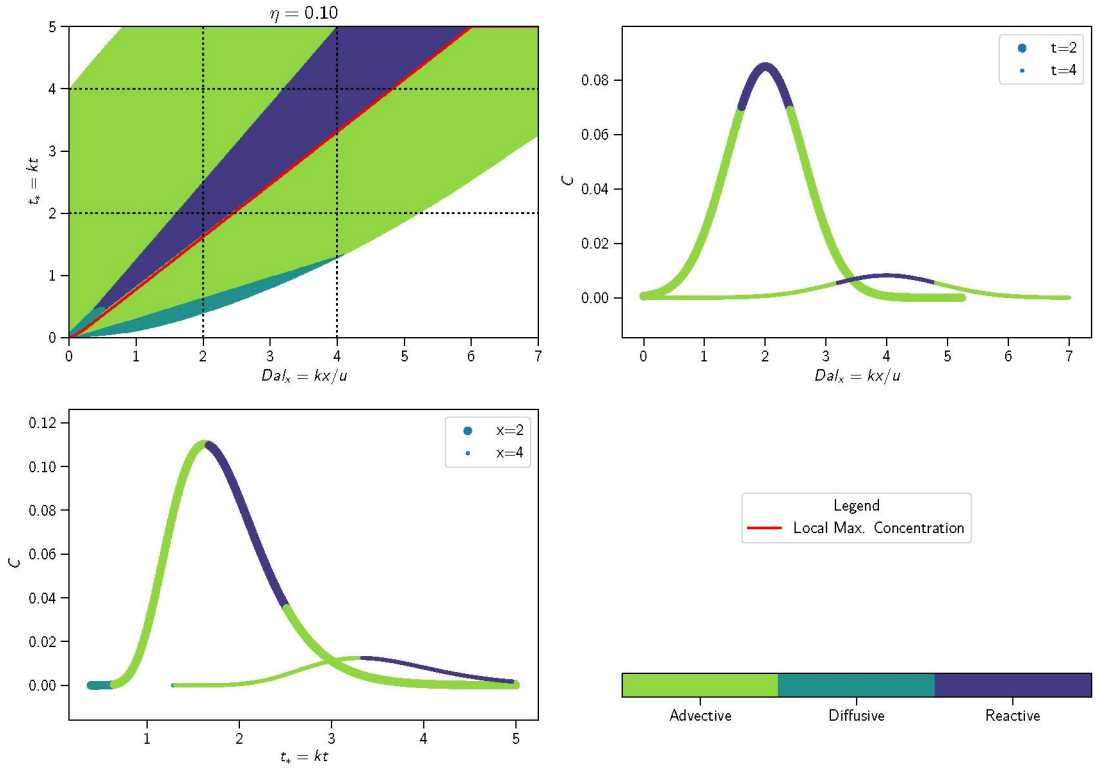

Figure 28 – Classification of the dominant flux for a one dimensional channel where estuary number is equal to 0.1. The upper-left plot is the classification plotted in space (x-axis) and time (y-axis) plane, the upper-right plot is the concentration evolution distribution over the space for two non-dimensional times, the bottom-left plot is the concentration distribution over the time for two non-dimensional space.

loading. Both analysis were conducted using the non-dimensional form III (Equation 2.24) where space is normalized by using the local Damköhler I number. The plots for the other non-dimensional forms were produced but not included here because they are very similar to those presented here. The non-dimensional form V where the spatial dimension is normalized by the local Peclet number is shown in Figure 31 because the Peclet number represents the relationship between diffusion and advection.

The maximum concentrations (shown as red lines in the figures) occur in regions where either diffusion (dark green) or reaction (violet) processes dominate or is in the transition to dominate. This happens for the cases of instantaneous loading and

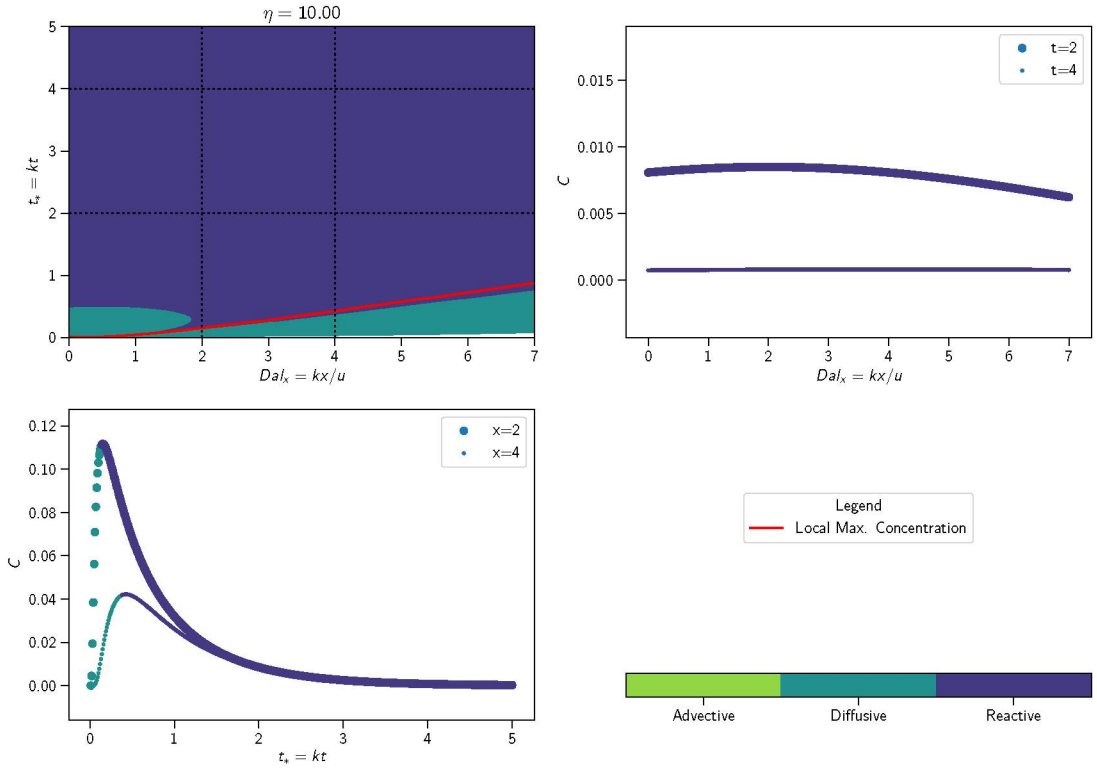

Figure 29 – Classification of the dominant flux for a one dimensional channel where estuary number of 10. Upper-left plot is the classification plotted in the space (x-axis) and time (y-axis) plane, the upper-right plot is the concentration evolution distribution over the space for two non-dimensional time, the bottom-left plot is the concentration distribution over the time for two non-dimensional space.

oscillatory loading (Figures 30 and 32).

It seems that larger advection dominated areas appeared in the plots with estuary numbers less than 1. And larger reaction and diffusion dominated areas for Estuary numbers greater than 1. Thus, estuary number can be used to classify the system according to the dominant transport process.

The Peclet number is the non-dimensional number which relates diffusive and advection rates (CHAPRA, 2008, p.163). Nevertheless, according to the results presented in Figure 31, regions with same Peclet numbers can be dominated by all, advection, diffusion or reaction.

Diffusive processes are negligible when the system is uniform because net diffusive fluxes depend on spatial gradients. As a consequence, previous classifications based on residence time could only state if a system presents a fast or a slow flushing characteristic. Therefore, the definition of dominant processes in a system with spatial variability has to address also the fact of diffusion and reaction. In that regard, a metric indicating which processes are dominating at a given time and location can be useful to produce new insights about the system. For example, if a system is dominated by advection most part of constituents will follow the streamlines. Furthermore, this classification could be an extension of the current lentic/lotic classification which considers also the influence of diffusive and reactive processes.

The estuary number has two advantages over the Peclet number: (i) it does not require a length scale and (ii) it takes into account the reaction process. Because of those advantages, the further focus is given to the Estuary number in the following analyses.

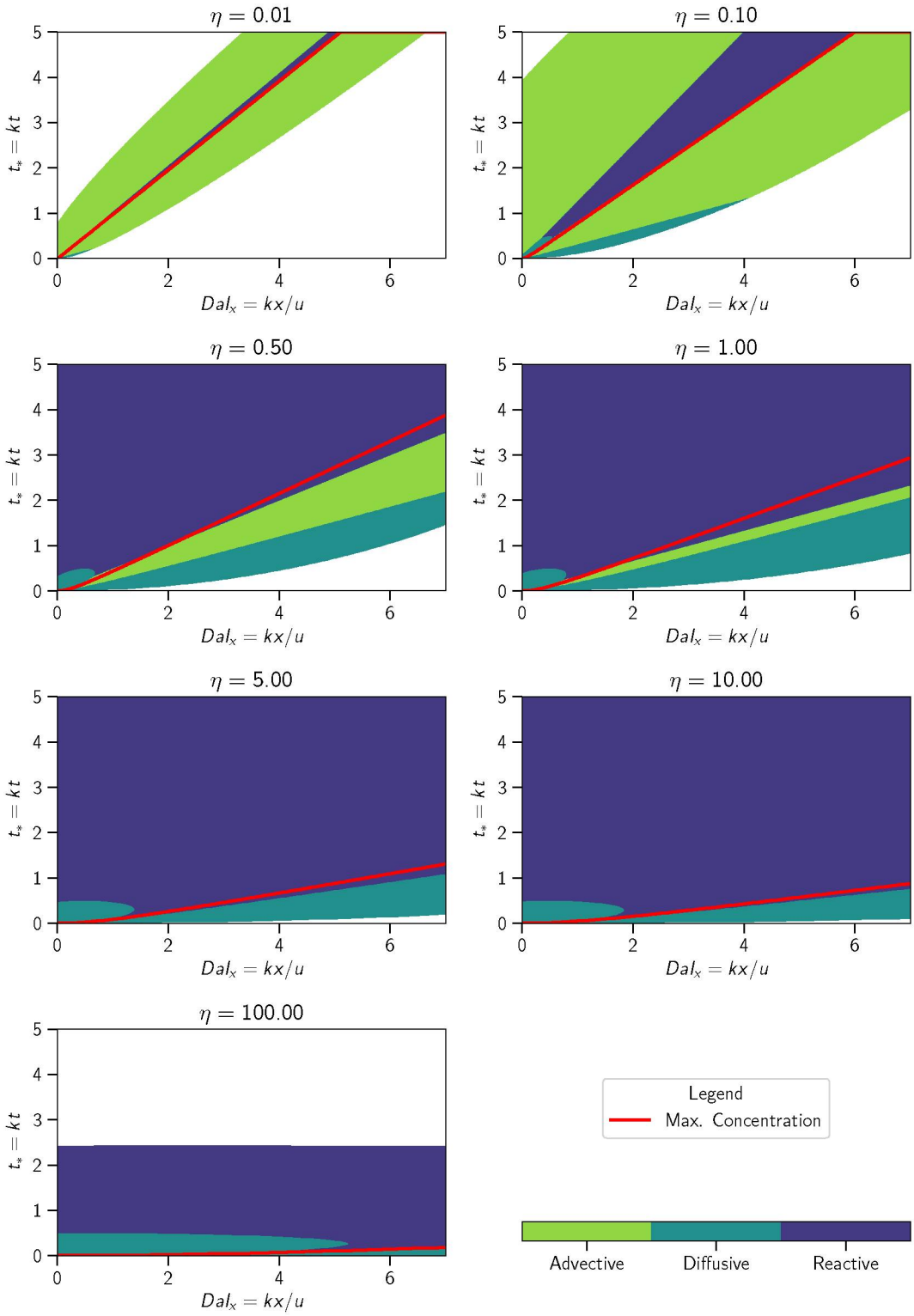

Figure 30 – Relevance of advective, diffusive, and reactive terms of the ADRE for instantaneous loading where the x-axis is normalized using the local Damköhler I number. Each plot presents an Estuary numbers (η) ranging from 0.01 to 100.

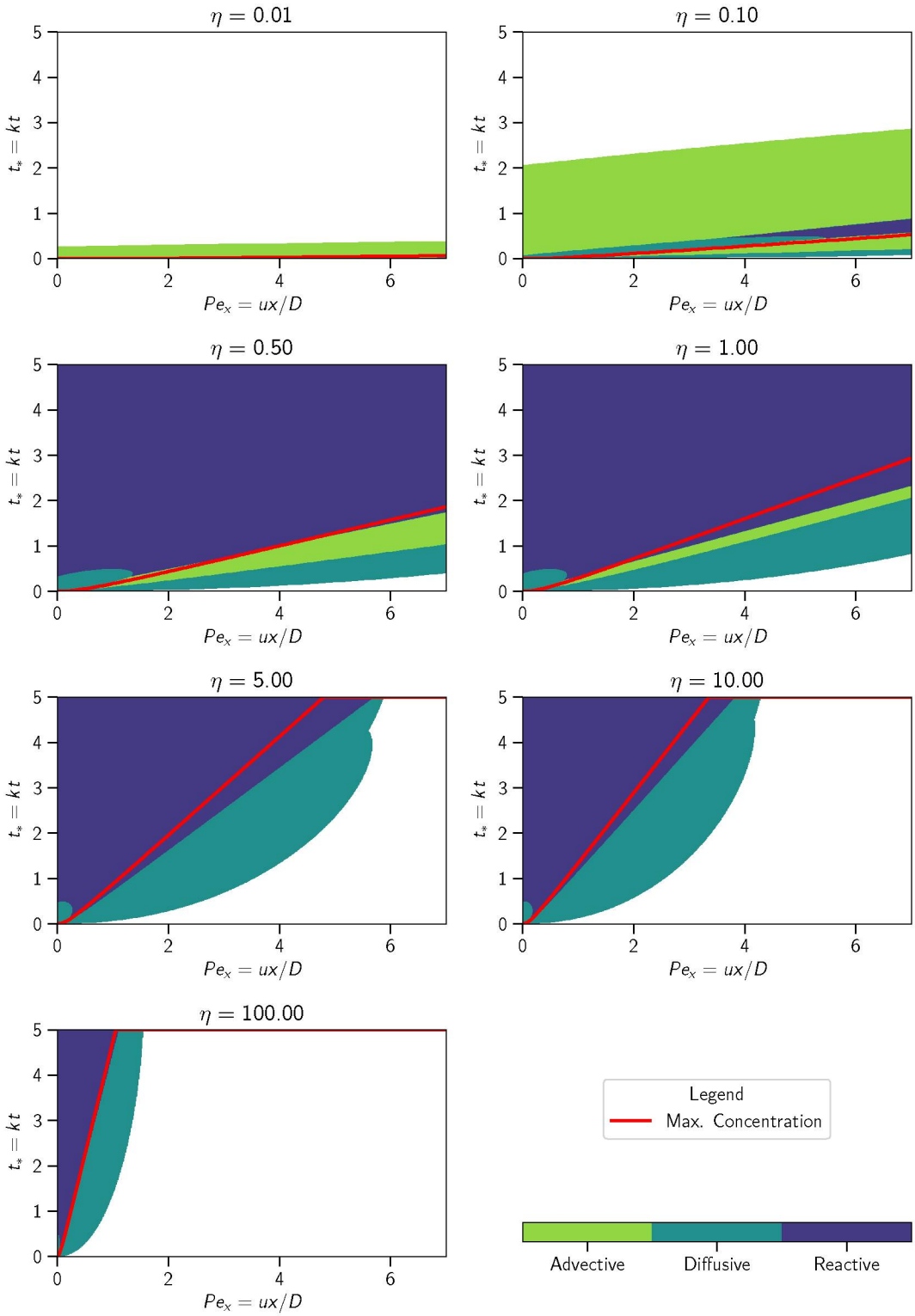

Figure 31 – Relevance of advective, diffusive, and reactive terms of the ADRE for instantaneous loading where the x-axis is normalized using the local Peclet number. Each plot presents an Estuary numbers (η) ranging from 0.01 to 100.

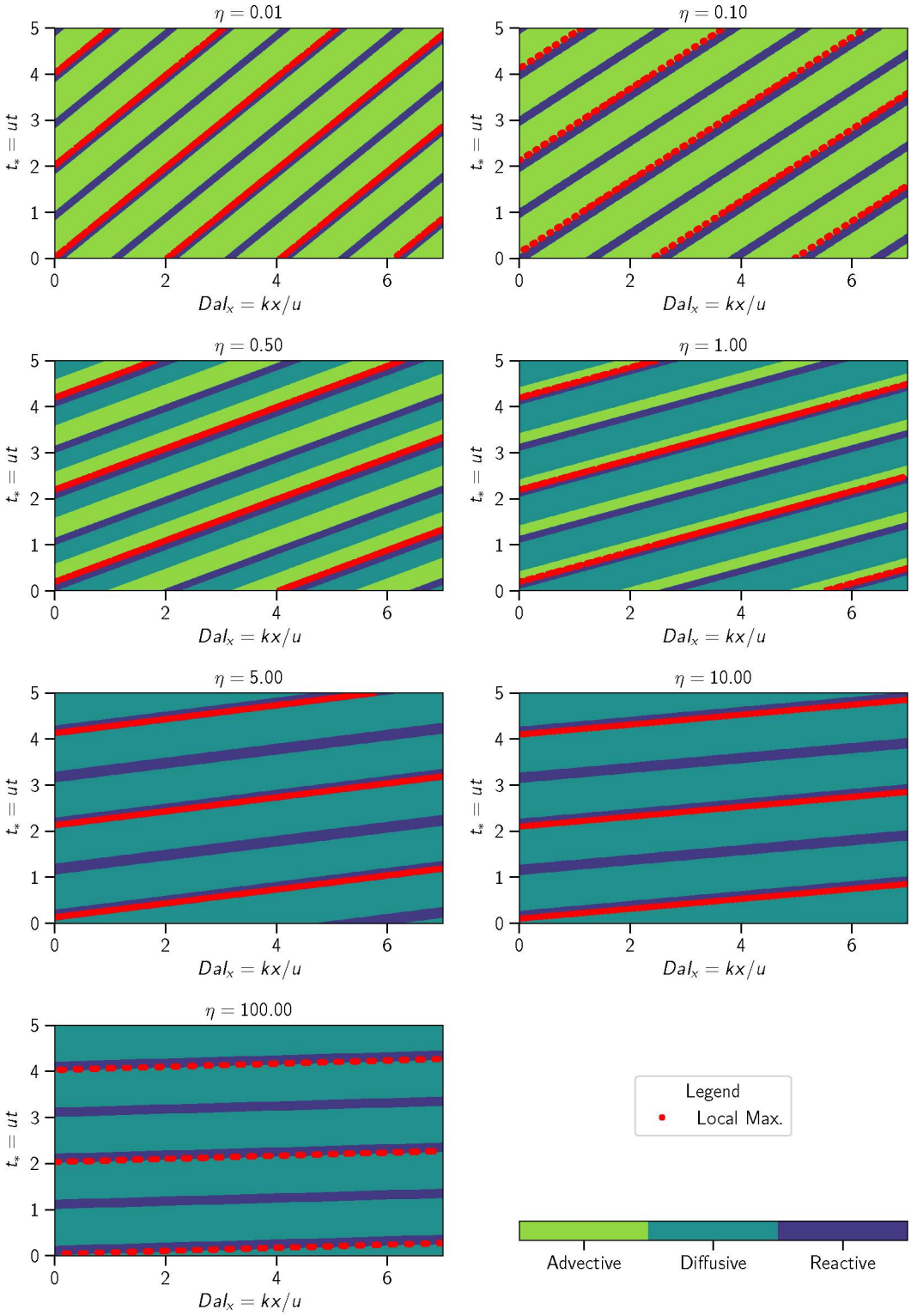

Figure 32 – Relevance of advective, diffusive, and reactive terms of the ADRE for oscillatory loading plotted for seven Estuary numbers (eta) ranging from 0.01 to 100. Red dots indicates the local maximum.

4.1.3 Summary of Analytical Results

- A total of 18 potential metrics were identified;
- The link between some metrics and the maximum concentration was illustrated through manipulation of analytical solutions of the 1D-ADRE;
- Initial dilution factors are increasing with increasing frequency of oscillating loadings. The effect is maximized when diffusion increases;
- The maximum concentration in ideal solutions is linked to the Estuary number. Either initial dilution or the recovery rate are functions of the Estuary number;
- Damkhöhler numbers indicate the length influenced by a loading, depending on the Estuary number;
- The non-dimensional scale Π_8 2.3 represents the maximum time extent, where concentration is reduced to 10% of the global maximum concentration;
- The classification of the dominant processes based on the fluxes was performed for ideal solutions of the 1D-ADRE. This classification was compared with other methods based on typical non-dimensional numbers used to perform this classification. Most of the non-dimensional numbers could not predict this classification. However, estuary number indicates which transport processes most dominates mass transfer;
- The maximum concentration occurs when diffusion or reaction dominates the system.

It can be concluded that the calibration of diffusivity coefficients and reaction rates is more relevant than for velocities when the aim is the prediction of maximum concentrations. Furthermore, in advection-dominated systems one may produce good predictions for mean concentrations but less precise predictions for maximum concentrations as illustrated in Figures 28 and 29.

4.2 CASE STUDY: 3D FLOW AND WATER QUALITY MODELING FOR VOSSOROCA RESERVOIR

The hydrodynamic model was calibrated based on temperature data from a thermistor chain deployed at the deeper part of the reservoir (MANNICH, 2013; POLLI et al., 2017). The background eddy viscosity and diffusivity were manually changed until the root mean square error between measured and the modeled temperature was less than 1^oC (the sensor uncertainty). At the end of the calibration, the model had a good agreement with the data at the floating platform ($RMS_{error} = 0.6^oC$). The comparison between measured and simulated temperature is shown in Figure 33. Higher differences ($\pm 2^oC$) were observed in the top layer during the stratified period but the overall differences are in between 1^oC.

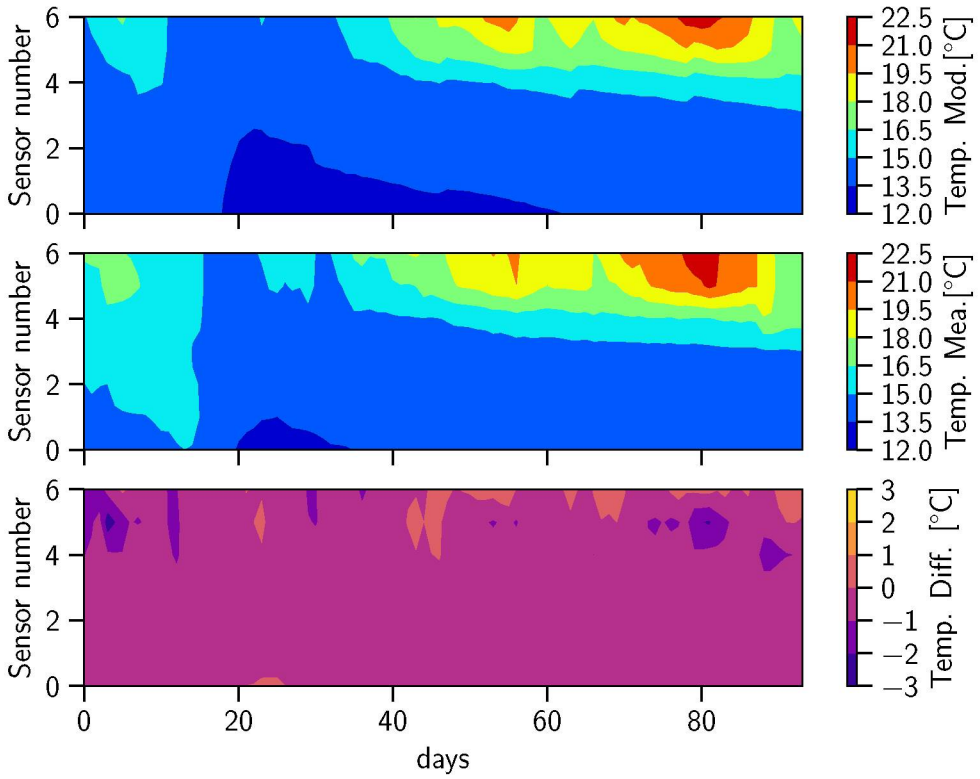

Figure 33 – Temporal evolution of vertical temperature variations at the floating platform. Top: modeled; middle: measured; down: difference between modeled and measured temperature.

4.2.1 System Assessment

The bulk residence time is often used to determine the trophic level of a reservoir for example through the Vollenweider model. Time averaged values of discharge, phosphorus loading and volume are typically used to obtain this estimations. On the other side, the bulk residence time can be estimated for specific time intervals too. Figure 34 shows daily estimation of residence time for Vossoroca reservoir from beginning of 2003 until end of 2015 using measured data and the Vollenweider plot. On average, Vossoroca's residence time is about 116 days (blue line in Figure 34), however daily estimations reveal high temporal variability (3 days – 5 years). Residence time thresholds estimated through Vollenweider (1975) and Salas, Martino et al. (1990) are represented in Figure 34 by a red solid line and by a dashed red line respectively. Reservoirs with longer residence times (above the limits) are considered to be eutrophic. According to Vollenweider model Vossoroca on average is a eutrophic reservoir and the opposite according to Salas model. The green points in the same Figure represent situations where the measurements of either total phosphorus concentration within the reservoir were higher than $48\ mg/m^3$ or chlorophyll concentration higher than $20\ mg/m^3$. These concentration limits are established by Carlson (1977) for eutrophic systems. The water quality data was obtained by the environmental protection agency of the state of Paraná (IAP (2004) and IAP (2017)). The higher phosphorus and chlorophyll concentrations in 2004 and 2006 agree with longer residence times and stronger residence time variations, however, in 2010 the reservoir faced high concentrations with short residence times.

These results indicate that trophic state estimations based on residence time alone may give contradicting results, and not necessarily show agreement with observations. For that reason further metrics were established and tested in this thesis, as follows.

The water quality simulation for Vossoroca reservoir was conducted from July, 1st of 2012 until October 2nd. Two phenomena occurred within this period, the transition from unstratified to stratified situation and an intense rainfall happened at the beginning of July. Water quality simulations were chosen to test the metrics, as they provide results in high temporal and spatial resolution, and once calibrated, may represent the modeled environment in a sufficiently realistic manner to apply the metric tests. The simulation period containing the stratification process on one hand, and

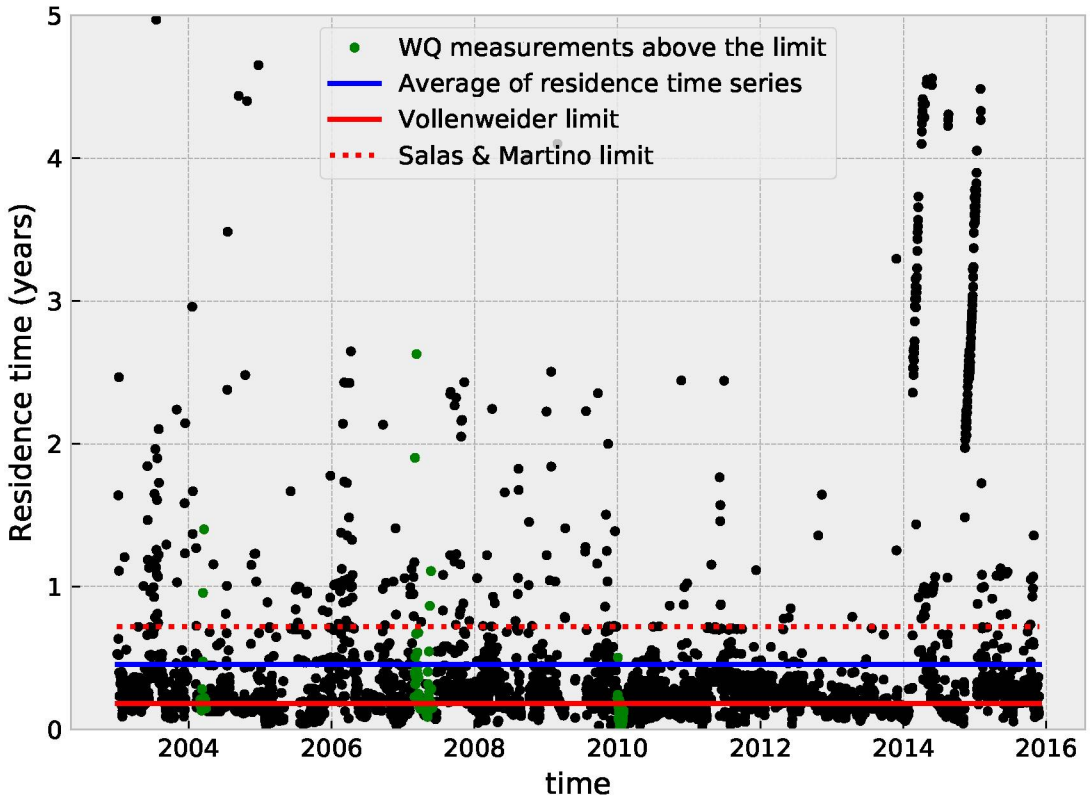

Figure 34 – Seasonality of bulk residence time. The blue line is the average residence time throughout the period. The red lines represent two threshold values: the solid line is the threshold proposed by Vollenweider and the dashed line is the one proposed by Salas & Martino for tropical lakes and reservoirs. The green points indicate months where chlorophyll or total phosphorou concentrations in the reservoir were then concentration limits defined by Carlson (1977) for eutrophic systems.

intense rainfall (high inflow) on the other hand is expected to provide good testing conditions for the new metrics in a challenging environment.

Three specific times were chosen to present and analyze the results related to the temporal variability. Table 7 summarizes the date and time and some drivers, such as wind condition, season and stratification intensity, which occurred during those moments.

The spatial variability is assessed using maps in the horizontal plane showing

properties in the surface and bed layer. In addition maps are plotted for a vertical plane along a longitudinal section. The longitudinal section begins at the main inlet and ends at the outlet as depicted in Figure 35.

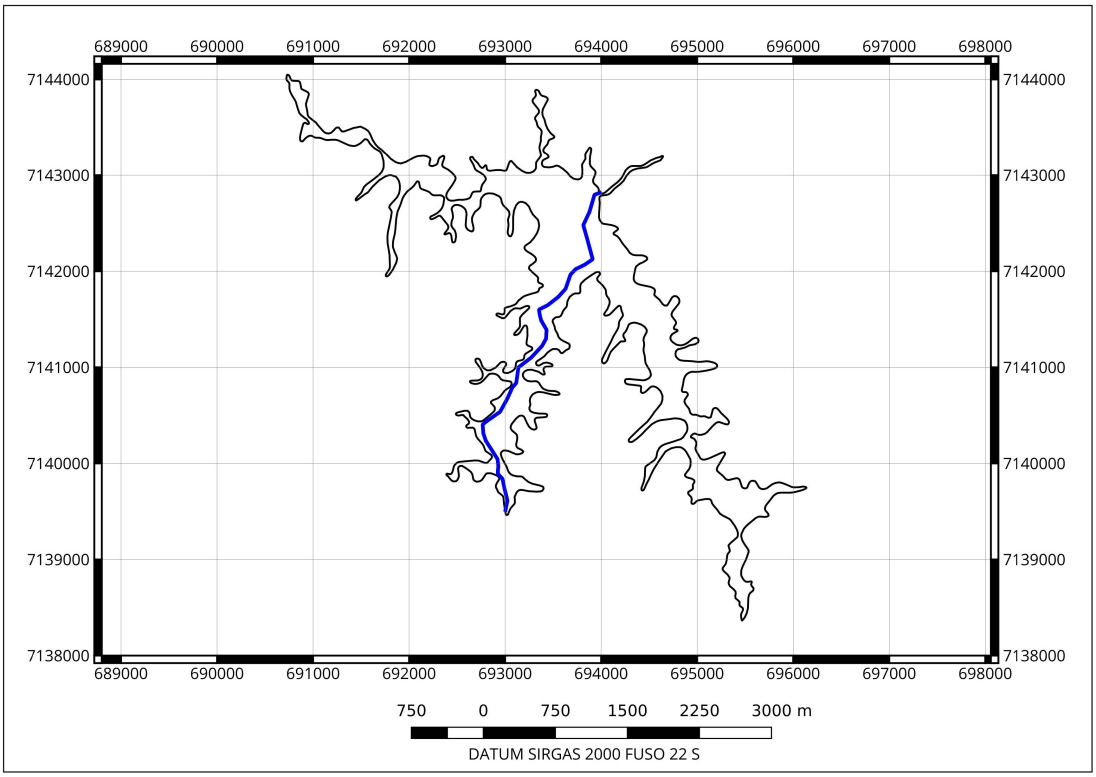

Figure 35 – Location of longitudinal section.

Table 7 – Forcing overview at three times chosen for visualization and analysis. The moments covered different situations with strong and mild winds and varying thermal stratification intensities.

id	Date	Wind	Season	Stratification
t1	2012/07/20	Strong	Winter	No
t2	2012/08/11	Strong	Transition	Weak
t3	2012/09/22	Mild	Spring	Strong

4.2.2 Assessment of effects of Temperature and Stratification

In this section, an overview of the thermal behavior of the reservoir is presented. First, the spatial variability is explored comparing temperature fields of the surface and the bottom.

During winter, there are small spatial variations of temperature over the horizontal and the vertical, as shown in Figures 36 and 37, respectively. The major differences can be observed close to the inlets where cold water enters from the rivers. During spring and winter, the temperature differences between surface and bottom start to increase (Figure 38). However, the horizontal variability is still negligible and the major difference occurs between deep and shallow regions along the bottom of the reservoir (Figure 39). At the beginning of summer, the vertical temperature difference is larger indicating a stratified water body (Figure 40). Furthermore, the bottom water temperature in shallow parts is warmer (Figure 41).

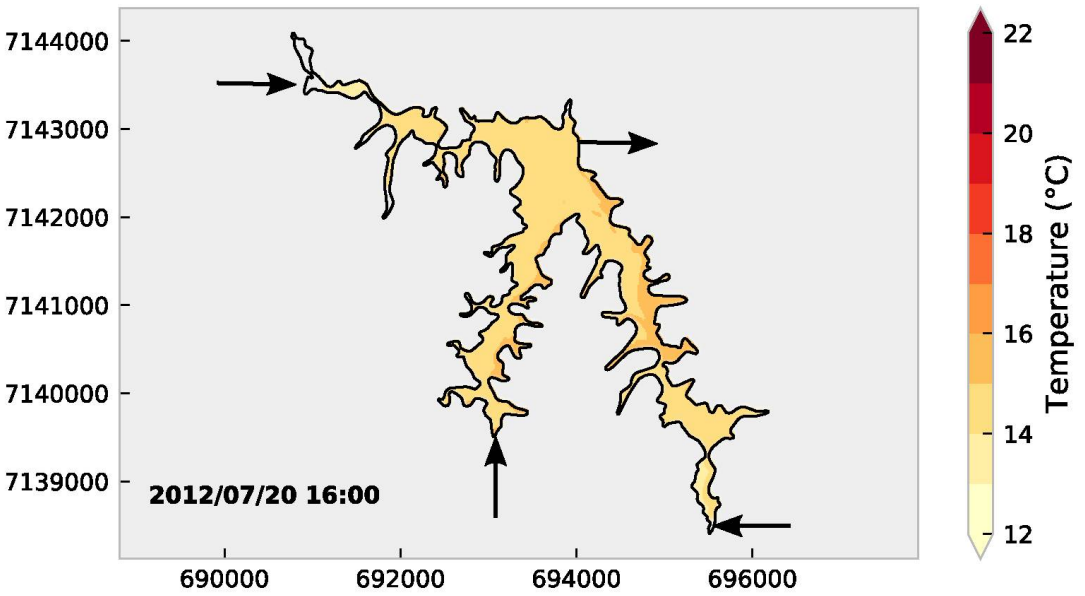

Figure 36 – Surface water temperature during the uniform temperature period.

Figure 42 shows the temperature field along the longitudinal section for each selected time. The reservoir transition to stratified conditions is clearly depicted in this figure. According to this result, the temperature difference between surface and bottom

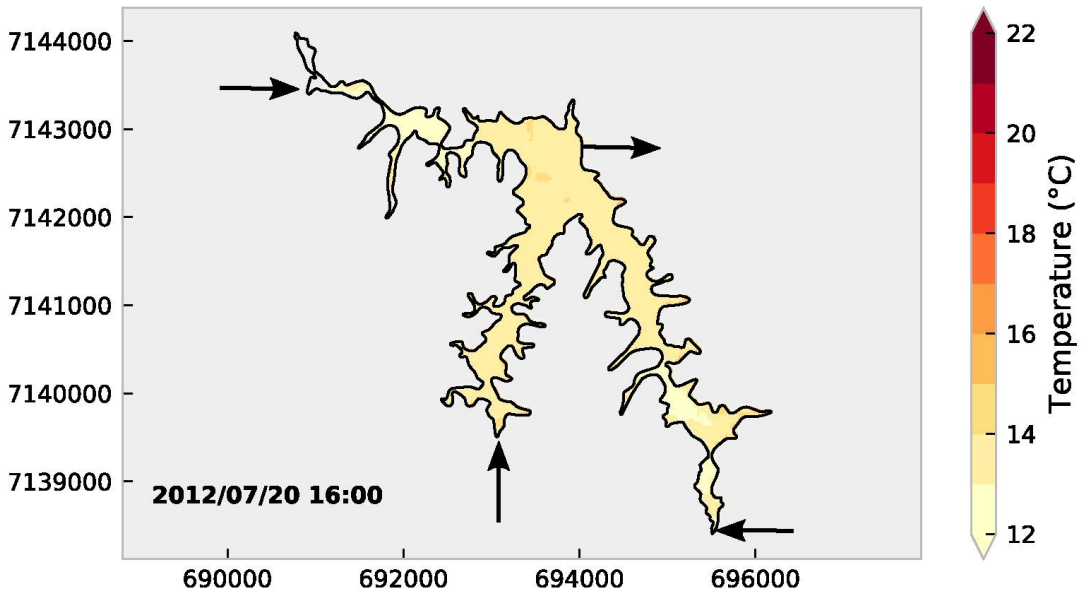

Figure 37 – Bottom water temperature during the uniform temperature period.

is larger than 2 degrees Celsius in areas with more than 4 meters depth, and in the deep areas the difference reaches up to 8 degrees Celsius.

During the selected times, the horizontal temperature variability at the surface was small. The horizontal variability of temperature seems to be more expressive at the bottom, where shallow areas are warmer than deeper regions. At the beginning of summer, when the reservoir becomes stratified the vertical variability is strong and dominates most parts of the reservoir.

A stratified water body has considerably different mixing characteristics compared to a mixed water body. Consequently, during stratified conditions, dissolved substance transport in this reservoir will be limited over the vertical. Thus, the reservoir can be divided according to a "active" volume of water at the surface, and a "passive" volume of water at the bed. This distinction illustrates the bulk measures including the whole volume for residence time estimations do not necessarily represent the systems substance mixing characteristic completely.

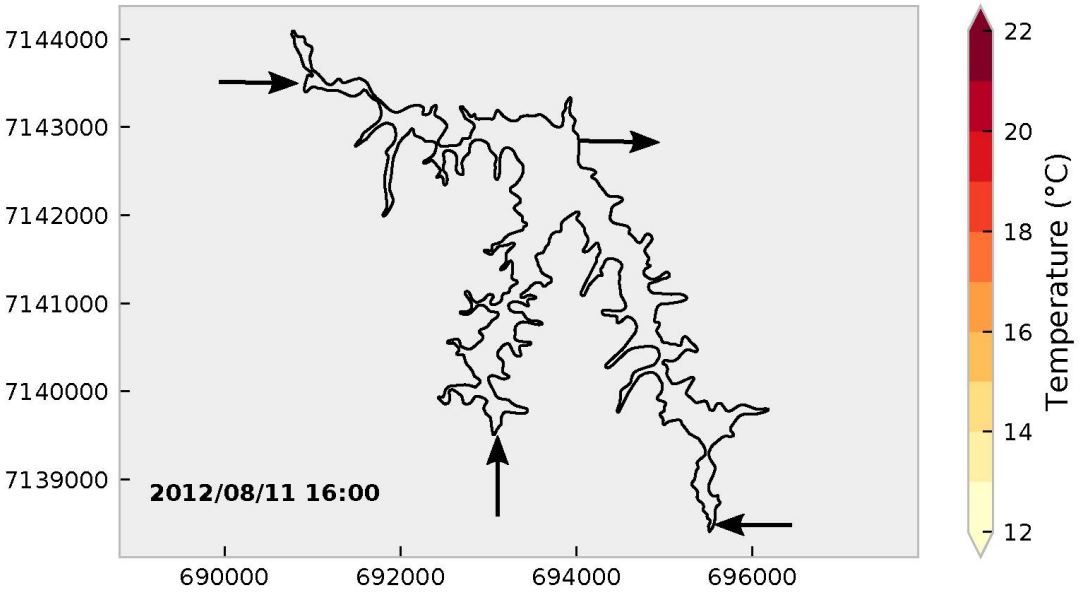

Figure 38 – Surface water temperature during the transition to stratified period.

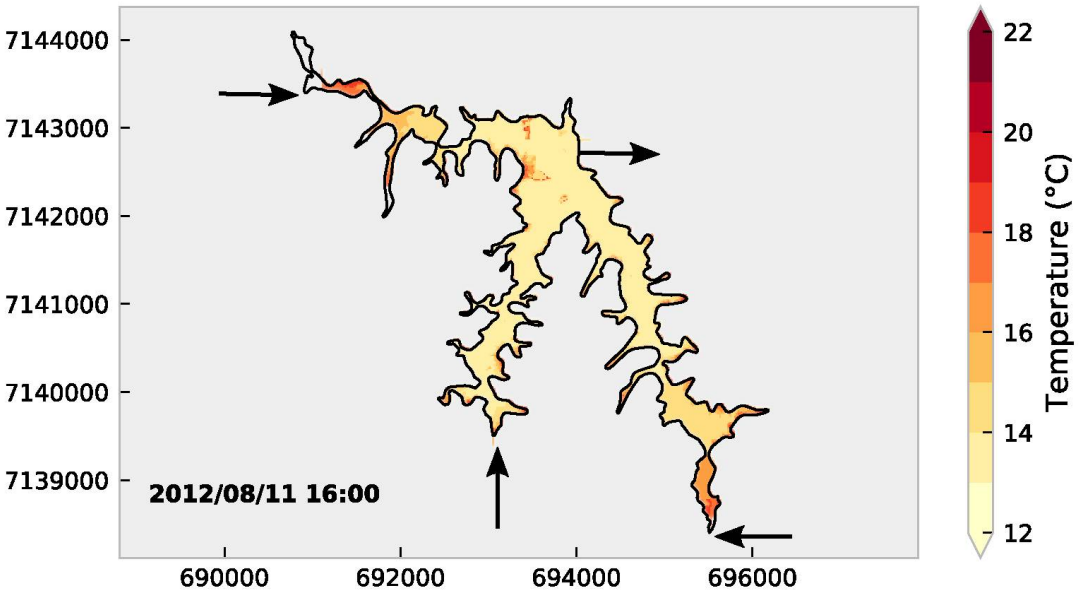

Figure 39 – Bottom Water temperature during the transition to stratified period.

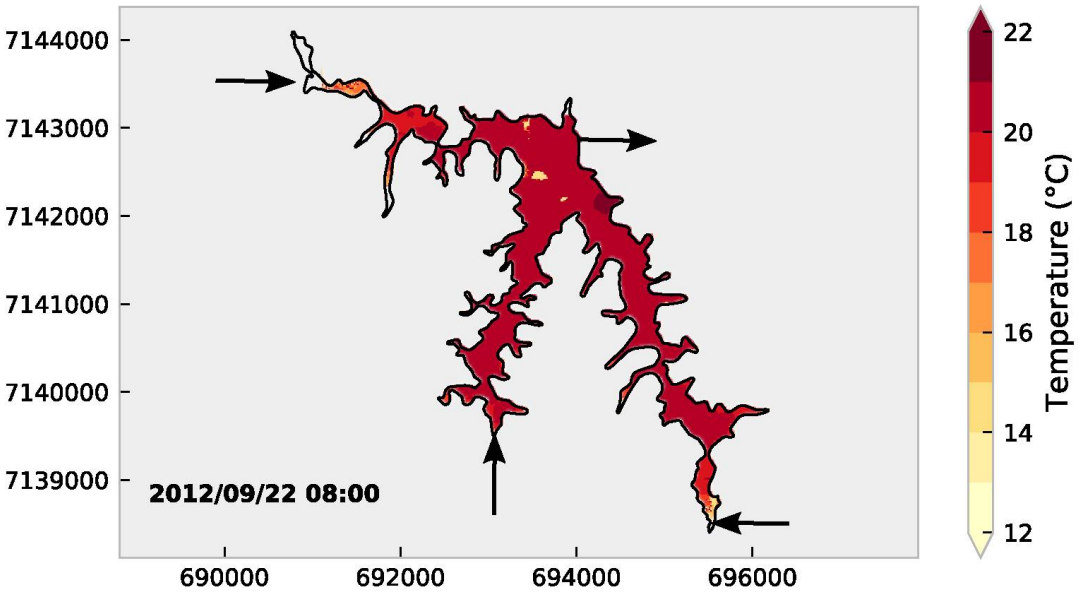

Figure 40 – Surface water temperature during the stratified period.

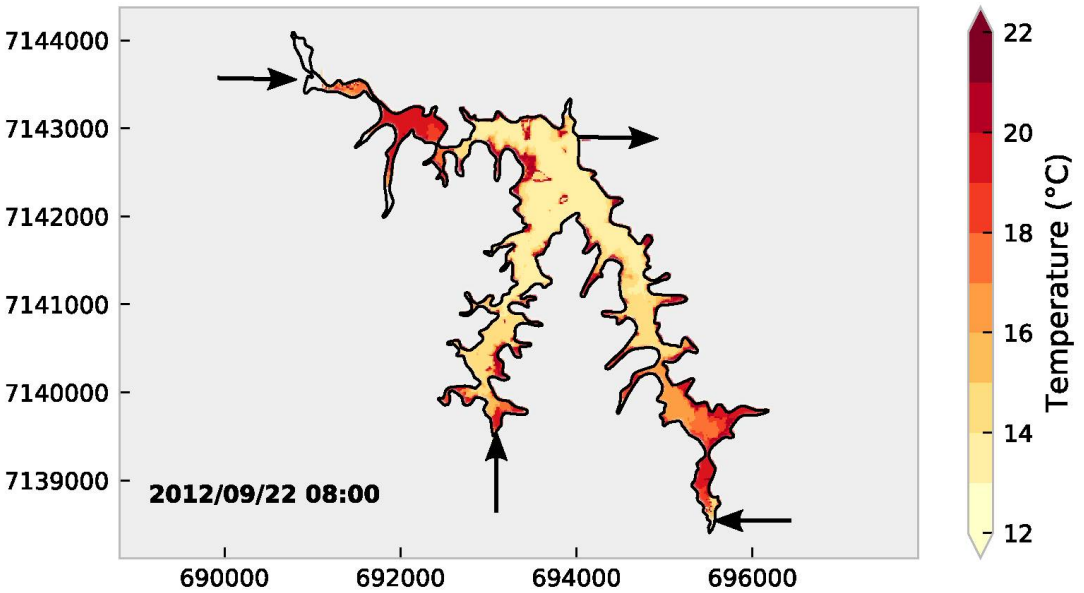

Figure 41 – Bottom water temperature during the stratified period.

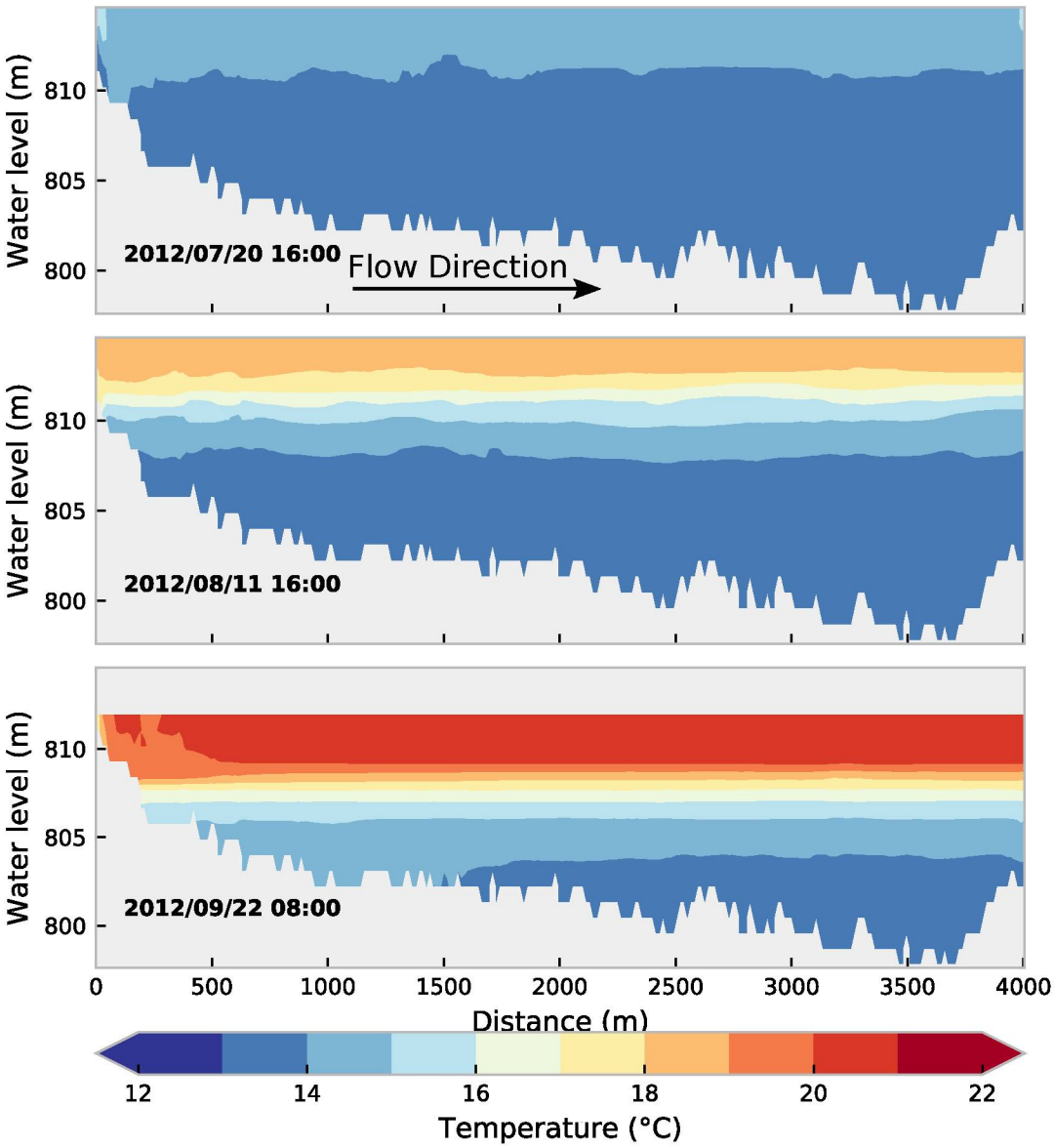

Figure 42 – Water temperature distribution along a longitudinal transect for the three chosen times.

4.2.3 Assessment of effects of Velocity Field

This section presents the velocity fields at the surface and the bottom of the reservoir. During strong wind events, the surface velocities are clearly wind induced as shown in Figure 43 and 45 (only few velocity vectors are shown for better visualization). At the bottom, velocities do not exhibit a uniform pattern but present regions, where bed velocities are directed in the opposite direction of the wind (i.e. in the middle of the right side arm, Figure 44 and 46). This strong three-dimensional behavior with inverting vertical velocity profiles is typical for closed basins with surface shear forces. During mild winds, the reservoir presents slow velocities at the surface and the bottom (Figures 47 and 48). The highest velocities are close to the inlets and the outlet.

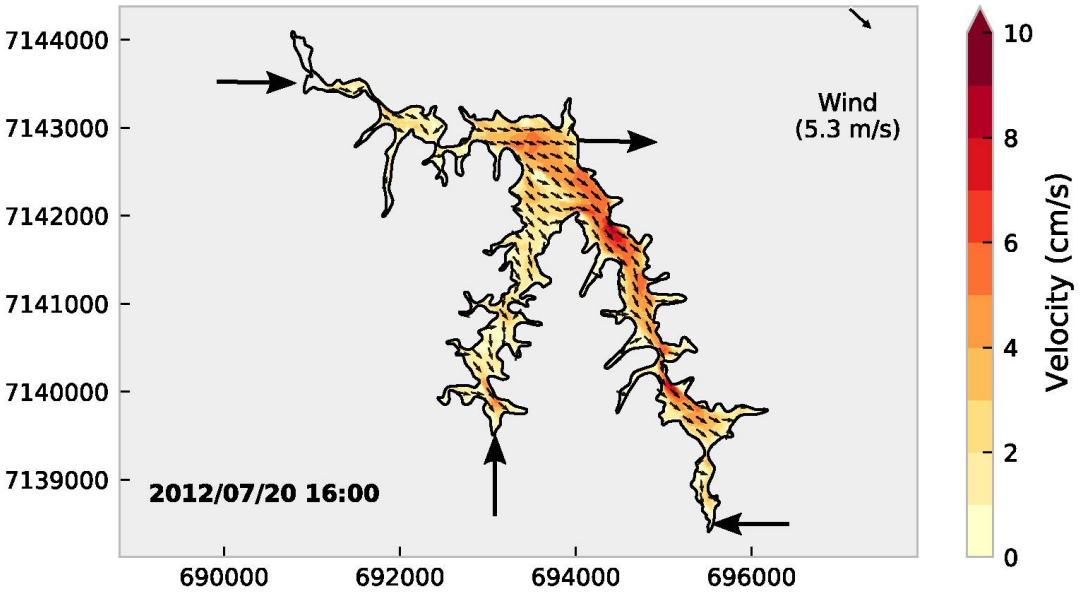

Figure 43 – Water surface velocity field during strong wind event from northwest and uniform temperature period.

Depending on stratification intensities and wind speed the system can show different behaviors with mixing occurring only in the surface layer during strong stratification or over the full vertical when winds are relatively fast and stratification is weak.

These results clearly indicate the importance of wind-induced velocities to

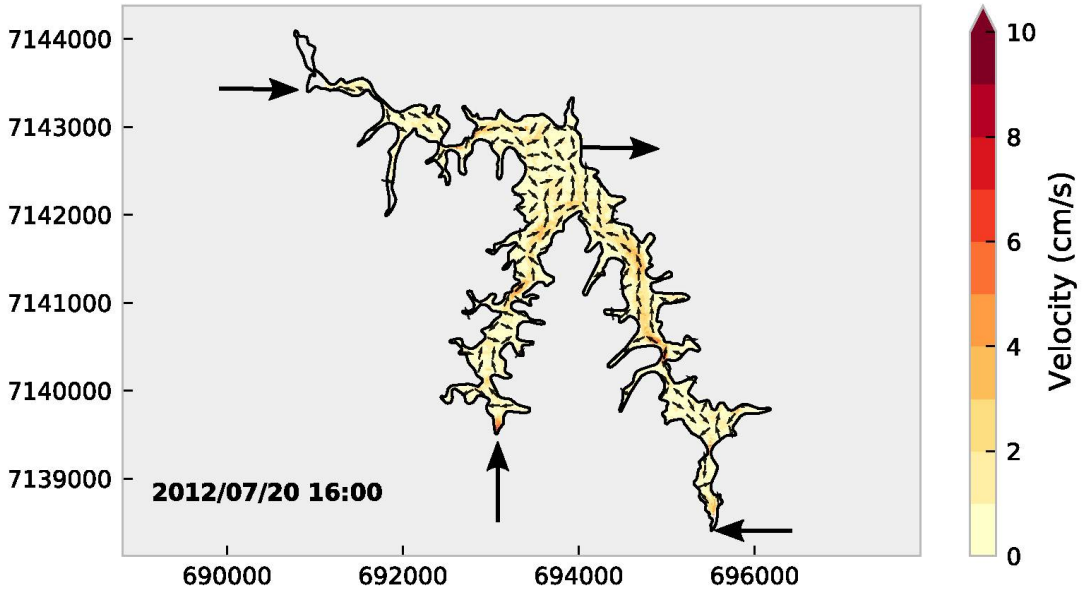

Figure 44 – Water bottom velocity field during strong wind event from northwest and uniform temperature period

determine lake mixing characteristics. Thus, in addition to the previously discussed spatial stratification related system sensitivity, we have the temporal wind related system sensitivity. The latter velocity sensitivity can be intensified for run-off-a-river reservoirs, where river induced velocities play a more dominant role than in the present case. Consequently, the system can be divided in terms of temporal periods with similar features. This distinction illustrates again that bulk measures including the whole volume and mean temporal forcings for residence time estimations do not necessarily represent the systems substance mixing characteristic correctly. Thus, besides a distinction of "active" volumes, or characteristic lengths (such as a mixing or transport length), a velocity scale is required for such system analysis bringing us even closer to the established metrics (chapter 3).

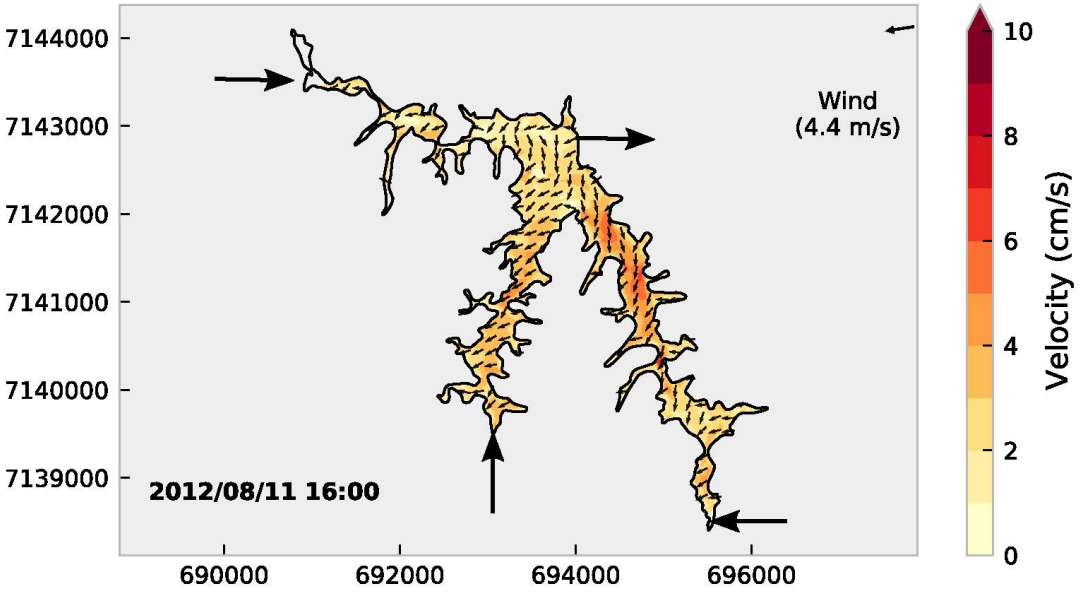

Figure 45 – Water surface velocity field during strong wind event from northeast and transition to stratified period.

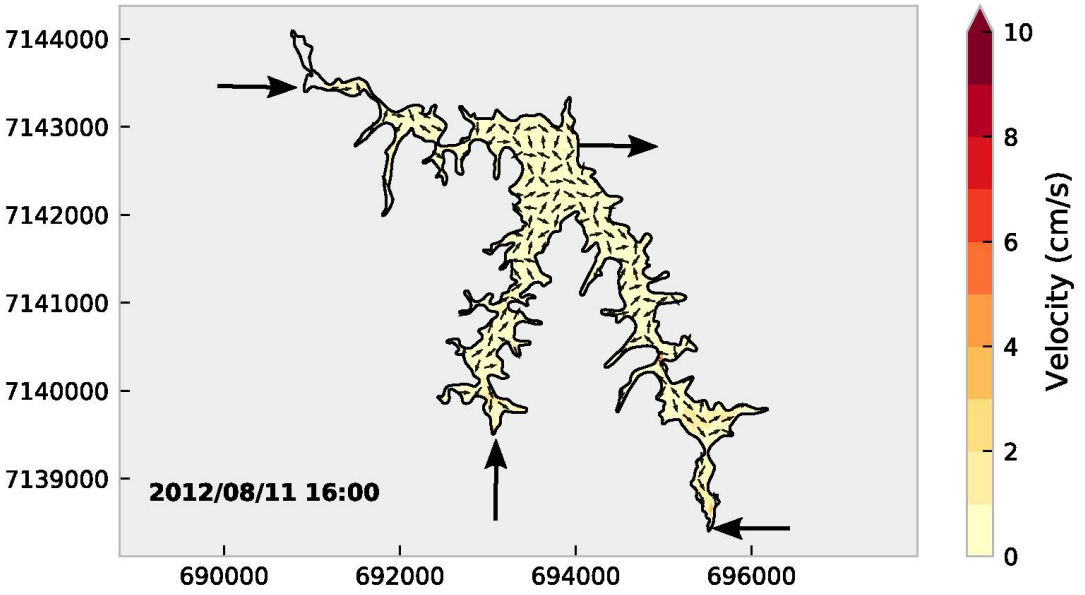

Figure 46 – Water bottom velocity field during strong wind event from northeast and transition to stratified period.

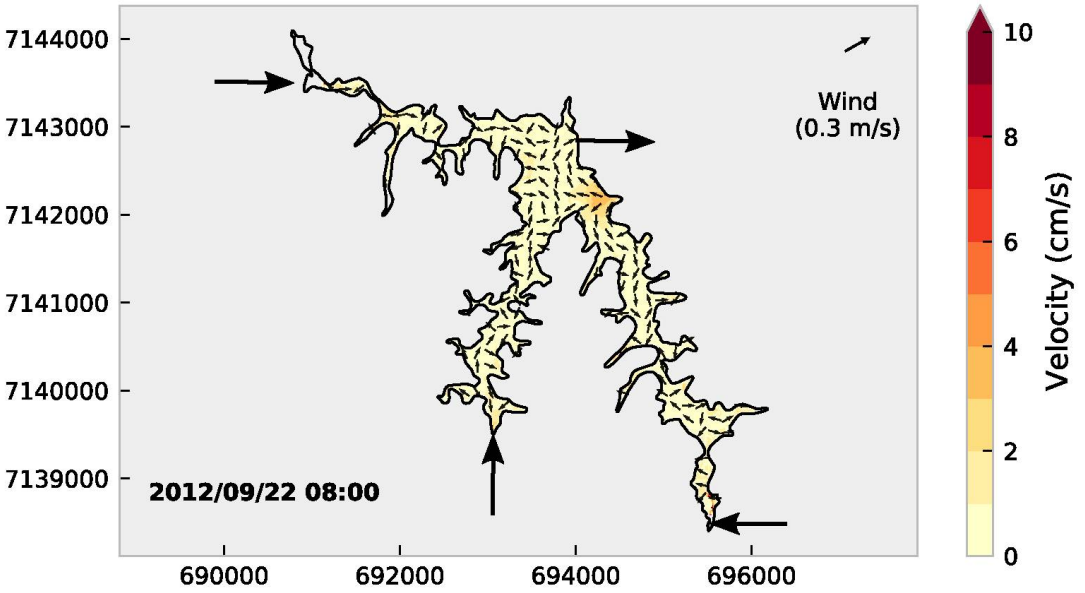

Figure 47 – Water surface velocity field during mild wind event from southwest and stratified period.

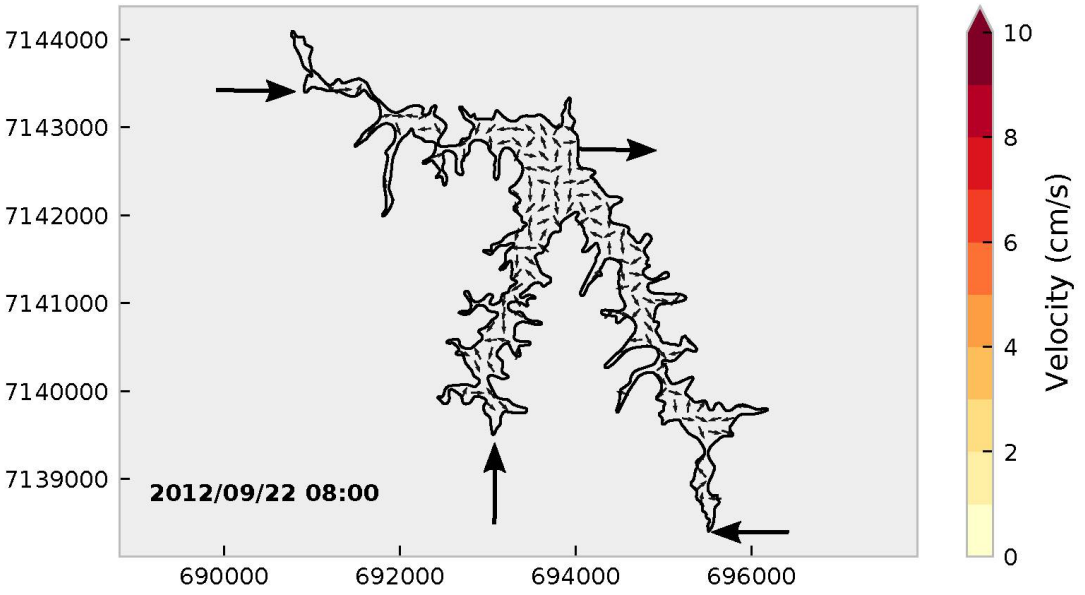

Figure 48 – Water bottom velocity field during mild wind event from southwest and stratified period.

4.2.4 Assessment of Water Quality Aspects

The results on temperature and velocity fields indicated potential consequences for substance transport. To corroborate those interpretations with quantitative measures a water quality model was coupled with the hydrodynamic model. The water quality model focused on eutrophication with a relatively simple model setup just considering the main nutrients (phosphate, nitrate, ammonium), light and Chlorophyll. Phosphate and chlorophyll are assessed here because they are often used to evaluate eutrophication (e.g. Trophic State Index and Vollenweider Plot). The presentation of the results follows the same maps and times as used for the hydrodynamics results . Horizontal plots are presented first followed by the plots of the longitudinal cross-sections.

In the end of July, apparently a density current is transporting phosphorus along the bottom of reservoir (Figure 49). Chlorophyll a follows a similar pattern (Figure 50). However, on contrary of orthophosphate, chlorophyll a is also present close to the surface.

The results show that the river water entering a reservoir transports significant amounts of substances into the system. This can also be found in literature, for example, approximately 90% of the total phosphorus transported in the Chesapeake Basin happened at the seven largest storms of the year (PIONKE; GBUREK; SHARPLEY, 2000). Fortunately, strong events happened during the period of simulation allowing the study of transport of substances under those conditions too. As the water quality model considered a constant loading for the fractions of phosphorus and nitrogen the concentration of substances are directly proportional to the river discharge.

In summary, besides the previously shown overall system sensitivity on spatial stratification related factors, and the temporal wind related factors the results on substance transport and water quality show an additional strong sensitivity related to the substance source and its loading. Consequently, the system analysis needs to include information on the source location (or its distance to points of interest) and its strength (e.g. concentration or load). Those parameters need to be included in a system metrics to correctly describe consequences for water quality analysis. The testing of the established metrics (Chapter 3) with the obtained results is done as follows.

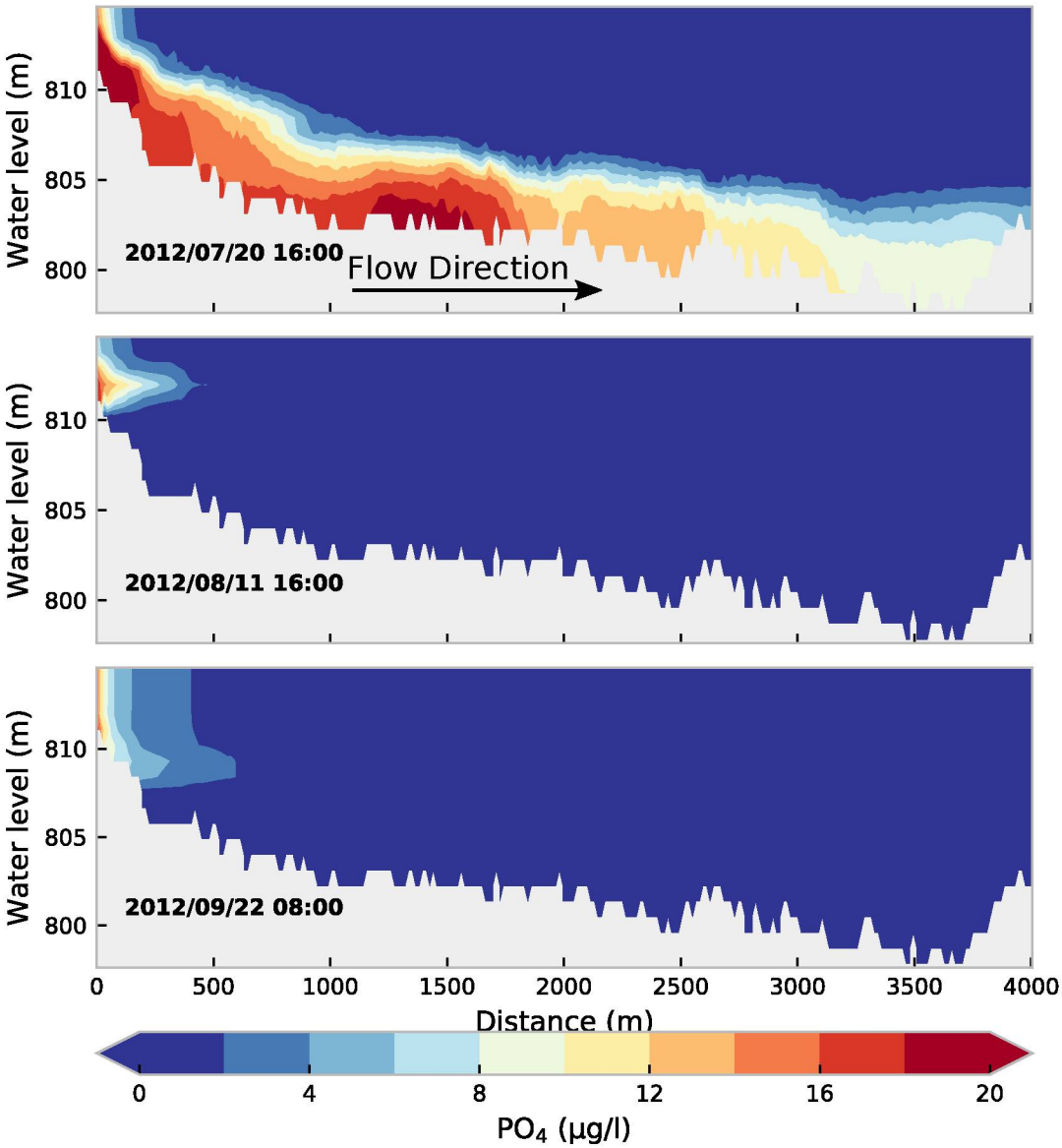

Figure 49 – Phosphate (PO_4) concentration field along longitudinal section.

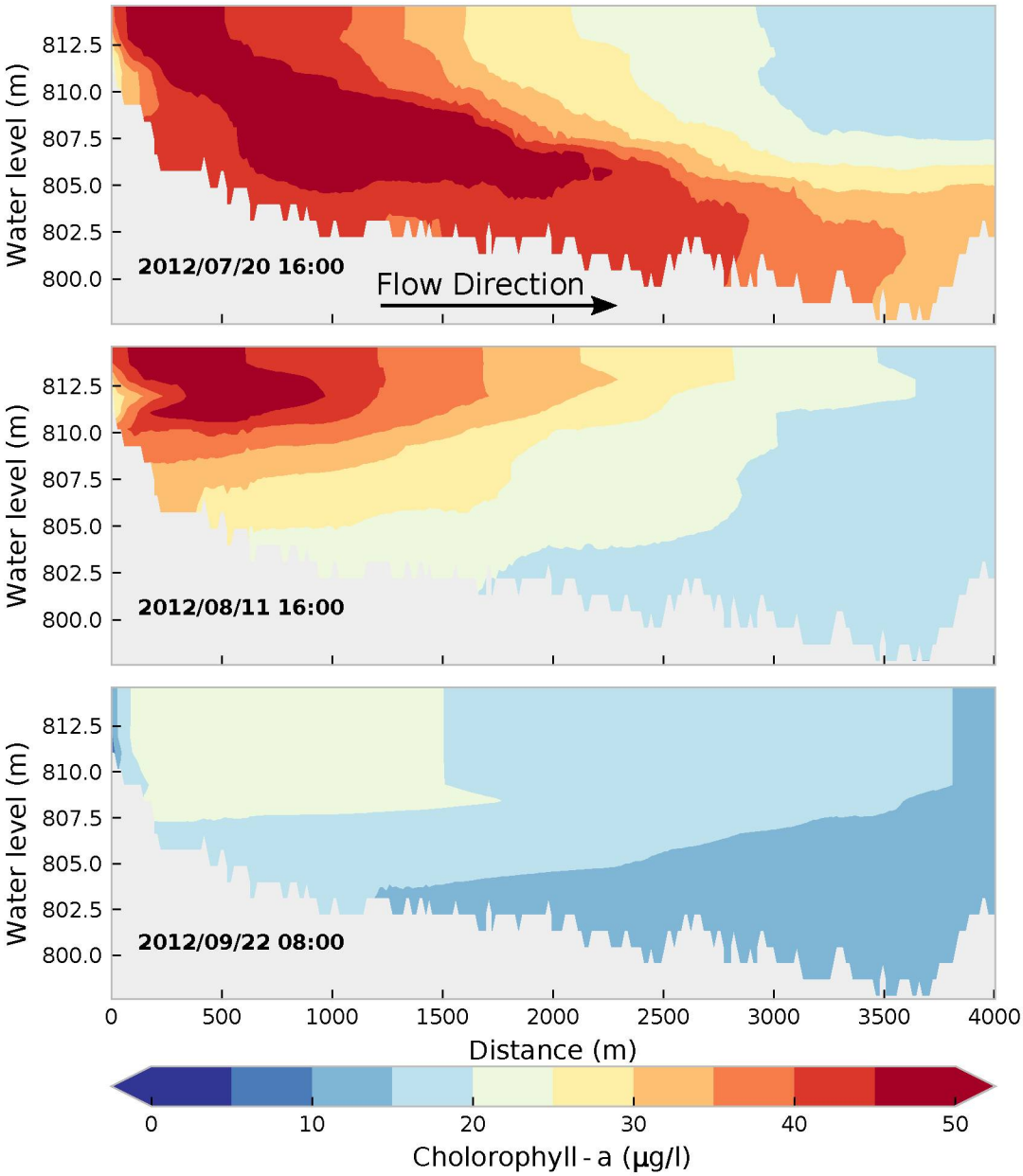

Figure 50 – Chlorophyll a concentration field along longitudinal section.

4.2.5 Combination of effects: Metric assessment

The simulation of hydrodynamics and water quality for the studied period of approximately 3 months took approximately one week computational time to run, using 6 cores on a multiprocessor machine, resulting in a half terabyte of data. The post-processing of such big data is not as straightforward as usual. Some analysis included in the Delft3d post-processing software and programming libraries were not prepared for such huge matrix. The main issue of processing simulation output data occurs when the data did not fit on the available random access memory (RAM). Nowadays, a typical computer has 8–16 gigabytes of RAM thus less than 3% of the produced data can be analyzed at once because the computer also needs extra memory to run the operational system, auxiliary processes, and to keep the output data while it is processed. Thu, the output data from the model had to be reorganized allowing the data to be processed by parts. Several new routines were programmed in Python and Matlab for that purpose. The processing was focused on calculating spatially and temporally varying metrics to be compared with flow and water quality features. The estuary number and age were select as principal metrics for this assessment, i.e., the metric proposed by this thesis and one metric often referred to in literature.

Stratification influence is discussed by comparing periods with different stratification intensities. The wind influence is included by considering velocity fields of different intensities, and all together with the source effects will be discussed for four specific rain events to illustrate the metric behavior for combined effects of different intensities.

The discharge of the main inlet (São João river) and the rainfall events chosen to be analyzed for the metrics testing are presented in Figure 51. River discharge during the events was $3 \pm 1\ m^3/s$ and the events were named Event 1 (E1), Event 2 (E2), Event 3 (E3), and Event 4 (E4) according to Figure 51.

The analysis of each event is conducted through a sequence of 3 specific time steps, at the peak of discharge, 6 and 10 hours after the peak discharge. The Estuary number (established metric), orthophosphate concentration (water quality aspect), and age (conventional metric) will be presented respectively one by one.

Event 1 had the biggest discharge ($4\ m^3/s$). Figure 52 shows the spatial

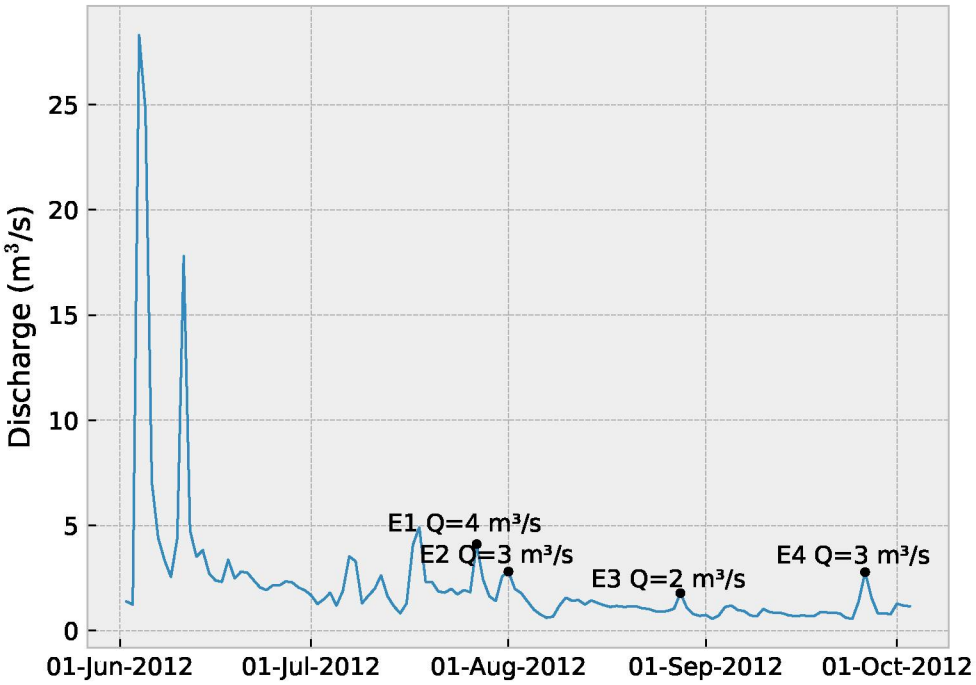

Figure 51 – Rainfall events chosen to be assessed. Event 1 (E1), Event 2 (E2), Event 3 (E3), and Event 4 (E4).

distribution of the Estuary number plotted along the longitudinal transect. Following the characterization done in the analytical analysis (Section 4.1) high values indicate regions which are more diffusive. For event 1 high values appeared at the water surface, within a layer of approximately 3 meters thickness almost all over the reservoir, with exception to a region close to the river inflow. There, until a distance of approximately 500 m from the inlet, the flux is predominantly advective. The effect on the substance transport (orthophosphate) is shown in Figure 53. The river water forms a surface plume which extents correlate with observations of the estuary number for the region up to 500 m from the inlet. The water age is shown in Figure 54 indicating that the surface river plume until 500 m from the inlet is composed by river water that entered the reservoir within the last 5 days (dark-blue area).

The discharge during Event 2 was $3\ m^3/s$. The estuary number, in this case, was higher (more diffusive) and of larger extent covering a layer of 7 meter approximately. Just 10 hours after the peak (third graph) this effect reduces significantly. In this case the Estuary number showed differences close to the inlet only after the peak passed. This indicates that the reservoir's physicochemical conditions during Event 2 were different to those during Event 1. Here the estuary number indicated a more diffusive/reactive environment than during event 1, where transport was more pronounced close to the river inlet. Consequently, the results of orthophosphate (Figure 56) showed a damping of the plume intensity and a quicker decay of the substance along the path. The river plume was weaker than in Event 1 and regions with higher intensity were concentrated before the plume reaches 500 m of distance from the river entrance. The water age confirmed that the water from 5 days was confined to the first 500 m from the river inlet.

The discharge during Event 3 was the lowest $2\ m^3/s$. This is also the period of the beginning of temperature stratification. The estuary number again presented higher values close to the water surface within a layer of 3 meters thickness, however, different to Event 1 and 2 (Figure 59) the values were more uniform close to the surface and exhibited small temporal variability.

The results for orthophosphate showed (Figure 60) characteristics of an interflow, where river water enters the reservoir at the thermocline depth. Despite the lowest flow rate, the river plume in this case reached regions farther than in Event 1 and 2. This fact also agrees with the lower estuary number in the mid-depth region. According to water age, the influence of the river water on orthosphosphate did not relate to the rainfall peak of Event 3 because the age is older than 5 days (Figure 61). Thus, the water quality aspect refers to a previous discharge event. According to Figure 51, the discharge remained almost constant during a long period before Event 2, and this constant discharge may be the reason of the identified river water plume. As a conclusion, the combined use of water age and estuary number preview of the system because water age provides information about the sources and the estuary number about the local characteristic of the system.

Event 4 is very similar to Event 3 regarding the patters of the Estuary number (Figure 62), orthophosphate (Figure 63), and water age (Figure 64). The major difference

is the intensity, as the discharge was slightly higher $3\ m^3/s$ but the river plume also showed an interflow reaching a farther distance then the previous events analyzed. The interflow may be an important way of transport during the transition to a temperature stratified regime. Younger water ages are restricted to the river entrance, this may be also induced by the higher diffusive/reactive environment close to the surface. Figure 64 shows that river water may affect water age 3 km far away from the river entrance during the maximum flow rate.

Figures 65, 66, 67, and 68 shows the Orthophosphate, estuary number, and water age in the same figure to make easier to compare the figures.

The exceedance probability for estuary number and orthophosphate was calculated to verify the relationship between both parameters. The estuary number limited considered was $\eta = 1$ and for phosphorus limit was the concentration of 10 μg/l based on the CONAMA limit for total phosphorous (CONAMA, 2005). The exceedance probability is shown in terms of percentage of the simulation period, thus an exceedance time of 50% means that the parameter was bigger than the limit in half of the simulation.

The exceedance probability of estuary number for the transect is shown in Figure 69 and the exceedance probability of orthophosphate is shown in Figure 70. The visual comparison between Figures 69 and 70 shows an agreement that when estuary number is greater than one (dominated by diffusion) the probability of orthophosphate exceed the limit is lower. It can be also noted a vertical transition close to the depth of 808 m.

In average, the orthophosphate exceeds the limit 36% of the simulated period. The places where estuary number is most of the time greater than 1 (diffusive) the orthophosphate probability to exceed the limit is 15% and where the estuary number is less than 1 the probability of exceedance is 39%. Thus, the estuary number seems to indicate places with more or less susceptible to water quality issues.

The results indicate that the use of one metric using the estuary number allows to characterize and to classify water quality aspects by using a combination of hydrodynamic parameters with a reaction parameter in a single non-dimensional metric. In contrary to previously used metrics, this especially holds also for spatially and temporally varying systems. Consequently, complex water quality simulations, which

usually require expensive and rare measurements for validation and calibration can be sometimes substituted be using hydrodynamic model results processed in terms of the estuary number. Hydrodynamic model setups are much easier to be validated and faster to be simulated.

In conclusion, the study case of river water flowing into a reservoir with is approximately a one-dimensional process, showed that regions with higher estuary number have characteristics of a diffusive/reactive environment, i.e. intense and fast decay than regions with lower estuary number. Furthermore, the estuary number can be exploited as a goal parameter for redesign a reservoir to get better mixing and consequently better water quality.

A potential use of this metric would be in a decision tree model. Figure 71 represents a proposal for a simple model to assess water quality and required modeling efforts based on metrics. In a first step spatial non-uniformity is addressed using known metrics from lake and reservoir analysis (WÜEST; LORKE, 2003) and applying the Vollenweider model. The second step includes some metrics identified in this thesis to decide upon the influence of the inflow on the system. The last step represents the key practical contribution of this work by using the process classification and metric combinations for characterizing transport phenomena and affected areas. The latter analysis thus can result in additional demands for monitoring or multidimensional modeling.

Summary

- The analysis of hydrodynamics and water quality in an unsteady three-dimensional model is a complex task owing to the large amount of data to be analyzed;
- In that regard, metrics as residence time and non-dimensional numbers can help to summarize features simplifying the analysis;
- Age presents similar results as a conservative tracer, confirming the Lagrangian aspect of this metric. Thus, depending on where the tracer is released the result will be different. Because of that, many authors suggested using well-defined time scales. This feature could be used when a specific phenomenon has to be

understood. For example, studying how long particles remain suspended after resuspension.

- Non-dimensional numbers as the Estuary number provide a system-wide diagnosis, i.e., a snapshot of the current state of the system. The application would be to understand general behavior or to improve decision making of engineering projects. For example, engineering structures aiming to reduce maximum concentration can be placed in a reservoir focusing in an increase of Estuary number.

- Estuary number may indicate regions and time when the system is more susceptible to face water impairment.

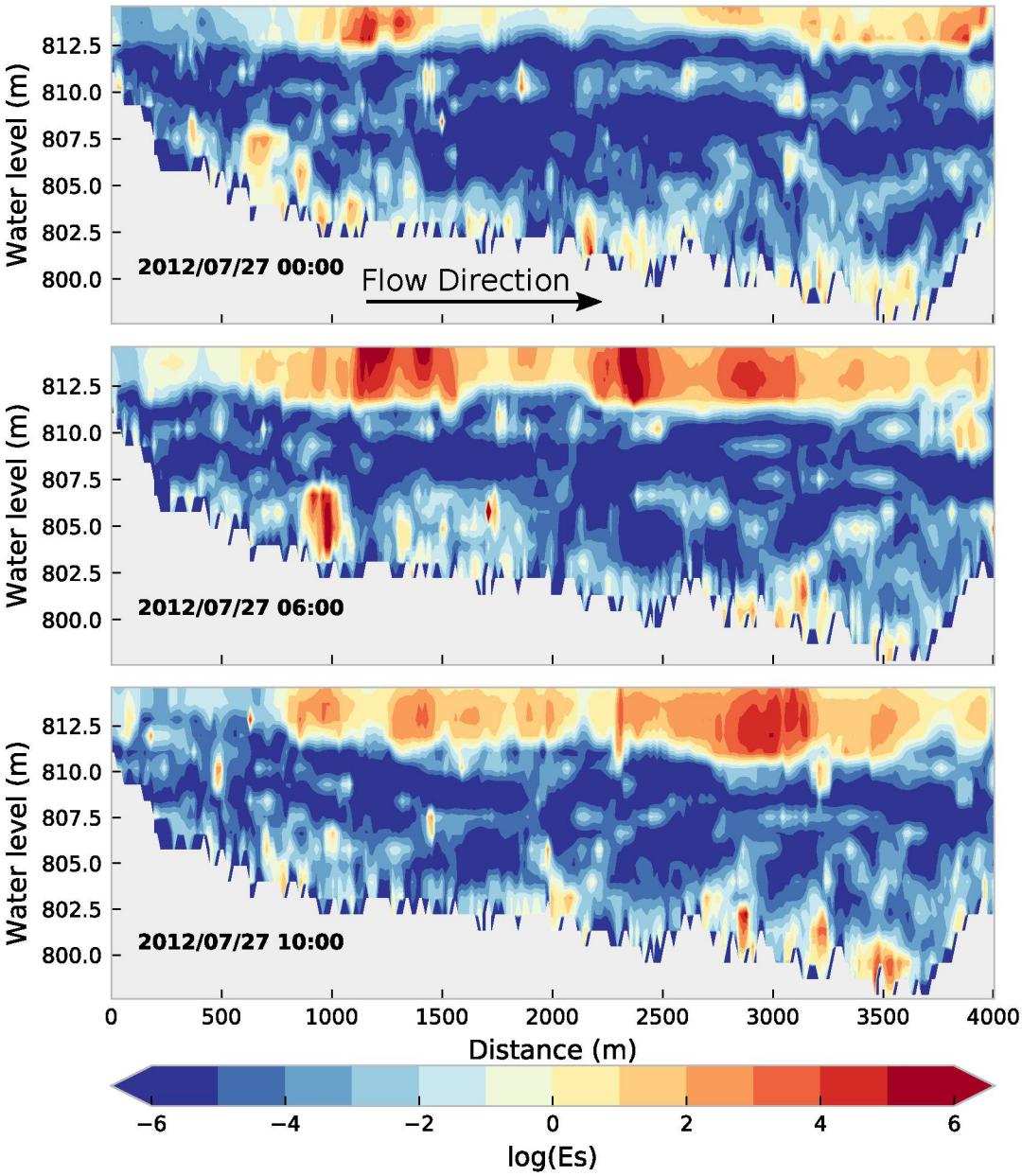

Figure 52 – Estuary number distribution during Event 1. The time of maximum discharge is presented in the plot at the top, 6 hours after the peak in the middle, and 10 hours after the peak at the bottom.

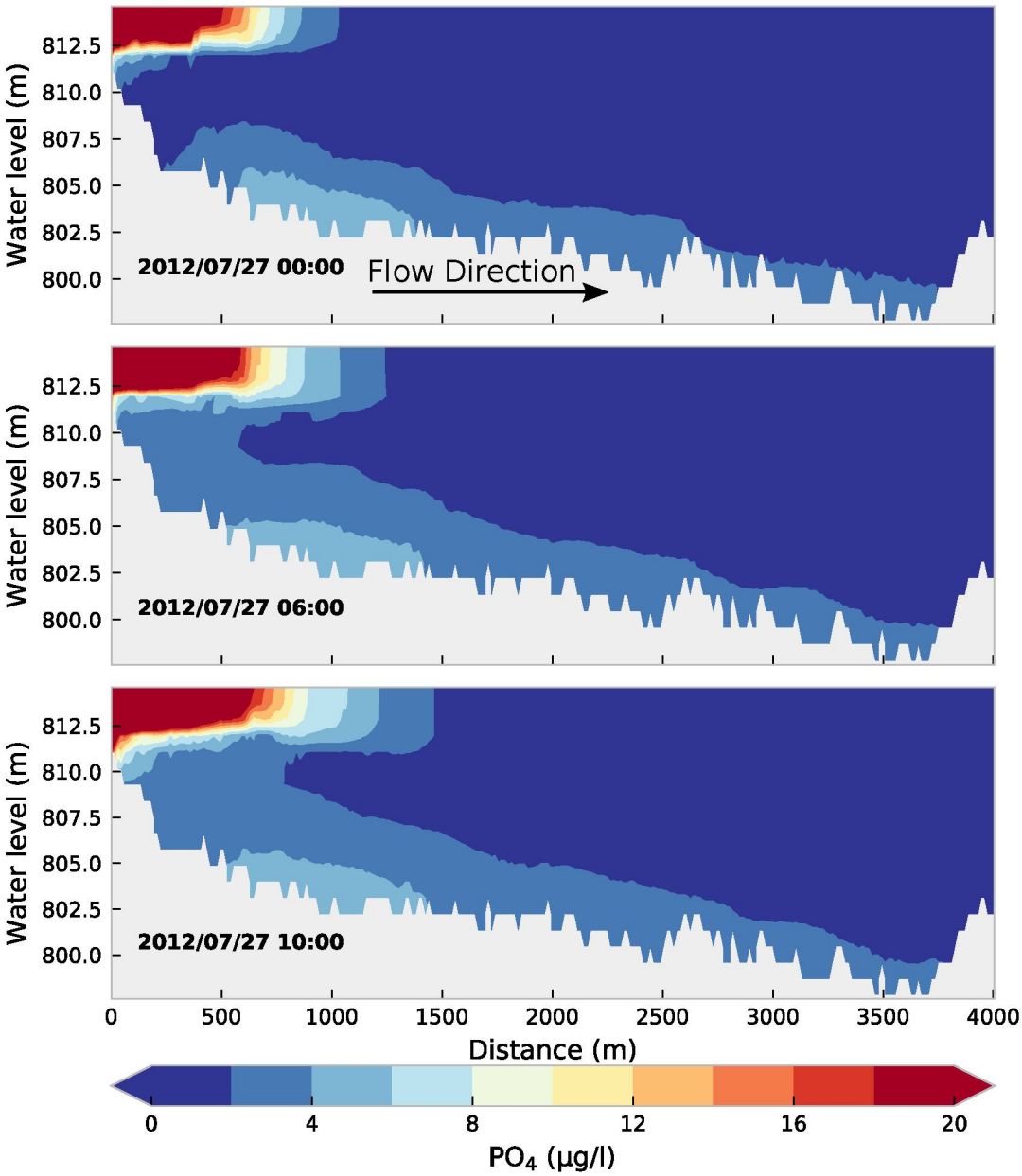

Figure 53 – Orthophosphate distribution during Event 1. The time of maximum discharge is presented in the plot at top, 6 hours after the peak in the middle, and 10 hours after the peak at the bottom.

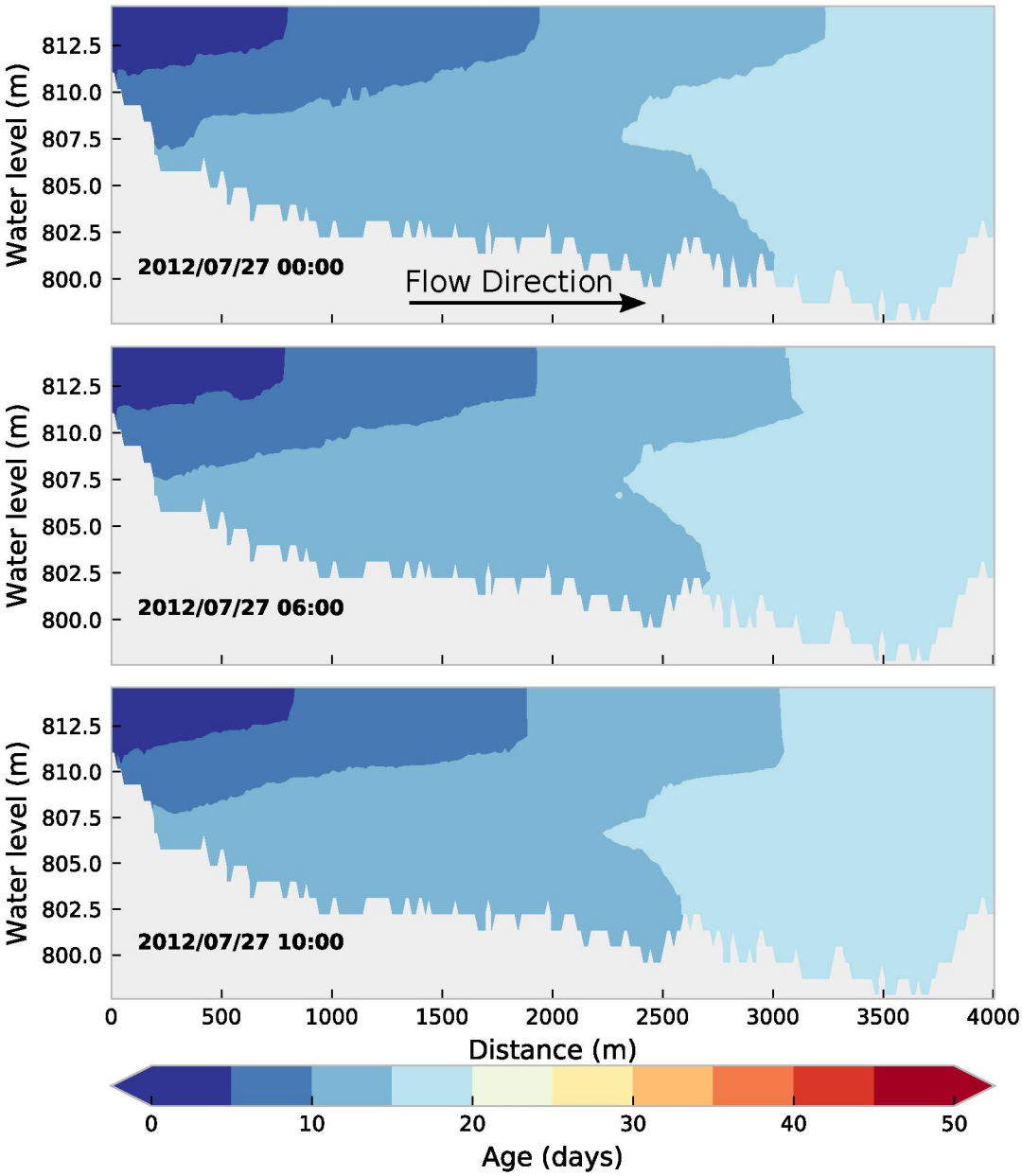

Figure 54 – Water age distribution during Event 1. The time of maximum discharge is presented in the plot at top, 6 hours after the peak in the middle, and 10 hours after the peak at the bottom.

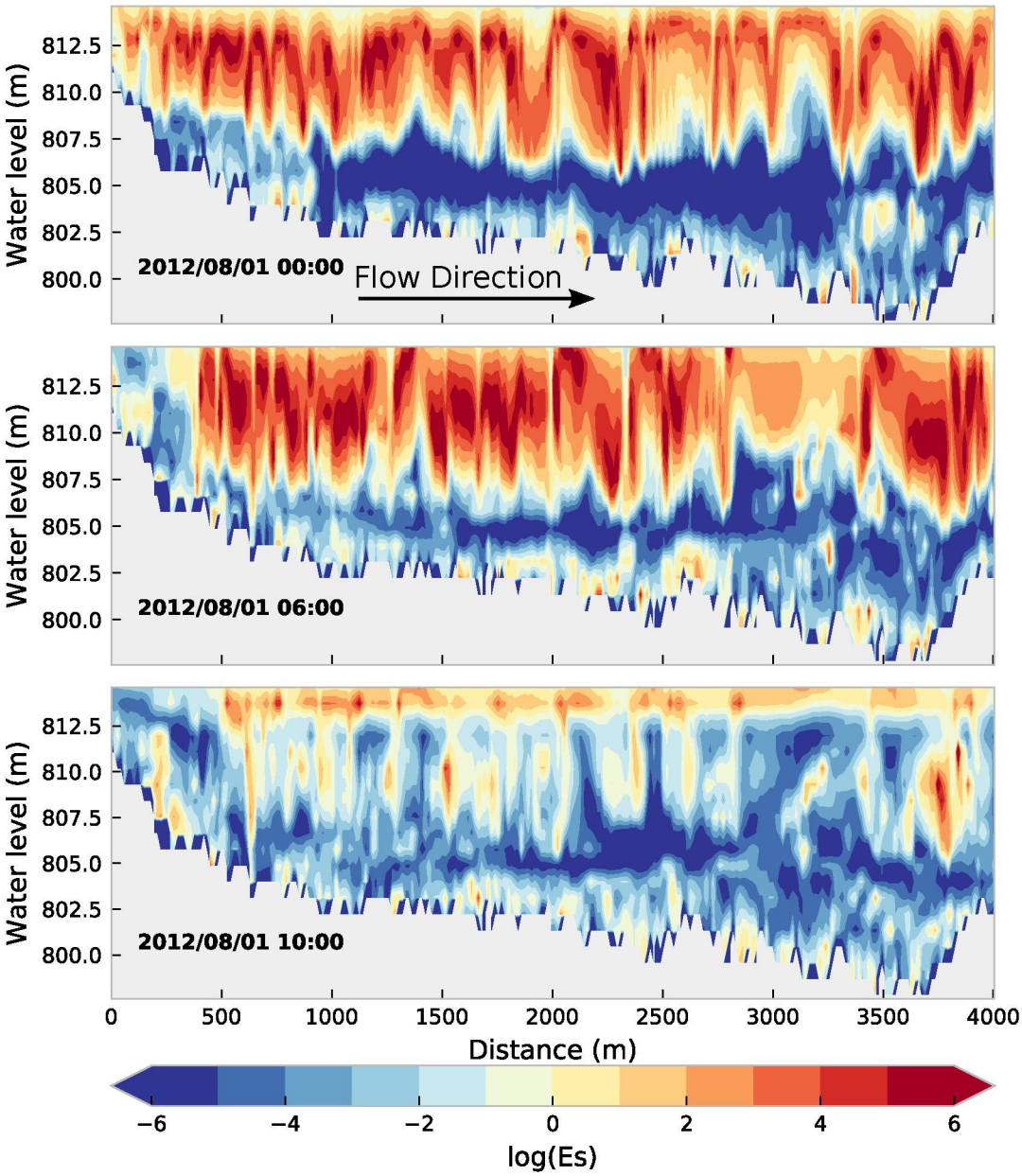

Figure 55 – Estuary number distribution during Event 2. The time of maximum discharge is presented in the plot at top, 6 hours after the peak in the middle, and 10 hours after the peak at the bottom.

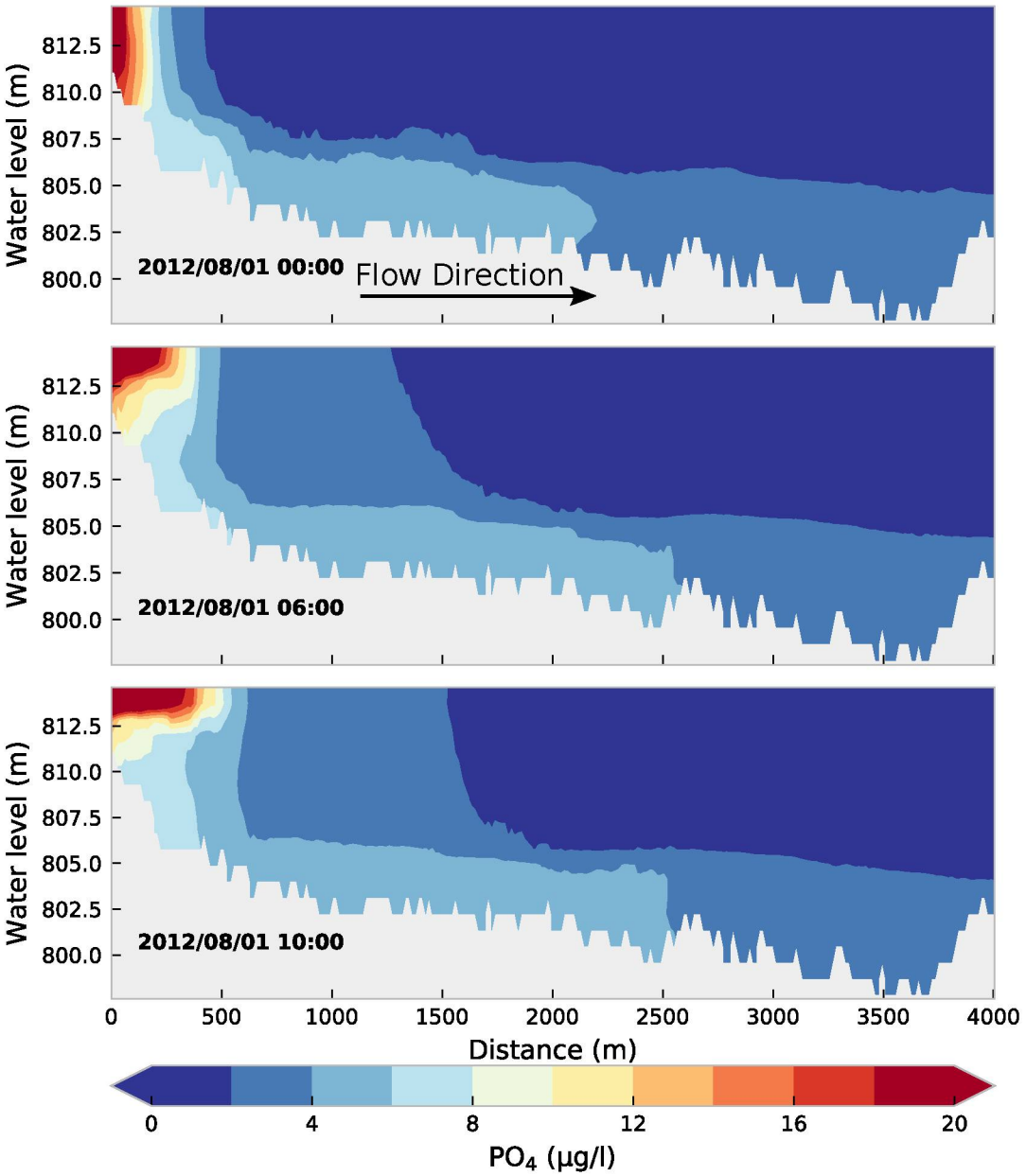

Figure 56 – Orthophosphate distribution during Event 2. The time of maximum discharge is presented in the plot at top, 6 hours after the peak in the middle, and 10 hours after the peak at the bottom.

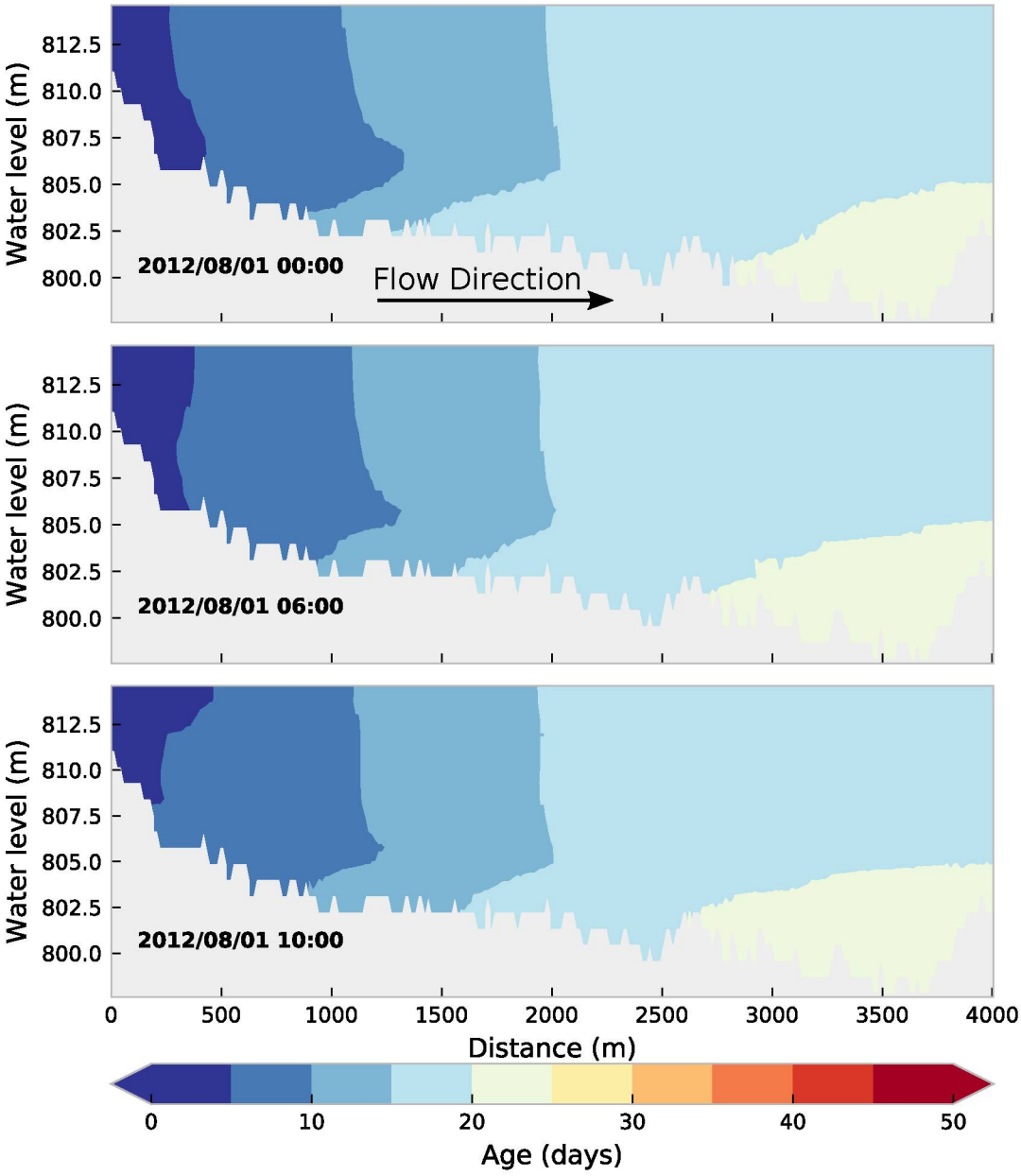

Figure 57 – Water age distribution during Event 2. The time of maximum discharge is presented in the plot at top, 6 hours after the peak in the middle, and 10 hours after the peak at the bottom.

Figure 58 – Event 2

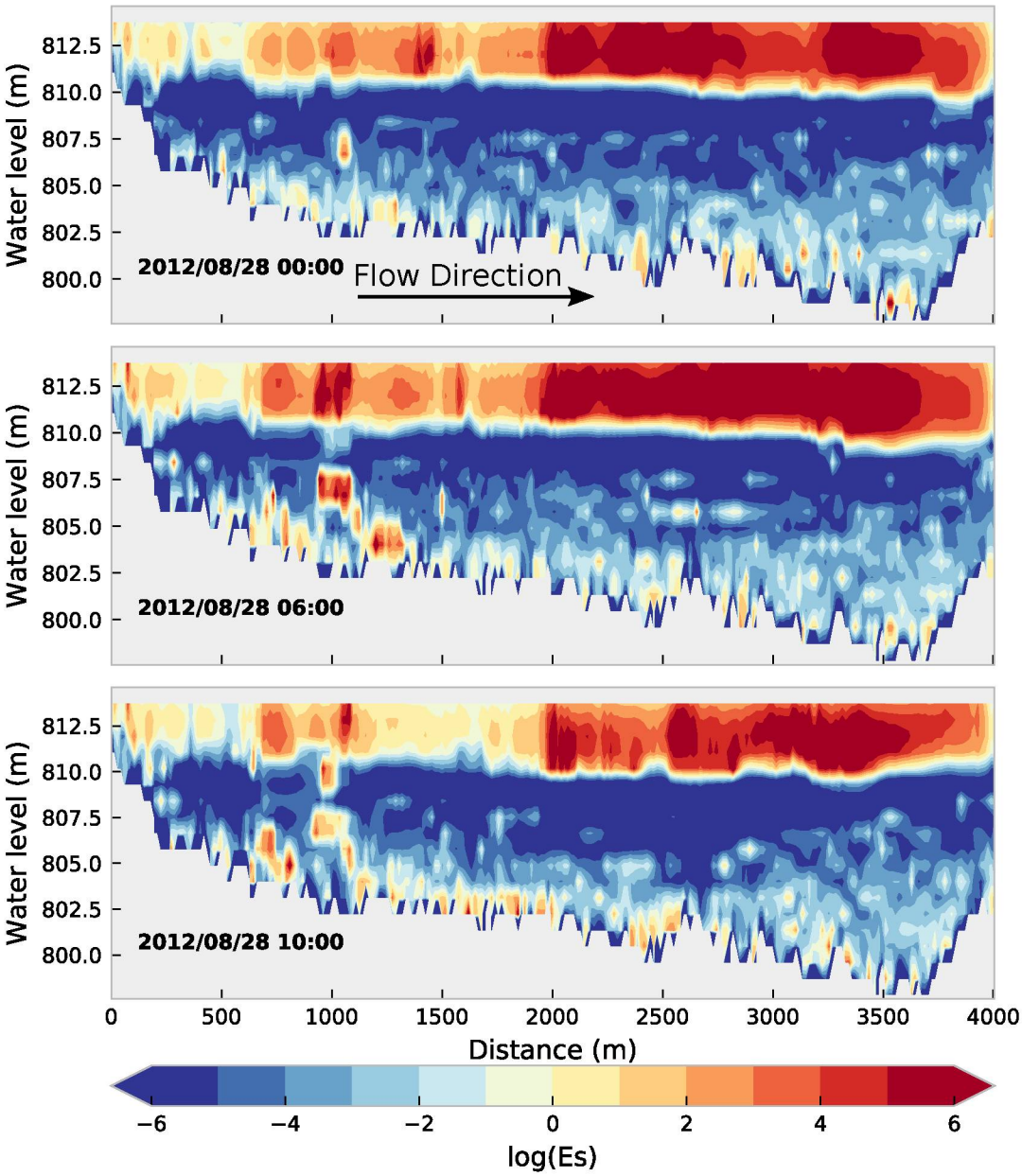

Figure 59 – Estuary number distribution during Event 3. The time of maximum discharge is presented in the plot at top, 6 hours after the peak in the middle, and 10 hours after the peak at the bottom.

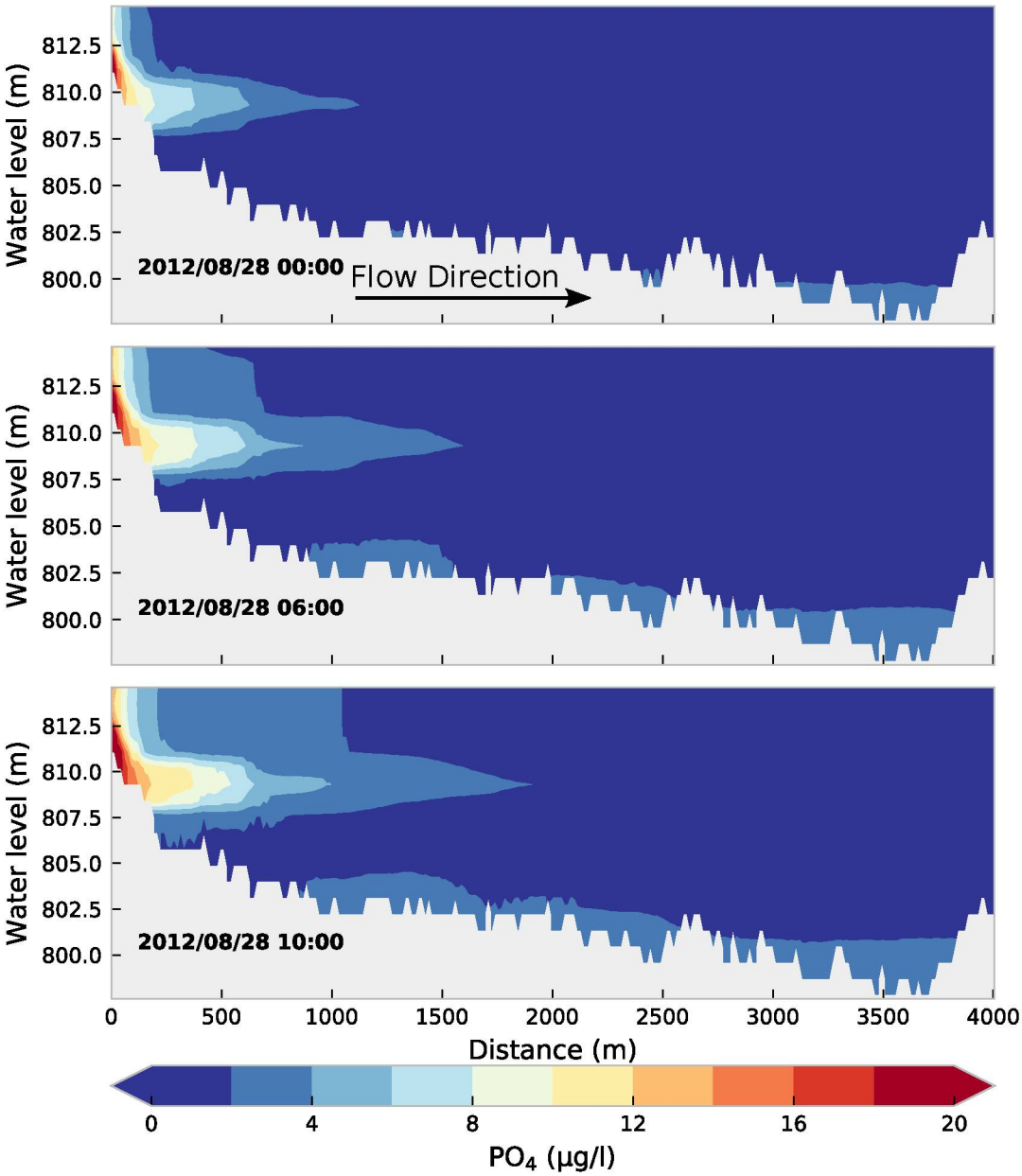

Figure 60 – Orthophosphate distribution during Event 3. The time of maximum discharge is presented in the plot at top, 6 hours after the peak in the middle, and 10 hours after the peak at the bottom.

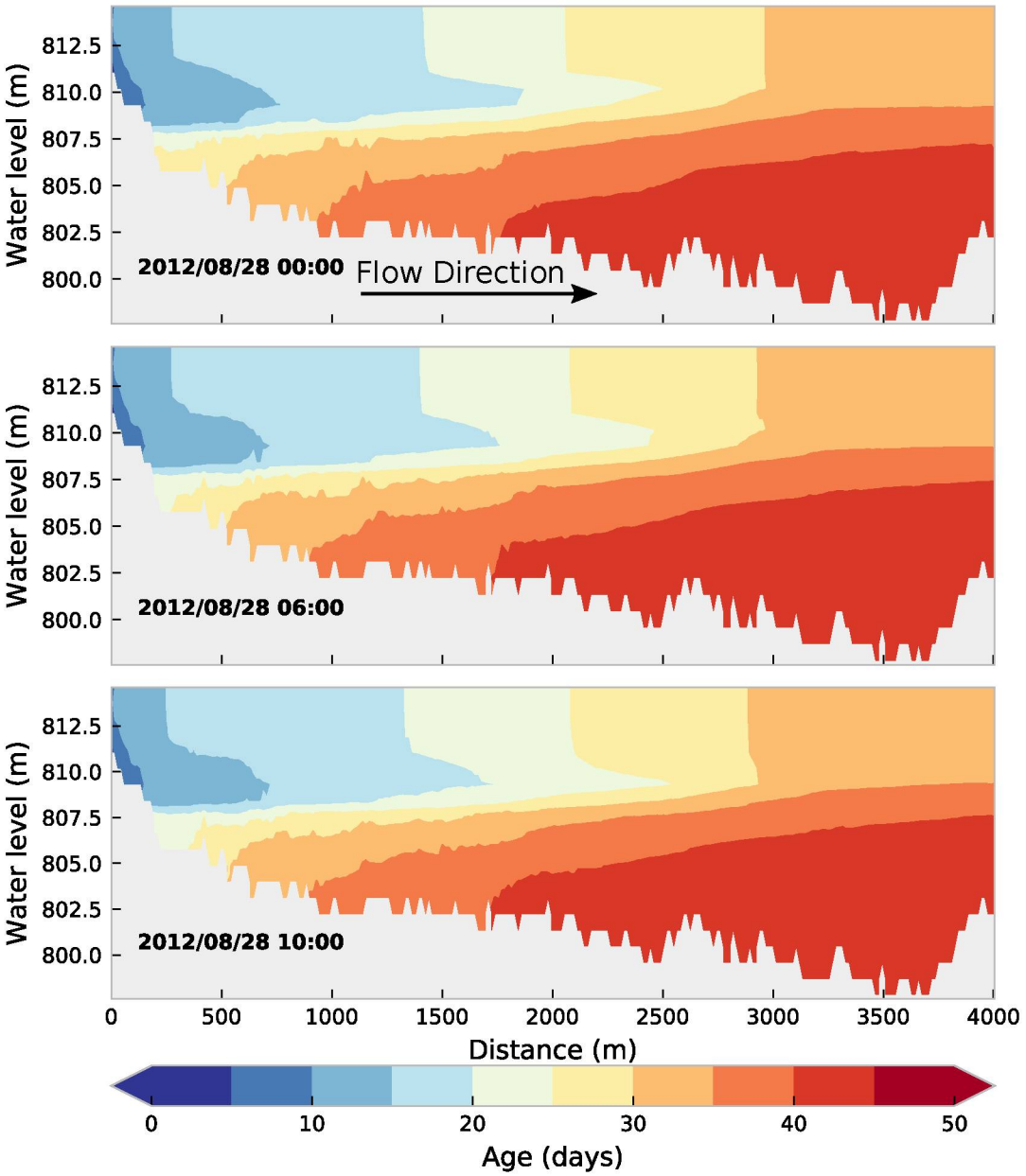

Figure 61 – Water age distribution during Event 3. The time of maximum discharge is presented in the plot at top, 6 hours after the peak in the middle, and 10 hours after the peak at the bottom.

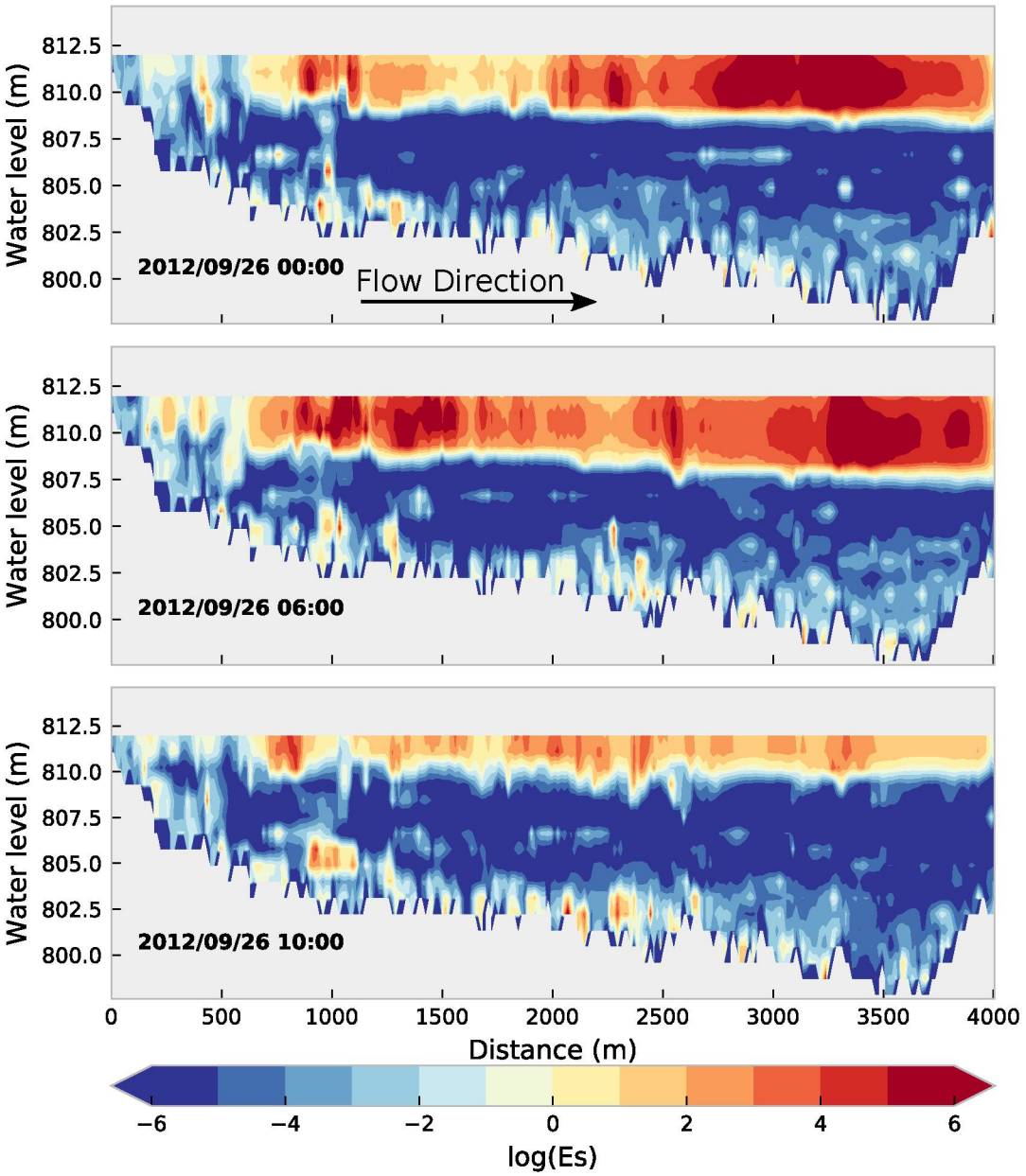

Figure 62 – Estuary number distribution during Event 4. The time of maximum discharge is presented in the plot at top, 6 hours after the peak in the middle, and 10 hours after the peak at the bottom.

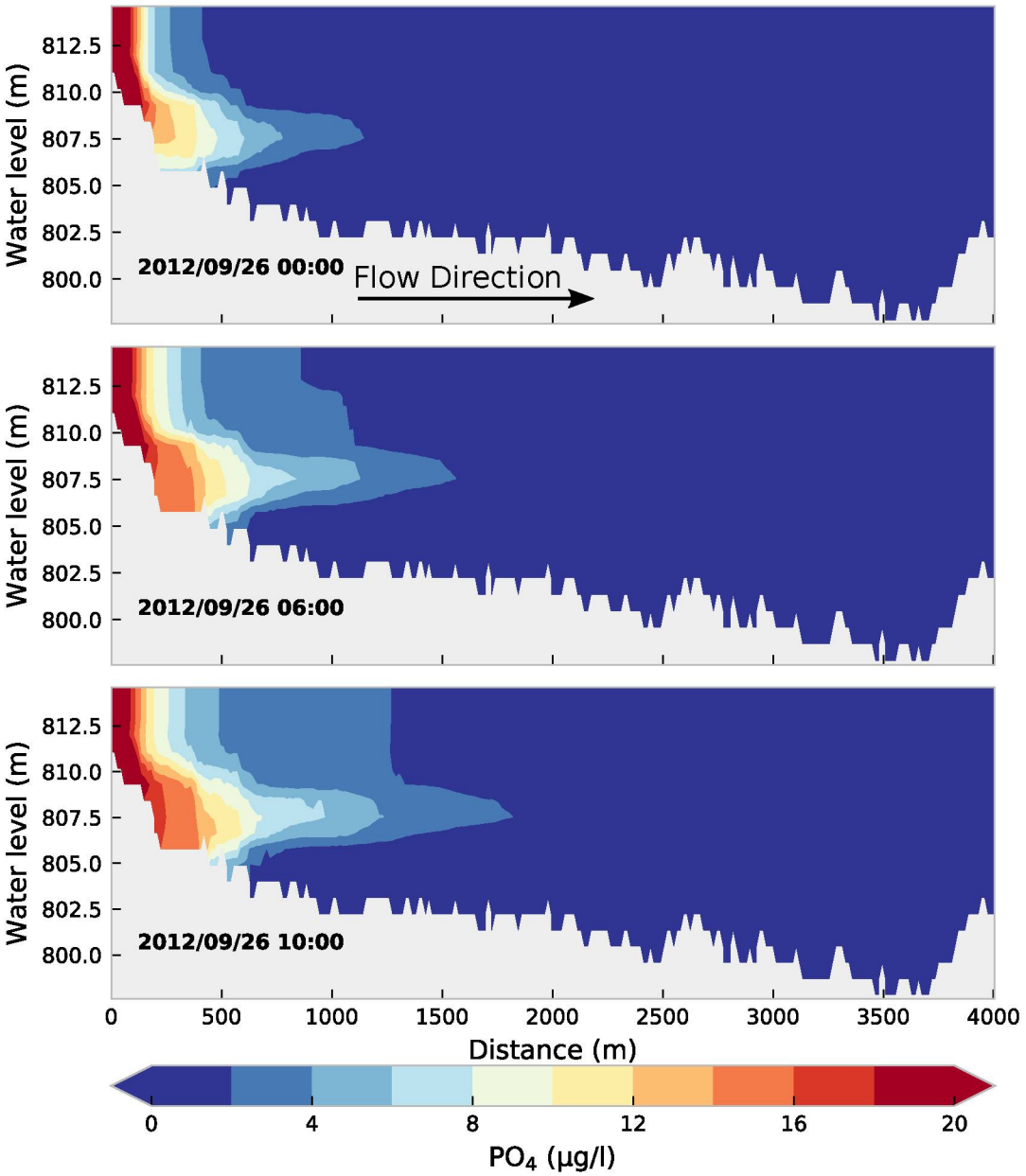

Figure 63 – Orthophosphate distribution during Event 4. The time of maximum discharge is presented in the plot at top, 6 hours after the peak in the middle, and 10 hours after the peak at the bottom.

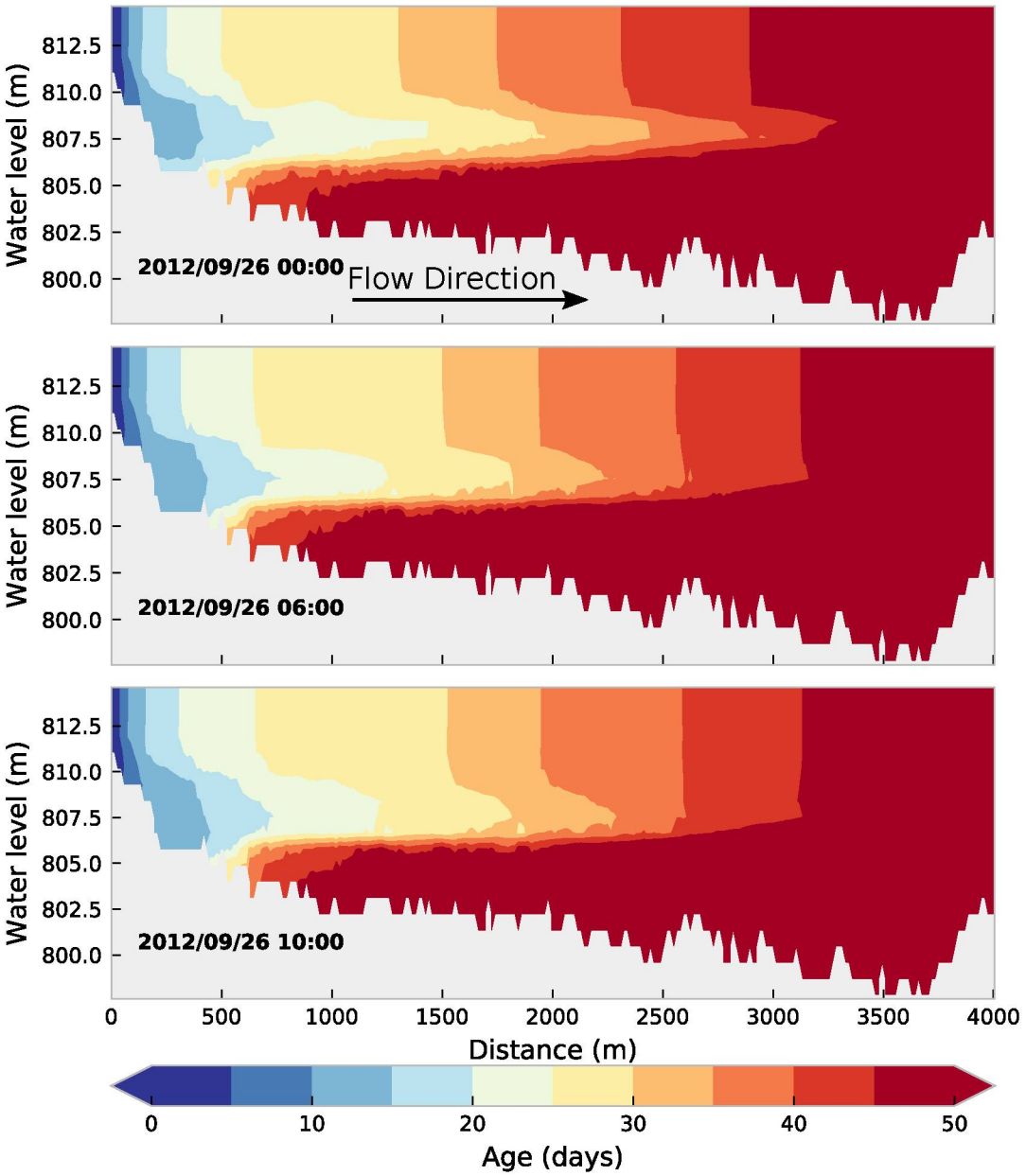

Figure 64 – Water Age distribution during Event 4. The time of maximum discharge is presented in the plot at top, 6 hours after the peak in the middle, and 10 hours after the peak at the bottom.

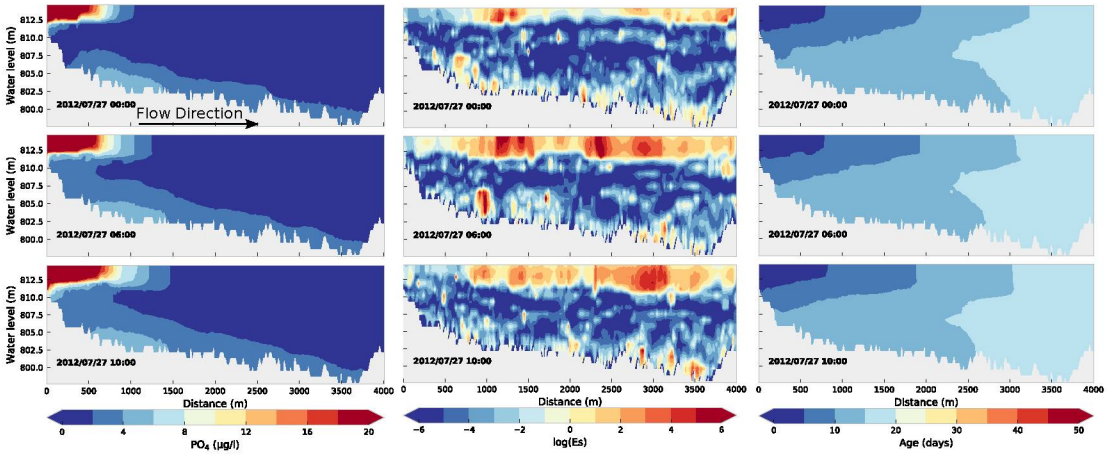

Figure 65 – Orthophosphate, estuary number, and water age distribution during Event 1. The time of maximum discharge is presented in the plot at the top, 6 hours after the peak in the middle, and 10 hours after the peak at the bottom.

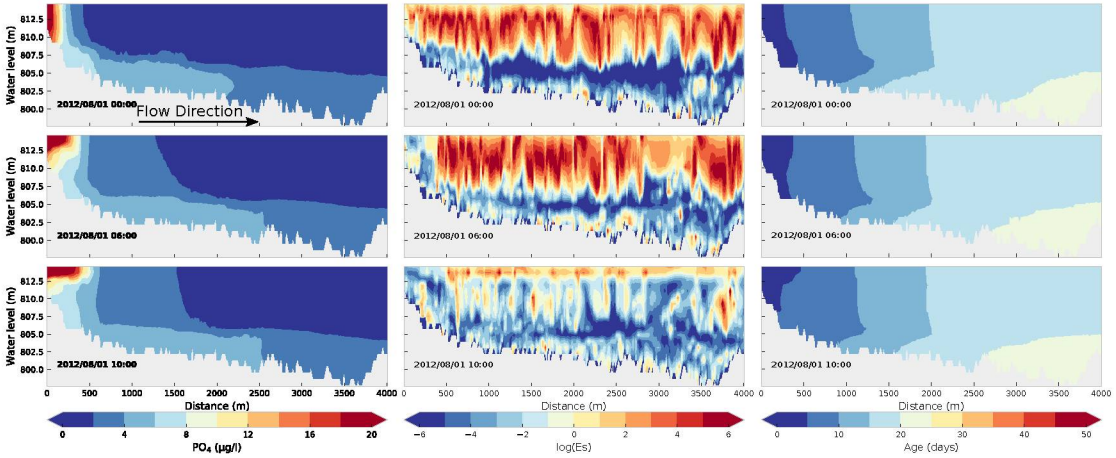

Figure 66 – Orthophosphate, estuary number, and water age distribution during Event 2. The time of maximum discharge is presented in the plot at top, 6 hours after the peak in the middle, and 10 hours after the peak at the bottom.

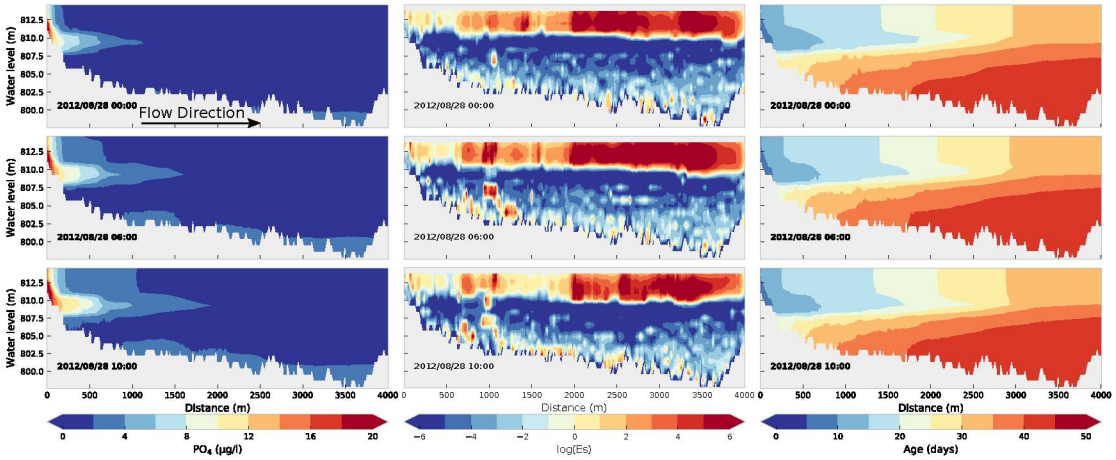

Figure 67 – Orthophosphate, estuary number, and water age distribution during Event 3. The time of maximum discharge is presented in the plot at top, 6 hours after the peak in the middle, and 10 hours after the peak at the bottom.

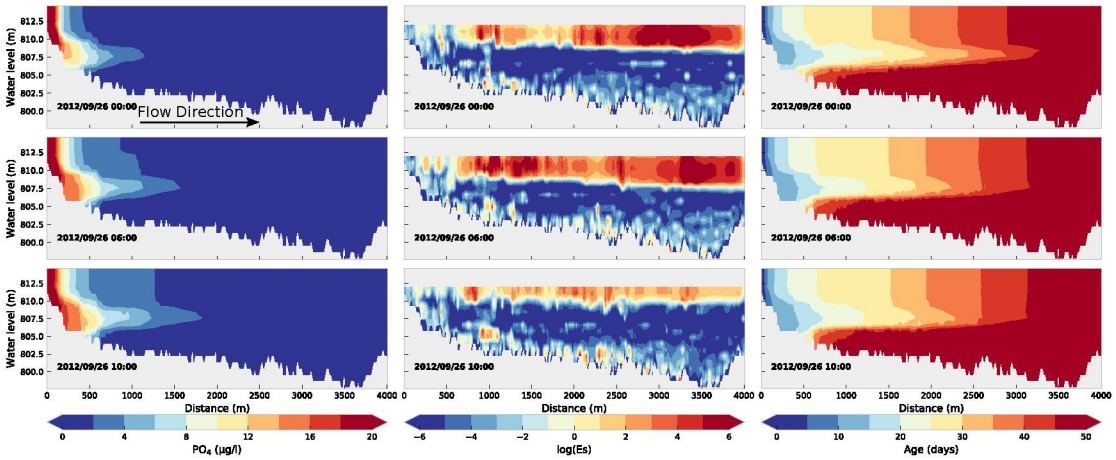

Figure 68 – Orthophosphate, estuary number, and water age distribution during Event 4. The time of maximum discharge is presented in the plot at top, 6 hours after the peak in the middle, and 10 hours after the peak at the bottom.

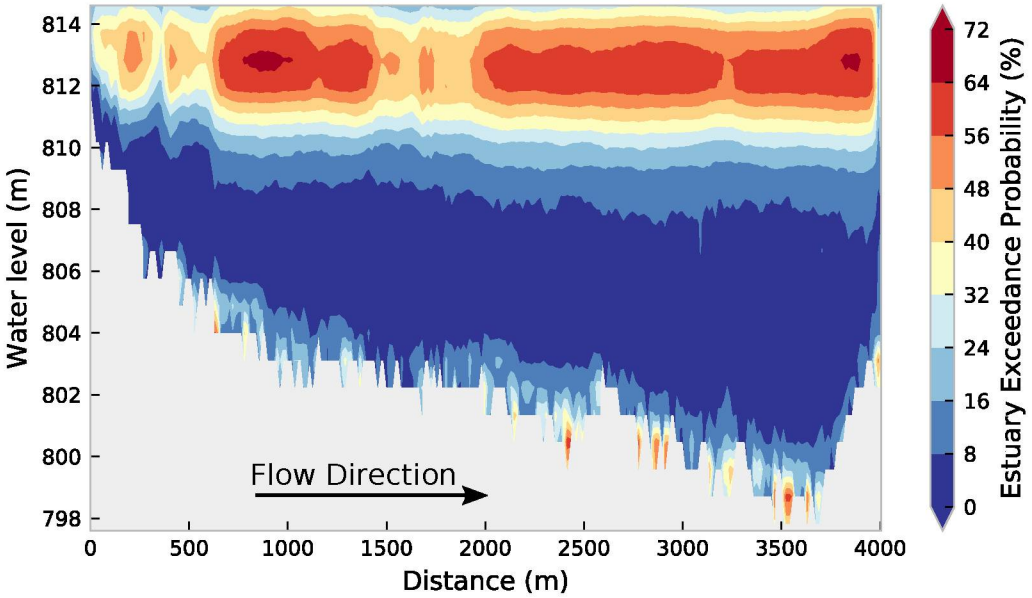

Figure 69 – Exceedance probability for estuary number, i.e. the percentage of the simulation period where estuary number was higher than 1.

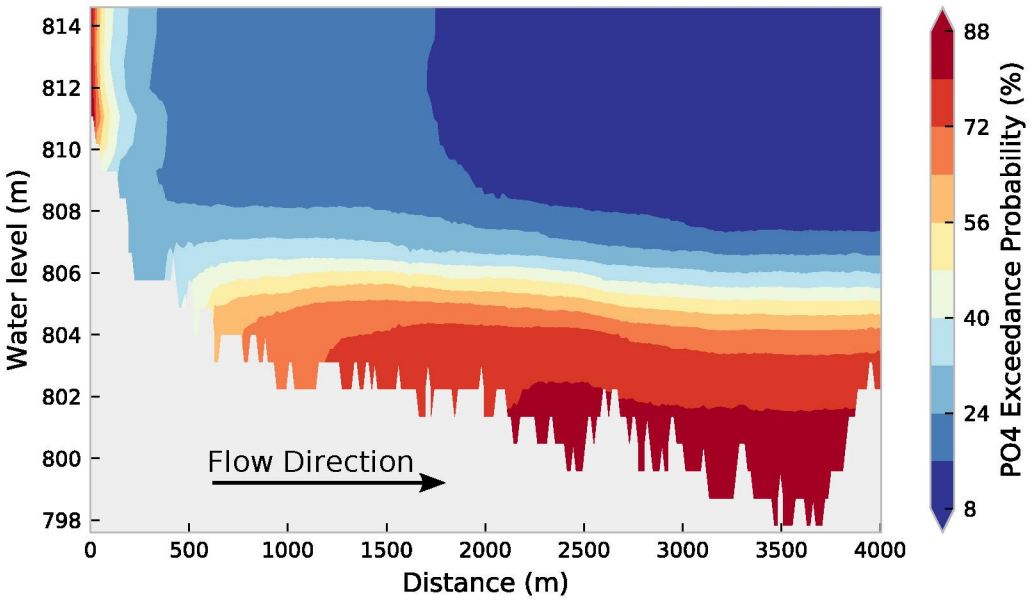

Figure 70 – Exceedance probability for orthophosphate, i.e. the percentage of the simulation period where orthophosphate was higher than 10 μg/l.

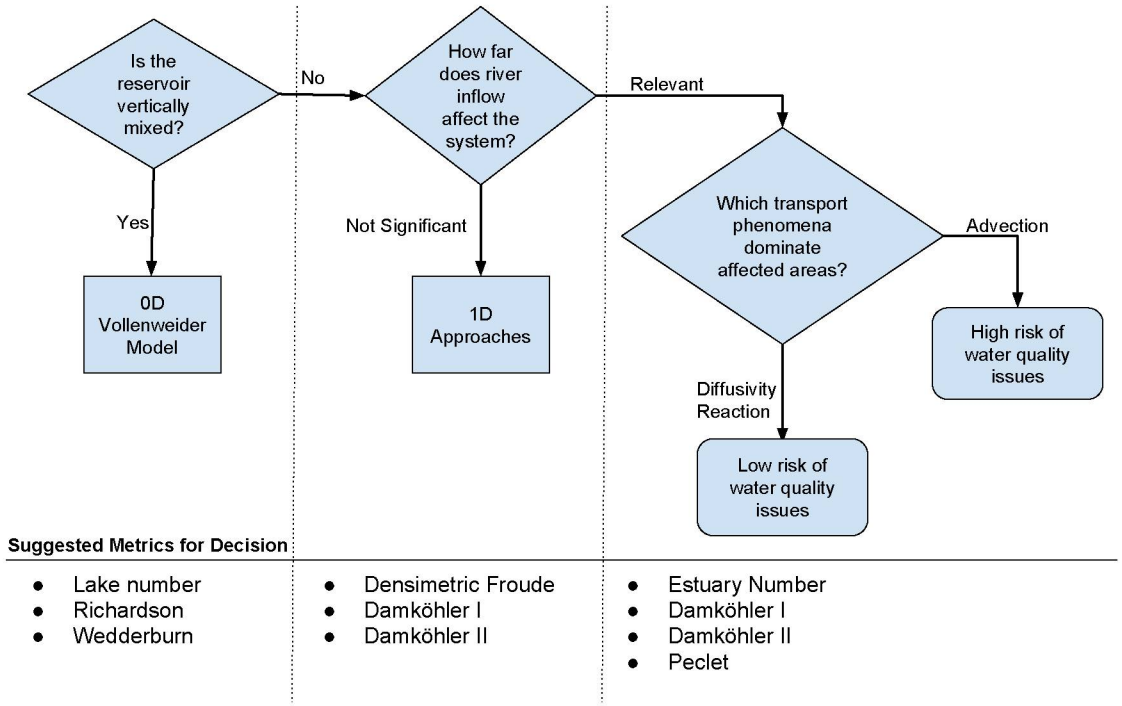

Figure 71 – Potential decision tree model based on the authors experience and results from this thesis. The aim of this model is to choose the right assessment tool for water quality. The decision is made based on metrics indicating the vertical mixing, river inflow dynamics, and dominant transport phenomena.

5 CONCLUSIONS

Previous works on reservoir water quality analysis used mainly descriptions of external processes to characterize or assess the system. Typical examples are the Lake Number and residence time, which were linked to water quality through the Vollenweider plot for example. The novelty of the presented approach is the assessment based on internal processes and using the external processes as boundary conditions only. A comprehensive list of metrics was derived from dimensional analysis, and three principle metrics were considered the most suitable for a non-uniform and unsteady environment regarding the linking of the physicochemical process and water quality aspects.

The three non-dimensional numbers were Estuary, Damköhler I and Damköhler II which showed a relationship with water quality especially regarding maximum concentration. The link of those numbers with water quality was quantitatively and qualitatively analyzed and assessed using analytical methods and a case study.

This link not only allows to classify the system characteristics in terms of water quality characteristics and concentration but also in terms of dominant processes. Results showed that reaction and diffusion processes dominate mass flux transfers in the system when estuary number is greater than one. In those cases, Damköhler II is a relevant spatial metric which is proportional to the location where fluxes are in equilibrium. The advective processes dominate the system when estuary is lower than one, in those cases, Damköhler I is a relevant spatial metric.

The Estuary number was identified as a new and original key metric because of its relationship with shape parameters (initial dilution and recovery rate) from the one-dimensional solutions of the ADRE. Higher estuary numbers relate to systems with higher initial dilution and recovery rates.

The applications of estuary number were evaluated through three-dimensional modeling of hydrodynamics and water quality for the assessment of eutrophication. River water entering the reservoir, rich in nutrients, was assessed qualitatively through the estuary number. Two classes, advective and diffusive/reactive were estimated varying in space and time. The plume of river water reached farther regions where and when the

estuary number was more advective during a flood event. The concentrations had a stronger reduction on concentrations in regions classified as diffusive. The analytically found non-dimensional numbers and the proposed classification scheme thus showed to be an important and useful metric for reservoir water quality assessment. This even allowed to propose an assessment scheme as illustrated in Figure 71. Thus, they have the potential to guide the choice of the right tool for a reservoir through, for example, a decision tree like model, to decide whether and when to use more-dimensional or water quality models.

Moreover, another great advantage of using non-dimensional metrics has been illustrated by the similarity analysis. There model/prototype similarity can be achieved through estuary number and Damköhler number. The concentration dynamics was similar when estuary and Damköhler number between model and prototype were equal. The numbers thus can be used to up or downscale measurements or model results of differently sized reservoirs.

5.1 RECOMMENDATIONS

In this section, there is a list of recommendations for future works or just insights verified during the construction of the thesis.

- The results of this thesis are predominantly based on analytic and modeling approaches, thus experimental analysis in field and lab scale are recommended to improve the classification schemes and to validate spatial and temporal extents of affected regions to provide even more evidence of the importance of Estuary number.

- Sink and sources terms were not specifically considered. This might be important for the analysis of systems with high internal loading or similar processes. It is recommended to adopt the herein proposed schemes in that regard, for example using the sediment as source and analyzing the process relevance with the non-dimensional numbers with a focus on vertical transport;

- The attention herein was put on the effects of metrics on maximum concentration, however other parameters related to water quality may be investigated by further

studies, e.g. mean concentration.

- Test estuary and Damköhler non-dimensional numbers for comparing reservoirs and/or experiments as a metric of similarity relation between physical model and prototypes or large and small lakes;
- Explore and improve the framework proposed herein in terms of water quality management and assessment.

5.2 TECHNICAL AND SCIENTIFIC CONTRIBUTIONS

The following documents were published during the development of this thesis:

- 2015 – **36th IAHR World Congress**, "Interpretation and Applicability of Residence Time in Reservoir", Authors: Julio W. Y Bernardo, Tobias Bleninger.
- 2015 – **36th IAHR World Congress**, "MATHEMATICAL MODELING OF GHG BALANCE IN A SUBTROPICAL RESERVOIR IN SOUTH BRAZIL" Authors: MÄNNICH, M. ; RESENDE, J. F. ; FERNANDES, C. V. S. ; BERNARDO, J. W. Y. ; BLENINGER, T. B..
- 2015 – **XXI Simpósio Brasileiro de Recursos Hídricos**, "Relevance Indicator of Nutrient Load within Reservoir Caused by Rainfall Events", Authors: Julio W. Y Bernardo, Cristovão V. S. Ferndes, M. Mannich, Tobias Bleninger.
- 2015 – **XXI Simpósio Brasileiro de Recursos Hídricos**, "REDE SEM FIO DE SENSORES APLICADA NO MONITORAMENTO INTELIGENTE DE RESERVATÓRIOS", Authors: NADAS, J. P. B. ; BRAGA, S. M. ; BRAGA, A. S. ; BERNARDO, J. W. Y.
- 2015 – **XXI Simpósio Brasileiro de Recursos Hídricos**, "MODELAGEM HIDRODINÂMICA PARA O DERROCAMENTO DO RIO TOCANTINS: PEDRAL DO LOURENÇO", Authors: TOMAS, G. P. ; BERNARDO, J. W. Y. ; RATTON, P. ; BLENINGER, T. B. ; GODOY, P.
- 2015 – **Specialist Conference on Natural Organic Matter in Drinking Water**, "Analysis of anthropogenic and natural sources in the characterization of

organic matter in rivers and reservoirs", Authors: M. M. Santos, H. G. Knapik, C. V. S. Fernandes, J. C. R. Azevedo, J. W. Y. Bernardo

- 2015 – **Revista Brasileira de Recursos Hídricos**, "CICLAR: Modelo 0D para Dinâmica de Carbono em Lagos e Reservatórios", Authors: MANNICH, M. ; RESENDE, J. F. ; FERNANDES, C. V. S. ; BERNARDO, J. W. Y. ; ZAHN, E. ; BLENINGER, T.

- 2016 – **19th International Physical Processes in Natural Waters Workshop**, "Non-uniformity of Residence time in a Brazilian Reservoir", Authors: Julio W. Y Bernardo, Tobias Bleninger.

- 2016 – **19th International Physical Processes in Natural Waters Workshop**, "A hydrodynamic approach to sediment distribution verified by hydroacoustic seabed classification in a complex shaped reservoir". Authors: HILGERT, S. ; BERNARDO, J. W. Y. ; BOUTON, N. ; BLENINGER, T. ; FUCHS, S.

- 2016 – **19th International Physical Processes in Natural Waters Workshop**, "Daily variation of CO2 fluxes in two Brazilian sub-tropical reservoirs." Authors: MANNICH, M. ; Fernandes, C. V. S. ; BERNARDO, J. W. Y. ; BLENINGER, T.

- 2016 – **XXXVII Ibero-Latin American Congress on Computational Methods in Engineering**, "EVOLUTION OF PERMEABLE INCRUSTRATIONS GEOMETRIES IN TISSUES VIA GENETIC ALGORITHM", Authors: RESENDE, J. F. ; BERNARDO, J. W. Y. ; ERRERA, M. R. . 2016, Brasilia.

- 2017 – **AMBIO** "Assessment of long-term changes in carbon stock by construction of hydropower reservoirs" Authors: Julio W. Y. Bernardo, M. Mannich, Stephan Hilgert, Cristovão V. S. Fernandes, Tobias Bleninger.

- 2017 – **European Geosciences Union General Assembly 2017**, "Three dimensional heat transport modeling in Vossoroca reservoir.", Authors: POLLI, B. A. ; BERNARDO, J. W. Y. ; HILGERT, S. ; BLENINGER, T. B.

- 2018 – **INTERNATIONAL JOURNAL OF ADVANCED ENGINEERING RESEARCH AND SCIENCE**, "Feasibility and Environmental Sustainability

of a 103.5 kWp floating Photovoltaic Electrical System with a Case Study in a Hydroelectric Power Plant, Santa Clara Hpp, Located in the South of Brazil Region.", Authors: PORTELLA, KLEBER FRANKE ; PALUDO, RODRIGO ; CARNEIRO, GELSON LUIZ ; BERNARDO, JÚLIO WERNER YOSHIOKA ; SIECIECHOWICZ, MARIANNE SCHAEFER FRANÇA ; BRAGANÇA, MARIANA D'OREY GAIVÃO PORTELLA ; ARRUDA, NICOLE MACHUCA BRASSAC DE ; ALBERTI, EMERSON LUIZ ; FR, AUGUSTUS CAESER.

- 2018 – (Submitted) **International Journal of Heat and Mass Transfer**, "....", Authors: Bernardo, J.W.Y. and Bleninger, T.

The following list describes routines and technical installations developed during the development of this thesis:

- Some open source code at GitHub (https://github.com/juliowerner);
- Graphical user interface to run Delft-3d model in parallel;
- Development of a low energy consumption datalogger in LME;
- Instrumentation of Vossoroca's reservoir;
- Temperature and level sensors deployed at the main inlet;
- High spatial resolution chain of thermistors;
- Basic setup of Delft3d Model for Vossoroca Reservoir;

REFERENCES

AFZAL, A.; ANSARI, Z.; FAIZABADI, A. R.; RAMIS, M. Parallelization strategies for computational fluid dynamics software: state of the art review. **Archives of Computational Methods in Engineering**, Springer, v. 24, n. 2, p. 337–363, 2017.

ALOSAIRI, Y.; IMBERGER, J.; FALCONER, R. A. Mixing and flushing in the persian gulf (arabian gulf). **Journal of Geophysical Research: Oceans**, v. 116, n. 3, p. 1–14, 2011. ISSN 21699291.

ANA. **Diretrizes para Estudo de Prognóstico de Qualidade da Água**. [S.l.], 2010. Disponível em: <http://arquivos.ana.gov.br/institucional/sof/DiretrizesparaEstudoPrognosticodeQualidadedaAgua.pdf>.

ANA. **Conjuntura dos recursos hídricos no Brasil: 2013**. [S.l.], 2013.

ANDUTTA, F. P.; HELFER, F.; MIRANDA, L. B. de; DELEERSNIJDER, E.; THOMAS, C.; LEMCKERT, C. An assessment of transport timescales and return coefficient in adjacent tropical estuaries. **Continental Shelf Research**, Elsevier, n. May, 2016. ISSN 02784343. Disponível em: <http://linkinghub.elsevier.com/retrieve/pii/S0278434316302552>.

ANDUTTA, F. P.; KINGSFORD, M. J.; WOLANSKI, E. 'sticky water' enables the retention of larvae in a reef mosaic. **Estuarine, Coastal and Shelf Science**, Elsevier Ltd, v. 101, p. 54–63, 2012. ISSN 02727714. Disponível em: <http://dx.doi.org/10.1016/j.ecss.2012.02.013>.

AVIGLIONE, J. ao H.; KIIHLL, L. R. B.; CARAMORI, P. H.; OLIVEIRA, D. **Cartas climáticas do Estado do Paraná**. [S.l.].

BARROSO, G. F.; GONÇALVES, M. A.; GARCIA, F. d. C. The morphometry of lake palmas, a deep natural lake in brazil. **PloS one**, Public Library of Science, v. 9, n. 11, p. e111469, 2014.

BERNARDO, J. W. Y. **Interpretations and Applicability of Residence Time In Reservoirs**. Dissertação (Mestrado) — Universidade Federal do Paraná, 2013.

BERNARDO, J. W. Y.; BLENINGER, T. Interpretation and applicability of residence times in reservoirs. In: **E-proceedings of the 36th IAHR World Congress**. The Hague: IAHR, 2015. p. 28–31.

BIRKEL, C.; SOULSBY, C. Linking tracers, water age and conceptual models to identify dominant runoff processes in a sparsely monitored humid tropical catchment. **Hydrological Processes**, v. 30, n. 24, p. 4477–4493, 2016. ISSN 10991085.

BOLIN, B.; RODHE, H. A note on the concepts of age distribution and transit time in natural reservoirs. **Tellus**, Wiley Online Library, v. 25, n. 1, p. 58–62, 1973.

BROECKER, W. S.; PENG, T.-H.; TRUMBORE, S.; BONANI, G.; WOLFLI, W. The distribution of radiocarbon in the glacial ocean. **Global Biogeochemical Cycles**, Wiley Online Library, v. 4, n. 1, p. 103–117, 1990.

BRYE, B. de; BRAUWERE, A. de; GOURGUE, O.; DELHEZ, E. J. M.; DELEERSNIJDER, E. Reprint of water renewal timescales in the scheldt estuary. **Journal of Marine Systems**, Elsevier B.V., v. 128, p. 3–16, 2013. ISSN 09247963. Disponível em: <http://dx.doi.org/10.1016/j.jmarsys.2012.03.002>.

CARLSON, R. E. A trophic state index for lakes1. **Limnology and oceanography**, Wiley Online Library, v. 22, n. 2, p. 361–369, 1977.

CASTELLANO, L.; AMBROSETTI, W.; BARBANTI, L.; ROLLA, A. The residence time of the water in lago maggiore (n. italy): first results from an eulerian-lagrangian approach. **Journal of Limnology**, v. 69, n. 1, p. 15–28, 2010.

CATALÁN, A. N.; MARCÉ, R.; KOTHAWALA, D. N.; TRANVIK, L. J. Organic carbon decomposition rates controlled by water retention time across inland waters. **Nature Geoscience**, Nature Publishing Group, v. 9, n. May, p. 501 —- 504, 2016. ISSN 1752-0894.

CHAPRA, S. C. **Surface water-quality modeling**. [S.l.]: Waveland press, 2008.

CLARIVATE. **Web of Science**. 2018. Disponível em: <http://www.webofknowledge.com/>.

CONAMA, R. 357, de 17 de março de 2005. **Conselho Nacional do Meio Ambiente-CONAMA**, v. 357, 2005.

DANCKWERTS, P. Continuous flow systems: Distribution of residence times. **Chemical Engineering Science**, v. 2, n. 1, p. 1–13, 1953. ISSN 00092509.

DEFNE, Z.; GANJU, N. K. Quantifying the residence time and flushing characteristics of a shallow, back-barrier estuary: Application of hydrodynamic and particle tracking models. **Estuaries and Coasts**, Springer, v. 38, n. 5, p. 1719–1734, 2015.

DELEERSNIJDER, E.; CAMPIN, J. M.; DELHEZ, E. J. M. The concept of age in marine modelling i. theory and preliminary model results. **Journal of Marine Systems**, v. 28, n. 3-4, p. 229–267, 2001. ISSN 09247963.

DELEERSNIJDER, E.; DELHEZ, E.; BECKERS, J. M. Some properties of generalized age-distribution equations in fluid dynamics. **SIAM Journal on Applied Mathematics**, v. 61, n. 5, p. 1526–1544, 2001. ISSN 0036-1399.

DELEERSNIJDER, E.; DELHEZ, E. J.; MOUCHET, A. **CART**. 2018. Disponível em: <www.climate.be/CART>.

DELEERSNIJDER, E.; MOUCHET, A.; DELHEZ, E.; BECKERS, J.-M. Transient behaviour of water ages in the world ocean. **Mathematical and Computer Modelling**, v. 36, n. 1-2, p. 121–127, 2002. ISSN 08957177. Disponível em: <http://www.sciencedirect.com/science/article/pii/S0895717702001085>.

DELESALLE, B.; SOURNIA, A. Residence time of water and phytoplankton biomass in coral reef lagoons. **Continental Shelf Research**, Elsevier, v. 12, n. 7-8, p. 939–949, 1992.

DELHEZ, E. J.; CAMPIN, J.-M.; HIRST, A. C.; DELEERSNIJDER, E. Toward a general theory of the age in ocean modelling. **Ocean Modelling**, v. 1, n. 1, p. 17–27, 1999. ISSN 14635003. Disponível em: <http://www.sciencedirect.com/science/article/pii/S1463500399000037>.

DELHEZ, É. J. M. On the concept of exposure time. **Continental Shelf Research**, Elsevier, v. 71, p. 27–36, 2013. ISSN 02784343.

DELHEZ, É. J. M.; BRYE, B. de; BRAUWERE, A. de; DELEERSNIJDER, É. Residence time vs influence time. **Journal of Marine Systems**, v. 132, p. 185–195, 2014. ISSN 09247963.

DELTARES. **Delft3D-FLOW: User Manual**. Delft, Holanda, 2015.

DU, J.; SHEN, J. Decoupling the influence of biological and physical processes on the dissolved oxygen in the chesapeake bay. **Journal of Geophysical Research: Oceans**, p. 1–16, 2015.

EPE. Plano decenal de expansão de energia 2023. Ministério de Minas e Energia, p. 434, 2014.

EVANS, C. D.; FUTTER, M. N.; MOLDAN, F.; VALINIA, S.; FROGBROOK, Z.; KOTHAWALA, D. N. Variability in organic carbon reactivity across lake residence time and trophic gradients. **Nature Geoscience**, Nature Publishing Group, v. 10, n. 11, p. 832, 2017.

FUENTE, M. D. L.; SKINNER, L.; CALVO, E.; PELEJERO, C.; CACHO, I. Increased reservoir ages and poorly ventilated deep waters inferred in the glacial eastern equatorial pacific. **Nature communications**, Nature Publishing Group, v. 6, p. 7420, 2015.

GENUCHTEN, M. T. van; ALVES, W. J. **Analytical Solutions of the One-dimensional Convective-Dispersive-Solute Transport Equation**. [S.l.], 1982. 151 p.

GONCALVES, M. A.; GARCIA, F. C.; BARROSO, G. F. Morphometry and mixing regime of a tropical lake: Lake nova (southeastern brazil). **Anais da Academia Brasileira de Ciências**, SciELO Brasil, v. 88, n. 3, p. 1341–1356, 2016.

GOOGLE. **Google Scholar**. 2018. Disponível em: <http://scholar.google.com/>.

HÅKANSON, L. Models to predict secchi depth in small glacial lakes. **Aquatic sciences**, Springer, v. 57, n. 1, p. 31–53, 1995.

HARE, J. A.; CHURCHILL, J. H.; COWEN, R. K.; BERGER, T. J.; CORNILLON, P. C.; DRAGOS, P.; GLENN, S. M.; GOVONI, J. J.; LEE, T. N. Routes and rates of larval fish transport from the southeast to the northeast united states continental shelf. **Limnology and Oceanography**, Wiley Online Library, v. 47, n. 6, p. 1774–1789, 2002.

HUIJGEVOORT, M. H. van; TETZLAFF, D.; SUTANUDJAJA, E. H.; SOULSBY, C. Using high resolution tracer data to constrain water storage, flux and age estimates in a spatially distributed rainfall-runoff model. **Hydrological Processes**, v. 30, n. 25, p. 4761–4778, 2016. ISSN 10991085.

IAP. **Monitoramento da Qualidade das Águas dos Reservatórios do Estado do Paraná, no Período de 1999 a 2004**. [S.l.], 2004.

IAP. **Relatório da Qualidade das Águas dos Reservatórios do Estado do Paraná**. Parana„ 2017.

ICOLD. **Dams and the World's Water**. [S.l.]: ICOLD, 2007. 68 p. ISSN 0534-8293.

JIANG, C.; LIU, Y.; LONG, Y.; WU, C. Estimation of residence time and transport trajectory in tieshangang bay, china. **Water**, Multidisciplinary Digital Publishing Institute, v. 9, n. 5, p. 321, 2017.

JONES, A. E.; HODGES, B. R.; MCCLELLAND, J. W.; HARDISON, A. K.; KEVAN, B. Residence time-based classification of surface water systems index terms and keywords. **Water Resources Research**, v. 53, n. 7, 2017.

JOUON, A.; DOUILLET, P.; OUILLON, S.; FRAUNIE, P. Calculations of hydrodynamic time parameters in a semi-opened coastal zone using a 3d hydrodynamic model. v. 26, p. 1395–1415, 2006.

KEREKES, J. The index of lake basin permanence. **International Review of Hydrobiology**, Wiley Online Library, v. 62, n. 2, p. 291–293, 1977.

KUMAR, A.; JAISWAL, D. K.; KUMAR, N. Analytical solutions to one-dimensional advection-diffusion equation with variable coefficients in semi-infinite media. **Journal of Hydrology**, Elsevier B.V., v. 380, n. 3-4, p. 330–337, 2010. ISSN 00221694. Disponível em: <http://dx.doi.org/10.1016/j.jhydrol.2009.11.008>.

LARGIER, J.; WOLANSKI, E.; IMBERGER, J.; HERON, M. The importance of retention zones in the dispersal of larvae. v. 2004, n. 42, p. 105–122, 2004.

LEE, H. S.; CHUNG, S. W.; CHOI, J. K.; MIN, B. H. Feasibility of curtain weir installation for water quality management in daecheong reservoir. **Desalination and Water Treatment**, v. 19, n. 1-3, p. 164–172, 2010. ISSN 1944-3994. Disponível em: <http://www.tandfonline.com/doi/abs/10.5004/dwt.2010.1883>.

LEHNER, B.; LIERMANN, C. R.; REVENGA, C.; VÖRÖMSMARTY, C.; FEKETE, B.; CROUZET, P.; DÖLL, P.; ENDEJAN, M.; FRENKEN, K.; MAGOME, J.; NILSSON, C.; ROBERTSON, J. C.; RÖDEL, R.; SINDORF, N.; WISSER, D. High-resolution mapping of the world's reservoirs and dams for sustainable river-flow management. **Frontiers in Ecology and the Environment**, v. 9, n. 9, p. 494–502, 2011. ISSN 15409295.

LI, Y.; ZHANG, Q.; YAO, J. Investigation of residence and travel times in a large floodplain lake with complex lake-river interactions: Poyang lake (china). **Water**, Multidisciplinary Digital Publishing Institute, v. 7, n. 5, p. 1991–2012, 2015.

LOGAN, J.; ZLOTNIK, V. The convection-diffusion equation with periodic boundary conditions. **Applied mathematics letters**, Elsevier, v. 8, n. 3, p. 55–61, 1995.

LUCAS, L. V.; THOMPSON, J. K.; BROWN, L. R. Why are diverse relationships observed between phytoplankton biomass and transport time? **Limnology and Oceanography**, v. 54, n. 1, p. 381–390, 2009. ISSN 0024-3590.

MAHANTY, M.; MOHANTY, P.; PATTNAIK, A.; PANDA, U.; PRADHAN, S.; SAMAL, R. Hydrodynamics, temperature/salinity variability and residence time in the chilika lagoon during dry and wet period: Measurement and modeling. **Continental Shelf Research**, Elsevier, v. 125, p. 28–43, 2016.

MANNICH, M. **Estimativa de Emissões de Gases de Efeito Estufa em Reservatórios e Lagos - Contribuições para o Monitoramento e Modelagem 1D-Vertical**. 284 p. Tese (Doutorado) — UFPR, 2013.

MARI, X.; ROCHELLE-NEWALL, E.; TORRÉTON, J.-P.; PRINGAULT, O.; JOUON, A.; MIGON, C. Water residence time: A regulatory factor of the dom to pom transfer efficiency. **Limnology and Oceanography**, v. 52, n. 2, p. 808–819, 2007. ISSN 00243590.

MERCIER, C.; DELHEZ, E. J. Diagnosis of the sediment transport in the belgian coastal zone. **Estuarine, Coastal and Shelf Science**, v. 74, n. 4, p. 678–691, 2007. ISSN 02727714.

MONSEN, N. E.; CLOERN, J. E.; LUCAS, L. V.; MONISMITH, S. G. A comment on the use of flushing time, residence time, and age as transport time scales. **Limnology and Oceanography**, Wiley Online Library, v. 47, n. 5, p. 1545–1553, 2002.

MORILLO, S.; IMBERGER, J.; ANTENUCCI, J. Modifying the residence time and dilution capacity of a reservoir by altering internal flow-paths. **International Journal of River Basin Management**, v. 4, n. 4, p. 255–271, 2006. ISSN 18142060.

MOUCHET, A.; CORNATON, F.; DELEERSNIJDER, É.; ÉRIC, É. J. Partial ages: diagnosing transport processes by means of multiple clocks. **Ocean Dynamics**, v. 66, n. 3, p. 367–386, 2016. ISSN 16167228.

MUHTADI, A.; YUNASFI, Y.; MA'RUFI, M.; RIZKI, A. Morphometry and pollution load capacity of lake pondok lapan in langkat regency, north sumatra. **Oseanologi dan Limnologi di Indonesia**, v. 2, n. 2, p. 49–63, 2017.

NAGHETTINI, M.; PINTO Éber José Andrade de. **Hidrologia Estatística**. [S.l.]: CPRM, 2007.

NAUMAN, E. B. Residence time theory. **Industrial and Engineering Chemistry Research**, v. 47, n. 10, p. 3752–3766, 2008. ISSN 08885885.

NEITSCH, S. L.; ARNOLD, J. G.; KINIRY, J. R.; WILLIAMS, J. R. **Soil and water assessment tool theoretical documentation version 2009**. [S.l.], 2011.

ORLOB, G. T.; ROESNER, L. A.; NORTON, W. R. **Mathematical Model for the Prediciton of Thermal Energy Changes in Impoundments**. California, 1969. 190 p.

PEETER A. WUEST, G. P. D. M. I. F. Horizontal mixing in lakes. **Journal of Geophysical Research**, v. 101, n. c8, p. 18361—-18375, 1996.

PILOTTI, M.; SIMONCELLI, S.; VALERIO, G. Computing the transport time scales of a stratified lake on the basis of tonolli's model. **Journal of Limnology**, v. 73, n. 3, 2014. ISSN 1723-8633. Disponível em: <http://www.jlimnol.it/index.php/jlimnol/article/view/jlimnol.2014.897>.

PIONKE, H. B.; GBUREK, W. J.; SHARPLEY, A. N. Critical source area controls on water quality in an agricultural watershed located in the chesapeake basin. **Ecological Engineering**, Elsevier, n. 4, p. 325–335, 2000.

POLLI, B. A.; BERNARDO, J. W.; HILGERT, S.; BLENINGER, T. Three dimensional heat transport modeling in vossoroca reservoir. In: **European Geosciences Union General Assembly**. Viena: EGU, 2017. v. 19.

QI, H.; LU, J.; CHEN, X.; SAUVAGE, S.; SANCHEZ-PÉREZ, J. M. Water age prediction and its potential impacts on water quality using a hydrodynamic model for poyang lake, china. **Environmental Science and Pollution Research**, Environmental Science and Pollution Research, v. 23, n. 13, p. 13327–13341, 2016. ISSN 16147499.

RAST, W.; LEE, G. F. Summary analysis of the north american (us portion) oecd eutrophication project: Nutrient loading-lake response relationships and trophic state indices. n. January, 1978.

RAYSON, M. D.; GROSS, E. S.; HETLAND, R. D.; FRINGER, O. B. Time scales in galveston bay: An unsteady estuary. **Journal of Geophysical Research: Oceans**, n. 2, p. 1–18, 2016. ISSN 21699291.

REN, Y.; LIN, B.; SUN, J.; PAN, S. Predicting water age distribution in the pearl river estuary using a three-dimensional model. **Journal of Marine Systems**, Elsevier B.V., v. 139, p. 276–287, 2014. ISSN 09247963.

RENNELLA, A. M.; QUIRÓS, R. The effects of hydrology on plankton biomass in shallow lakes of the pampa plain. **Hydrobiologia**, v. 556, n. 1, p. 181–191, 2006. ISSN 00188158.

ROGERS, J. S.; MONISMITH, S. G.; FRINGER, O. B.; KOWEEK, D. A.; DUNBAR, R. B. A coupled wave-hydrodynamic model of an atoll with high friction: Mechanisms for flow, connectivity, and ecological implications. **Ocean Modelling**, Elsevier, v. 110, p. 66–82, 2017.

RUEDA, F.; MORENO-OSTOS, E.; ARMENGOL, J. The residence time of river water in reservoirs. **Ecological Modelling**, Elsevier, v. 191, n. 2, p. 260–274, 2006.

SALAS, H. J.; MARTINO, P. A simplified phosphorus trophic state model for warm-water tropical lakes. **Water Research**, Elsevier, v. 25, n. 3, p. 341–350, 1991.

SALAS, H. J.; MARTINO, P. et al. Metodologias simplificadas para la evaluacion de eutroficacion en lagos calidos tropicales. In: **Metodologías simplificadas para la evaluación de eutroficación en lagos cálidos tropicales**. [S.l.]: CEPIS, 1990.

SCHINDLER, D. W. Recent advances in the understanding and management of eutrophication. **Limnology and Oceanography**, v. 51, n. 1, p. 356–363, 2006. ISSN 00243590.

SCHINDLER, D. W. The dilemma of controlling cultural eutrophication of lakes. **Proceedings of the Royal Society B: Biological Sciences**, v. 279, n. 1746, p. 4322–4333, 2012. ISSN 1471-2954.

SEITZINGER, S. P.; MAYORGA, E.; BOUWMAN, A. F.; KROEZE, C.; BEUSEN, A. H. W.; BILLEN, G.; Van Drecht, G.; DUMONT, E.; FEKETE, B. M.; GARNIER, J.; HARRISON, J. A. Global river nutrient export: A scenario analysis of past and future trends. **Global Biogeochemical Cycles**, v. 24, n. 2, 2010. ISSN 08866236.

SILVA, C. P.; MARTI, C. L.; IMBERGER, J. Horizontal transport, mixing and retention in a large, shallow estuary: Río de la plata. **Environmental Fluid Mechanics**, v. 14, n. 5, p. 1173–1197, 2014. ISSN 15677419.

SILVA, C. P.; MARTI, C. L.; IMBERGER, J. Mitigating the effects of high biomass algal blooms on the drinking water intakes of the city of buenos aires, argentina. **Journal of Hydraulic Research**, v. 1686, n. January, p. 1–15, 2014. ISSN 0022-1686. Disponível em: <http://dx.doi.org/10.1080/00221686.2014.950609{\%}5Cnhttp://www.tandfonline.com/doi/abs/10.1080/00221686.2014.950>.

SMITS, J. G.; BEEK, J. K. van. Eco: a generic eutrophication model including comprehensive sediment-water interaction. **PloS one**, Public Library of Science, v. 8, n. 7, p. e68104, 2013.

SOBALLE, D. M.; KIMMEL, B. L. A large-scale comparison of factors influencing phytoplankton abundance in rivers , lakes , and impoundments. **Ecological Society of America**, v. 68, n. 6, p. 1943–1954, 1987. Disponível em: <http://www.jstor.org/stable/1939885>.

SPERLING, E. von. **Morfologia de lagos e represas**. [S.l.]: DESA/UFMG, 1999.

STROBEL, V. **academic-keyword-occurence**. 2018. Disponível em: <http://doi.org/10.5281/zenodo.1218409>.

STUMM, W.; MORGAN, J. J. **Aquatic chemistry: chemical equilibria and rates in natural waters**. [S.l.]: John Wiley & Sons, 2012. v. 126.

SYMONDS, A. M.; VIJVERBERG, T.; POST, S.; SPEK, B.-J. van der; HENROTTE, J.; SOKOLEWICZ, M. Comparison between mike 21 fm, delft3d and delft3d fm flow models of western port bay, australia. **Coastal Engineering Proceedings**, v. 1, n. 35, p. 11, 2017.

TAKEOKA, H. Fundamental concepts of exchange and transport time scales in a coastal sea. **Continental Shelf Research**, v. 3, n. 3, p. 311–326, 1984. ISSN 02784343.

U.S.EPA. **Water Quality Standards Handbook Chapter 3 : Water Quality Criteria**. [S.l.], 2017. 26 p.

VIERO, D. P.; DEFINA, A. Water age, exposure time, and local flushing time in semi-enclosed, tidal basins with negligible freshwater inflow. **Journal of Marine Systems**, v. 156, n. July 2016, p. 16–29, 2016. ISSN 09247963.

VOLLENWEIDER, R. A. Input-output models with special reference to the phosphorus loading concept in limnology. In: **Conference on Chemical-Ecological Considerations for Defining the Goals of Water Pollution Control**. [S.l.: s.n.], 1975.

WETZEL, R. G. **Limnology: lake and river ecosystems**. [S.l.]: gulf professional publishing, 2001.

WÜEST, A.; LORKE, A. Small-scale hydrodynamics in lakes. **Annual Review of Fluid Mechanics**, v. 35, n. 1, p. 373–412, 2003. ISSN 0066-4189.

ZARFL, C.; LUMSDON, A. E.; BERLEKAMP, J.; TYDECKS, L.; TOCKNER, K. A global boom in hydropower dam construction. **Aquatic Sciences**, v. 77, n. 1, p. 161–170, 2015.

Appendix

APPENDIX A – VOSSOROCA RESERVOIR

Hydrometeorological Description

A weather station has been deployed near the reservoir measuring short-wave incoming radiation, incoming short-wave radiation, air temperature, humidity, wind intensity, wind direction, soil temperature and precipitation. Table 8 presents descriptions of sensors. This station was installed in May 2012 but started to operate only in June 2012. Weather parameters are measured in a frequency of two minutes, the data until February 2015 is presented in Figure 72.

Frequency analysis of wind direction for the period between June 2012 and February 2015 are in Figures 73 and 74. The prevailing wind come from east and the mean velocity in this direction is 1.2 m/s.

Table 8 – Technical information about sensors deployed in weather station.

Equipment	Precision	Range
Tipping Bucket Rain Gauge	± 0.2 mm	0 – 635 mm/hr
Hygrometer	± 1.5 %	0 – 100 %
Resistance Temperature Detector	0.2°C	-40°C – 85 °C
Barometer	± 1 hPa	1 – 1500 hPa
Pyranometer (up and down)		0 – 2000 W/m^2 400 – 1100 nm
Anemometer	±0.3 m/s ±3°	0 – 100 m/s 0 – 360°

Hydrological data was provided by COPEL, it consist by inflow and outflow discharges. Figure 75 shows the data which were used as boundary condition in the model. The water temperature of river were estimated from air temperature through parametric equations from Neitsch et al. (2011).

Bathymetry

The data was measured using two different sets of equipments, each set was used twice totaling four field surveys. The first equipment (SET1) was composed of

EA400 single beam echo sounder, Kongsberg ©and a Global Position Systems (GPS) 1200+, Leica Geosystems ©. The second equipment (SET2) was composed of a single beam echo sounder (SDH-13A) and GPS with Real Time Kinect System (RTK) which provides a better position of GPS coordinates. Figure 77 shows the bathymetry using the complete dataset interpolated in a 10x10m grid. Thus, SET1 had a better precision in water level while SET2 had a better precision in positioning.

Data acquisition was only possible in cooperation with two institutes: *Institut für Wasser und Gewässerentwicklung (IWG)* from Karlsruhe Institute of Techonology and *Laboratório de Geodésia Espacial e Hidrografia (LAGEH)* from Federal University of Paraná (UFPR) .

Water Quality

Environmental agency published a report consolidating water quality parameters from 2001 to 2004 (IAP, 2004). Table 9 shows the water quality parameters presented in that report;

Table 9 – Water quality data provided by environmental agency (IAP) for Vossoroca Reservoir.

Parameter	2001-Jul	2002-Mar	2002-Jul	2003-Out	2004-Mar
Total Phosphorus (mgP/m^3)	28	67	42	11	15
Total Inorganic Nitrogen (mgN/m^3)	420	530	140	190	230
Chlorophyll-a (mg/m^3)	1.92	7.61	9.74	4.36	19.45
Sechi disk depth (m)	1.0	1.30	1.8	1.2	1.5

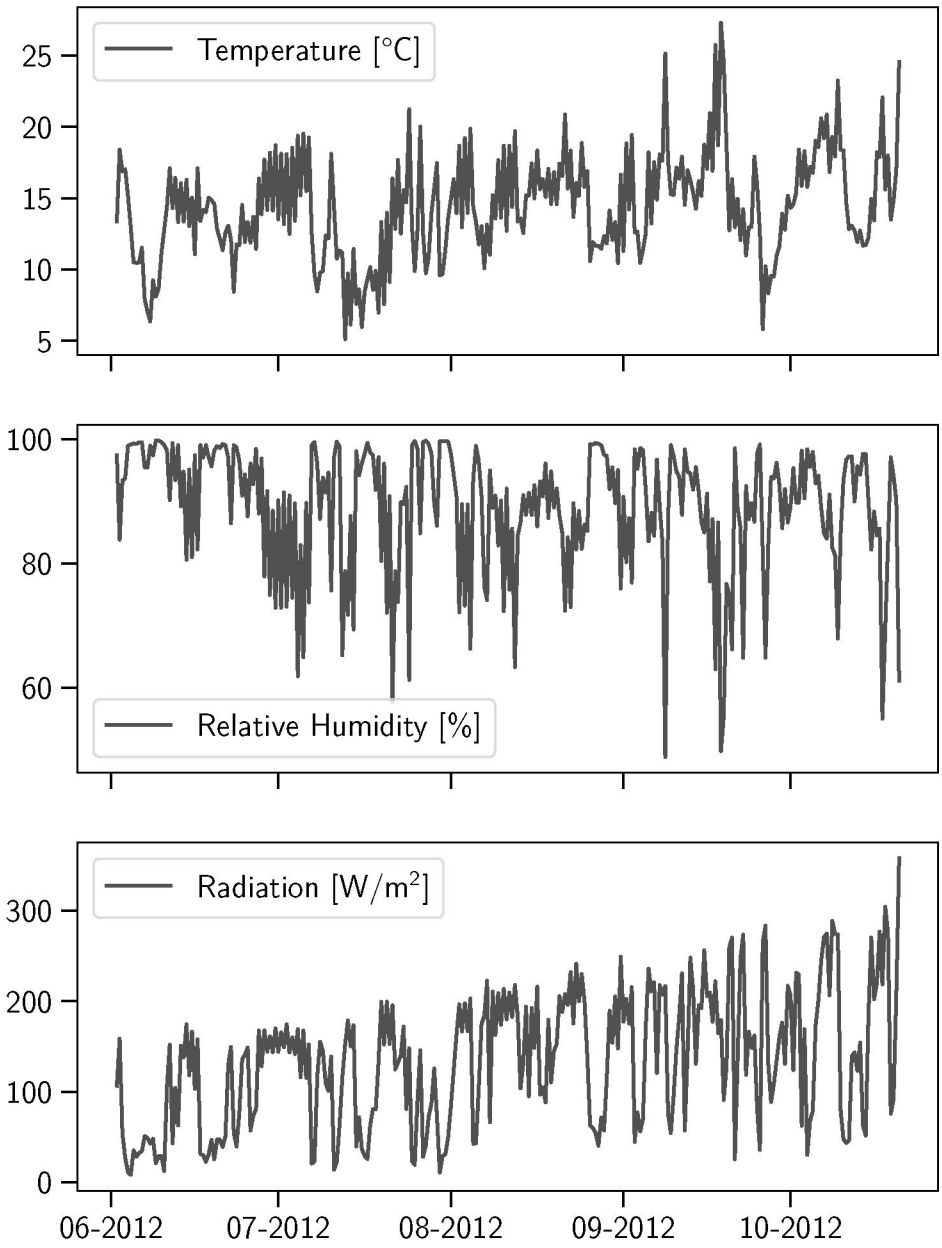

Figure 72 – Thermal boundary conditions from weather station located close to the reservoir.

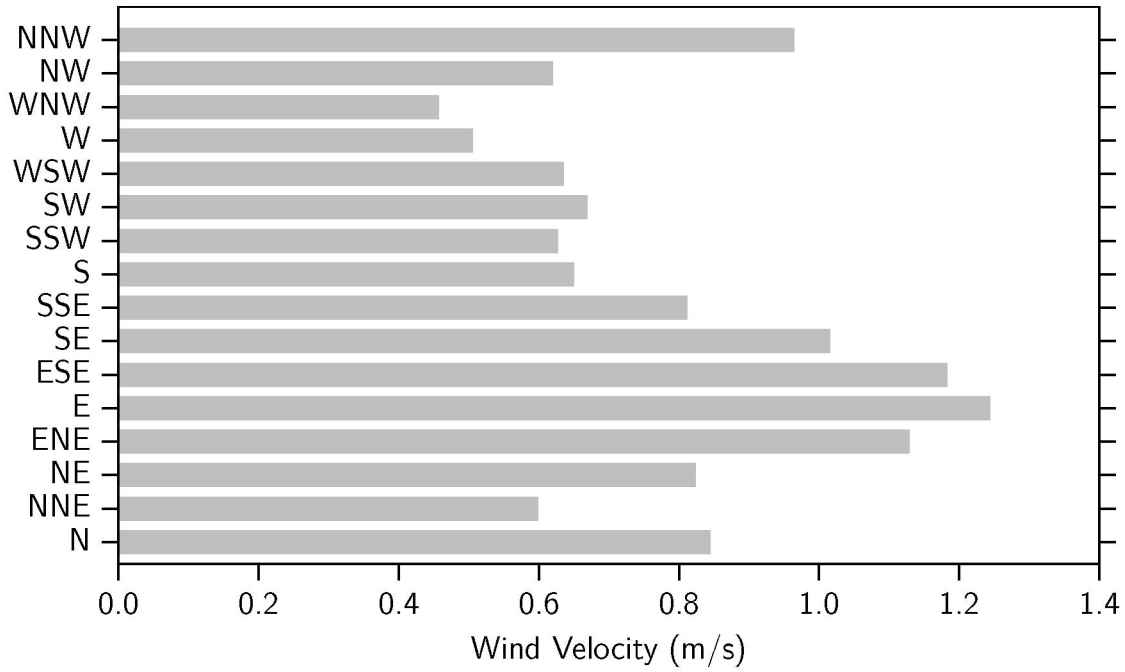

Figure 73 – Vossoroca's average Wind velocity for each direction from Jun/2012 until Feb/2015.

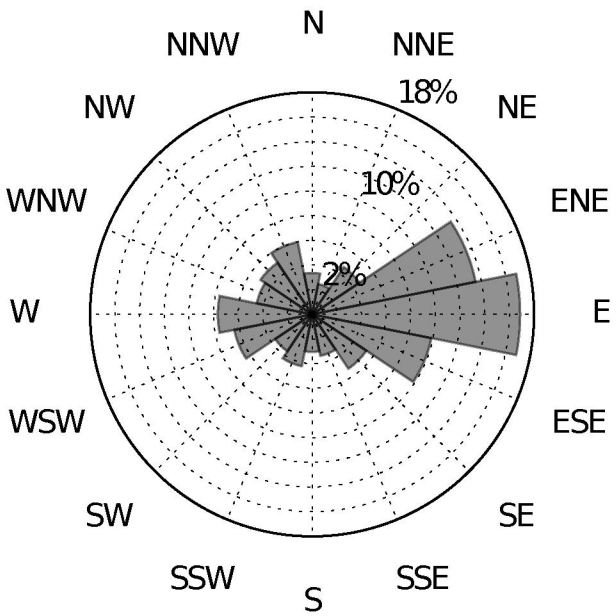

Figure 74 – Vossoroca's wind frequency analysis from Jun/2012 until Feb/2015.

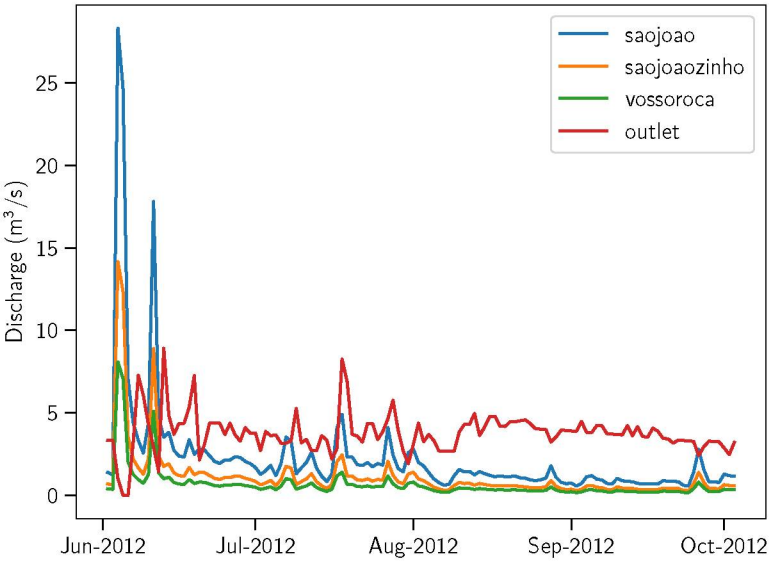

Figure 75 – Vossoroca's discharge data in 2012.

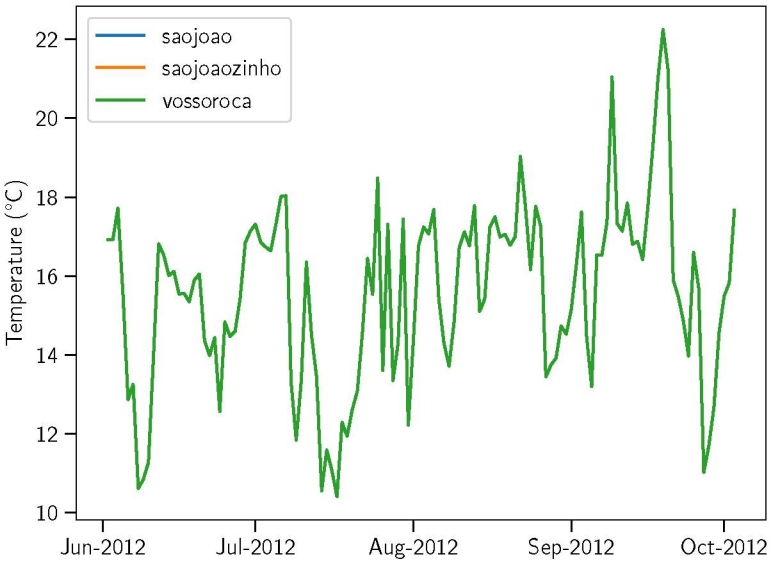

Figure 76 – River temperature estimated for inlets. The temperature were considered equal for all inlets.

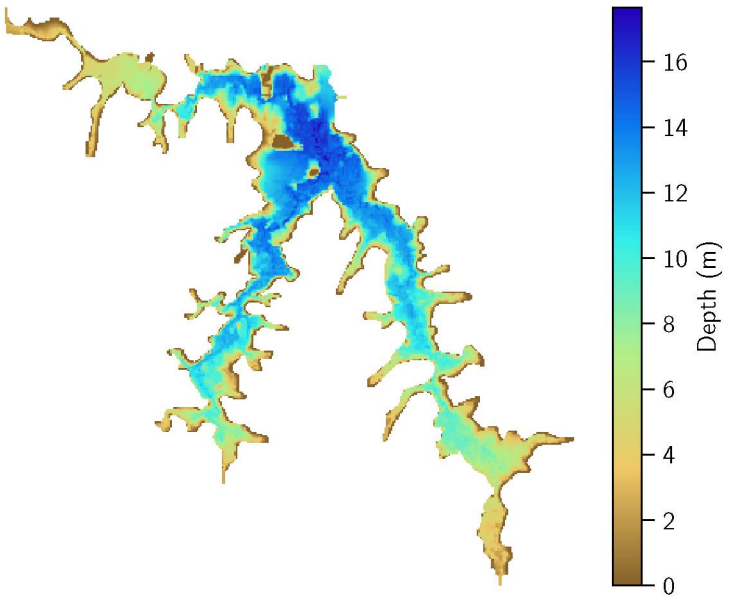

Figure 77 – Vossoroca Reservoir bathymetry showing depth values in meters below the maximum water level.

APPENDIX B – METRICS FOR UNIFORM SYSTEMS

The topic of this thesis is about non-uniform and unsteady system. Regarding these classes, a system can be classified qualitative, for example, by the inspection of the properties of water samples. However, what is explored in this section are quantitative methods which classified the system indirectly by physical properties.

A preliminary overview of expected hydrodynamic characteristics, as mixing level, could help the determination of the dimension to be considered in hydrodynamic modeling (i.e 1D, 2D, 3D approach). This system descriptor may be simple enough to provide an insight without many efforts and should somehow be verified later to guarantee reliable results. Furthermore, an indicator could help the comparison among systems and it has the potential to reveal new patterns.

The parameters were divided into two categories morphometric and dynamic parameters as will be explained below.

Morphometric parameters are those based only on shape and size characteristics as areas, perimeters, and depths. The shoreline development index, volume development index, average depth, relative depth are examples of this kind of descriptors. Such indicators often are related with water quality (MUHTADI et al., 2017; GONCALVES; GARCIA; BARROSO, 2016; BARROSO; GONÇALVES; GARCIA, 2014; HÅKANSON, 1995).

Mean depth (z_m) is the ratio of volume to superficial area: $z_m = \frac{V}{A_{sup}}$.

Shore line development index (SL) is the ratio between the shoreline (P, perimeter) of the water body to the perimeter of a circle with same superficial area of the water body:

$$SL = \frac{P}{\sqrt{4\pi A_{sup}}} \tag{B.1}$$

Volume development index (D_v) is the ratio between the reservoir volume and the volume of a cone with the same maximum depth.

$$D_v = 3\frac{z_m}{z_{max}} \tag{B.2}$$

Table 10 – Reservoir classification in circular, elongated, or dendritic through values of shore line development index (SPERLING, 1999).

Circular	Elongated	Dendritic
$D_p < 1.3$	$1.3 < D_p < 1.5$	$D_p > 1.5$

Relative depth (z_r) is the ratio of maximum depth to mean diameter of the superficial area.

$$z_r = z_{max}\sqrt{\frac{\pi}{4A_{sup}}} \tag{B.3}$$

This parameter relates an estimative of wind fetch to the depth, thus is a rough estimator of mixing by wind. Table 11 shows suggested ranges for this indicator.

Table 11 – Suggested critical value for mixing by wind trough relative depth (SPERLING, 1999)

Low Mixing	High Mixing
$z_r > 5\%$	$z_r < 5\%$

Index of Basin Permanence (IBP) is the ratio of the lake volume divided by the shoreline length (SL) and indicates the littoral effect on basin volume, when $IBP < 0.1e^3m^2$ the system is shallow and usually dominated by rooted aquatic plants (KEREKES, 1977).

Areal ratio is the ratio of drainage area (A_{bac}) and the superficial area of the water body (A_{sup}),

$$F_e = \frac{A_{bac}}{A_{sup}} \tag{B.4}$$

, higher values indicates great potential of substances carriage into the water body.

Dynamic parameters are those indicators which involve rates and are time dependent (dynamic) is present in the scales. Examples are residence time, densimetric Froude, Richardson, Brunt-Vaisala Frequency, Wedderburn, and Lake Number.

Residence time (t_r) is the average time at which the water remains in a reservoir when the system is completely mixed, or is the time necessary to empty the system. The residence time is estimated by the ratio of volume (V) and the outflow

(Q).

$$t_r = \frac{V}{Q} \tag{B.5}$$

Regarding system classification, residence time is used to classify the system as lotic, transitioning, or lentic by the limits shown in Table 12.

Table 12 – Limits of classification for Lotic ecosystem, transitioning ecosystem, and lentic ecosystem through residence time (CONAMA, 2005).

Lotic	Transition	Lentic
$t_r < 2$ days	2days $< t_r <$ 40days	$t_r > 40$ days

Densimetric Froude (F_d) is the ratio of inertial forces to buoyancy forces. This number measures if the flow can affect density structure of the system. The definition of densimetric Froude number is

$$F_d = \frac{u}{\sqrt{g'z}} \tag{B.6}$$

where g' is the reduced gravity $(\frac{\rho - \rho_0}{\rho_0} g)$. (ORLOB; ROESNER; NORTON, 1969) simplified the densimetric Froude to classify the system according to the stratification type. They used three classes (i) deep reservoir characterized by horizontal isotherms, (ii) weakly stratified reservoir which isotherms are tilted along longitudinal reservoir axis, and (iii) completely mixed which isotherms are vertical. Thus, according to them each class could be represented respectively by 1DV, 3D, and 1DH model. The Froude number simplified by (ORLOB; ROESNER; NORTON, 1969) is estimated by

$$F_d = 320 \frac{LQ}{z_m V}, \tag{B.7}$$

the limits proposed by the authors are in Table 13.

Table 13 – Classification of the reservoir according to resistance of stratification to horizontal flow through densimetric Froude.

Completely mixed	Weakly-stratified	Deep reservoir
$F_d > 1$	$0.1 < t_r < 1$	$F_d < 0.1$

This section showed some common parameter used to classify reservoirs. The morphological parameters require fewer data and they can be estimated at different

times producing a time series of the indicator (e.g. mean depth). On the other hand, the dynamic parameters could be estimated for each location within a system. Such transition from integral to local, and from steady to unsteady indicators are easy to achieve but there is no guarantee they are going to indicate the same properties or phenomena.

APPENDIX C – DERIVATION OF LOCAL MAXIMUM CONCENTRATION

Local maximum concentration is the maximum concentration in a given location. Then, for each place in a system, there is at least one maximum concentration. The maximum concentration was derived for the three ideal cases: new continuous loading, oscillatory loading, and instantaneous loading. The local maximum concentration for the new continuous loading is the concentration reached in the steady-state because the maximum concentration will reach the maximum concentration when t tends to infinity. This solution was found in Genuchten & Alves (1982) as solution C2.

The derivation of local maximum concentration for oscillatory loading is straightforward because the solution is in the form of $A\sin(B)$, where A is the amplitude. Thus, as the amplitude does not depend on time, the local maximum concentration is equal to the amplitude.

The derivation of local maximum concentration for the instantaneous loading was derived by derivatives. The first,

$$\frac{\partial C}{\partial t} = \frac{M(x^2 - 2Dt - 4Dkt^2 - t^2u^2)}{(\sqrt{4\pi Dt})Dt^2} \exp\left(\frac{-(x-ut)^2}{(4Dt)} - kt\right) \tag{C.1}$$

Then, it was supposed that

$$(x^2 - 2Dt - 4Dkt^2 - t^2u^2) \tag{C.2}$$

will reach zero faster than the remaining terms which requires that t tends to ∞, resulting that the time when the local maximum (t_{max}) occurs is:

$$t_{\max} = \frac{\sqrt{D^2 + 4KDx^2 + u^2x^2} - D}{u^2 + 4kD} \tag{C.3}$$

Figure 78 shows that the estimation for t_{max} through this derivation agrees with the local maximum concentration.

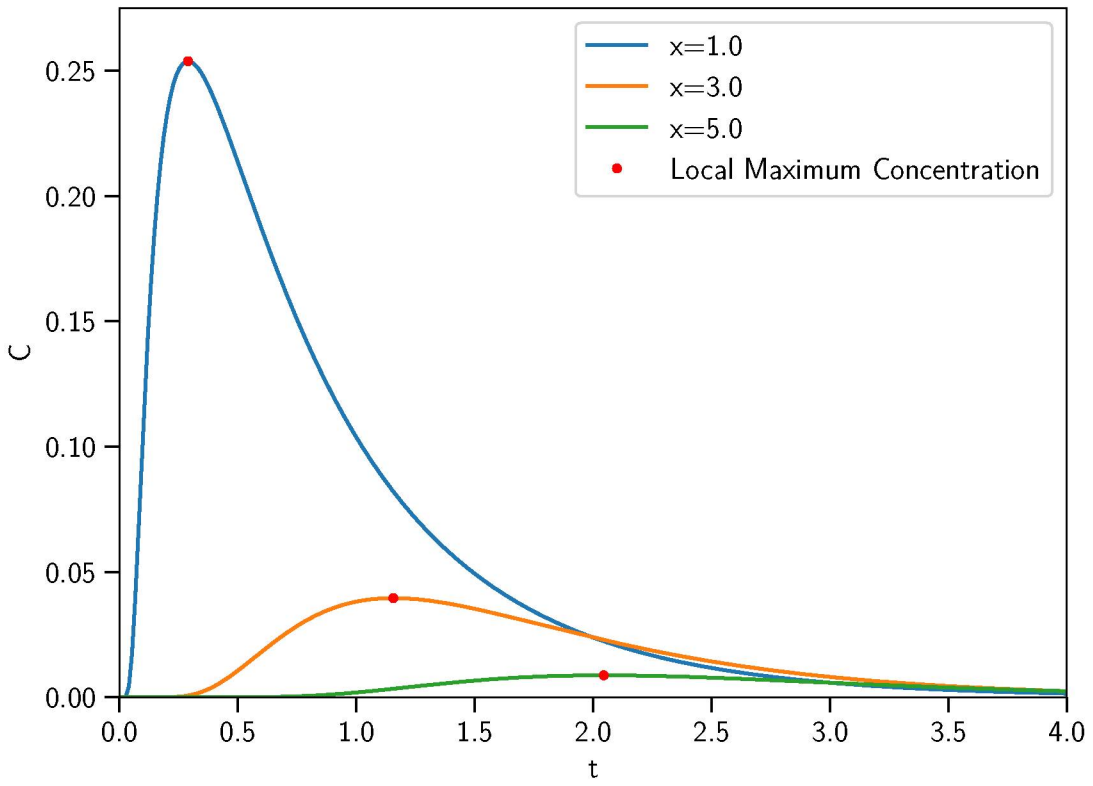

Figure 78 – Concentration time series for three locations (1 m, 2 m, and 5 m from release of an instantaneous loading) using the 1D-ADRE analytical solution. The red dots are the local maximum concentration derived through Equation C.3